A geospatial approach to display the hydrological impacts of permafrost disturbances on the geochemistry of streams, Lower Peel River and Western Mackenzie basin, northwestern Canada

Catherine Paquette

Thesis submitted to the
Faculty of Graduate and Postdoctoral Studies
in partial fulfillment of the requirements
for the M.Sc. Degree in Physical Geography

Department of Geography
Faculty of Arts
University of Ottawa

Supervisor:
Dr. Denis Lacelle

Thesis Committee:
Dr. Ian D. Clark
Dr. Michael Sawada

Abstract

Retrogressive thaw slumps are one of the most dynamic geomorphic features in ice-rich permafrost environments. These features impact aquatic environments by releasing previously frozen organic and inorganic sediments into nearby waterbodies. The objective of this study is to quantify the effect of thaw slumps growth on the hydro-geochemical regime of streams in the Richardson Mountains–Peel Plateau region, northwestern Canada (Fig. 1), within a geospatial hydrological framework (sub-basin, watershed and sub-watershed units). The sub-basin level is determined as the most effective to represent the geochemical properties because of the higher number of sample points within each unit. Based on correlation values, the average surface area of slumps has the most impact on stream geochemistry (as opposed to the number of slumps). Larger single slumps (>5ha) contribute more to changes in geochemistry than clusters of smaller slumps. These slumps can alter the geochemistry of the water to such levels as to exceed limits for freshwater aquatic life.

Résumé

Les glissements rétrogressifs de fonte sont parmi les formes de relief les plus dynamiques, se créant dans les environnements de pergélisol riche-en-glace. Ces glissements peuvent impacter les environnements aquatiques en relâchant du matériel organique et inorganique auparavant gelé dans les cours d'eau à proximité. L'objectif de cette étude est de quantifié l'effet du développement de glissements sur le régime hydro-géochimique des cours d'eau, dans la région des monts Richardson et du plateau Peel, au nord-ouest du Canada (Fig.1) à l'intérieur d'un cadre hydrologique géospatial (sous-bassin, bassin-versant et sous-bassin-versant). L'échelle des sous-bassins a été déterminée comme étant la plus efficace pour représenter l'état de géochimie dans les eaux à cause du plus haut nombre d'échantillons par unité. Basé sur les valeurs de corrélation, la superficie moyenne des glissements est le paramètre ayant le plus d'impact sur l'hydro-géochimie (contrairement au nombre de glissements). Les plus gros glissements (>5ha) contribuent davantage aux changements de la géochimie des eaux qu'un regroupement de plus petits glissements. Ces glissements peuvent changer la géochimie des eaux à un tel point que les valeurs excèdent les limites pour la vie aquatique en eau douce.

Acknowledgements

This thesis would not have been possible without funding provided by NSERC, the Northern Scientific Training Program and the Polar Continental Shelf Program, allowing the access to the remote locations needed to perform this research.

There have been many contributors to making this project a success. I am grateful to Ping Zhang and Nimal De Silva from the Department of Earth Sciences for their assistance in preparing and analyzing my water samples. I would like to thank Alex Brooker and Alex Forest for their company and help in the field. I am also grateful to Alex Brooker for his work identifying thaw slumps, providing me with the database necessary to perform my analyses.

I would specially like to thank my thesis supervisor Dr. Denis Lacelle for allowing me to further my passion for periglacial environments and for his tireless help in the research, analysis and writing of my thesis.

To my officemate Andréanne Bourgeois-Roy and to my fellow grad students, thank you for making the Geography Department a great place to study and work and thank you for all the support and advice all along this project.

Finally, I would like to thank my parents, Marc and Elizabeth, and my sibling, Stéphane and Émilie, for their support and love over the past two years. I am truly appreciative of the support you have given me.

Contents

List of Tables

List of Figures

Chapter 1. Introduction

1.1 Introduction

Air temperature in the Arctic has been increasing at a significant rate in recent decades. The *Arctic Climate Impact Assessment* (ACIA, 2004) has reported that between the 1950s and 2000s, the mean annual air temperature in the Arctic has increased by ca. 1°C; however, the change shows a strong seasonal contrast, with average winter air temperature increasing by 2-4°C. The climate warming in the Arctic has increased the vulnerability of various components of the terrestrial cryosphere, including snow, glaciers and permafrost. The thermal regime of permafrost in Arctic regions has already started to experience the effect of increasing air temperatures as revealed by a northward migration of the southern boundary of permafrost (Osterkamp and Romanovsky, 1999) and a warming of ground temperatures, with the rate of increasing ground temperature being more rapid in the continuous permafrost zone (Smith et al., 2010; Romanovsky et al., 2010; Lewkowicz et al., 2012). A consequence of warming permafrost is an associated increase in the rate of permafrost degradation or thermokarst (Jorgenson et al., 2006; Kokelj and Jorgenson, 2013).

Thermokarst features indicative of permafrost degradation include thickening of the active layer, development of channel networks and lake drainage, and thaw slumps (French, 2007). Thawing permafrost has the potential to significantly alter aquatic environments (Frey and McClelland, 2009; Rowland et al., 2010; Keller et al., 2010). The growth of retrogressive thaw slumps, one of the most dynamic geomorphic features in ice-rich permafrost environments, also impacts aquatic environments by releasing previously frozen organic and inorganic sediments into nearby streams and lakes. In regions containing thaw slumps, the suspended sediment load and solute concentrations in slump impacted streams and lakes can be orders of magnitude higher than from the adjacent unaltered landscape (Kokelj and Lewkowicz, 1999; Bowden et al., 2008; Lamoureux and Lafrenière, 2009; Lewis et al., 2012; Malone et al., 2013). Ongoing climate change in the Arctic, including warming air and ground temperature and increase in precipitation, will likely increase the number of active thaw slumps and their growth rates (Kokelj et al., in review). As a consequence, an increase in the amount of active thaw slumps is expected to affect high-latitude freshwater ecosystems through changes in water geochemistry, which might affect production, food chains, biogeochemical cycles and water quality (Mesquita et al. 2010). However, all studies that investigated the impacts of permafrost

degradation on freshwater ecosystems were performed within small fluvial catchments (i.e., along a single stream reach). As of yet, the potential spatial dimension of geochemical impacts of thawing permafrost are largely unknown.

1.2 Research Objectives

The objective of this study is to quantify the effect of the growth of thaw slumps on the hydro-geochemical regime of streams in the Richardson Mountains – Peel Plateau region, northwestern Canada (Fig. 1), within a geospatial hydrological framework (basin, sub-basin, watershed and sub-watershed units). This objective will be reached by: 1) compiling a database of the distribution of active and stable thaw slumps in the Richardson Mountains-Peel Plateau region using Landsat satellite images (Brooker , 2014); 2) using a digital elevation model to create a geospatial framework of drainage basins at various scales (sub-basins to sub-watersheds level), including a description of their main characteristics (surface area, drainage pattern and basin shape); 3) generate a database of geochemical composition of streams in the Richardson Mountains – Peel Plateau region; and 4) investigate relations between the distribution of thaw slumps and stream geochemistry at various hydrological scales. Overall, the thesis will help infer the spatial dimension at which the thaw slumps may impact aquatic ecosystems.

1.3 Structure of thesis

This thesis is divided into 6 chapters. Chapter 1 introduces the topic of study and includes a comprehensive review of the literature. Chapter 2 describes the study region, highlighting the glacial history, geology and surface sediments, soils and vegetation, regional climate as well as permafrost and ground ice conditions. Chapter 3 describes the methodologies used in the thesis. The results are presented in Chapter 4, and with the results discussed in Chapter 5. The research is summarized and conclusions are drawn in Chapter 6.

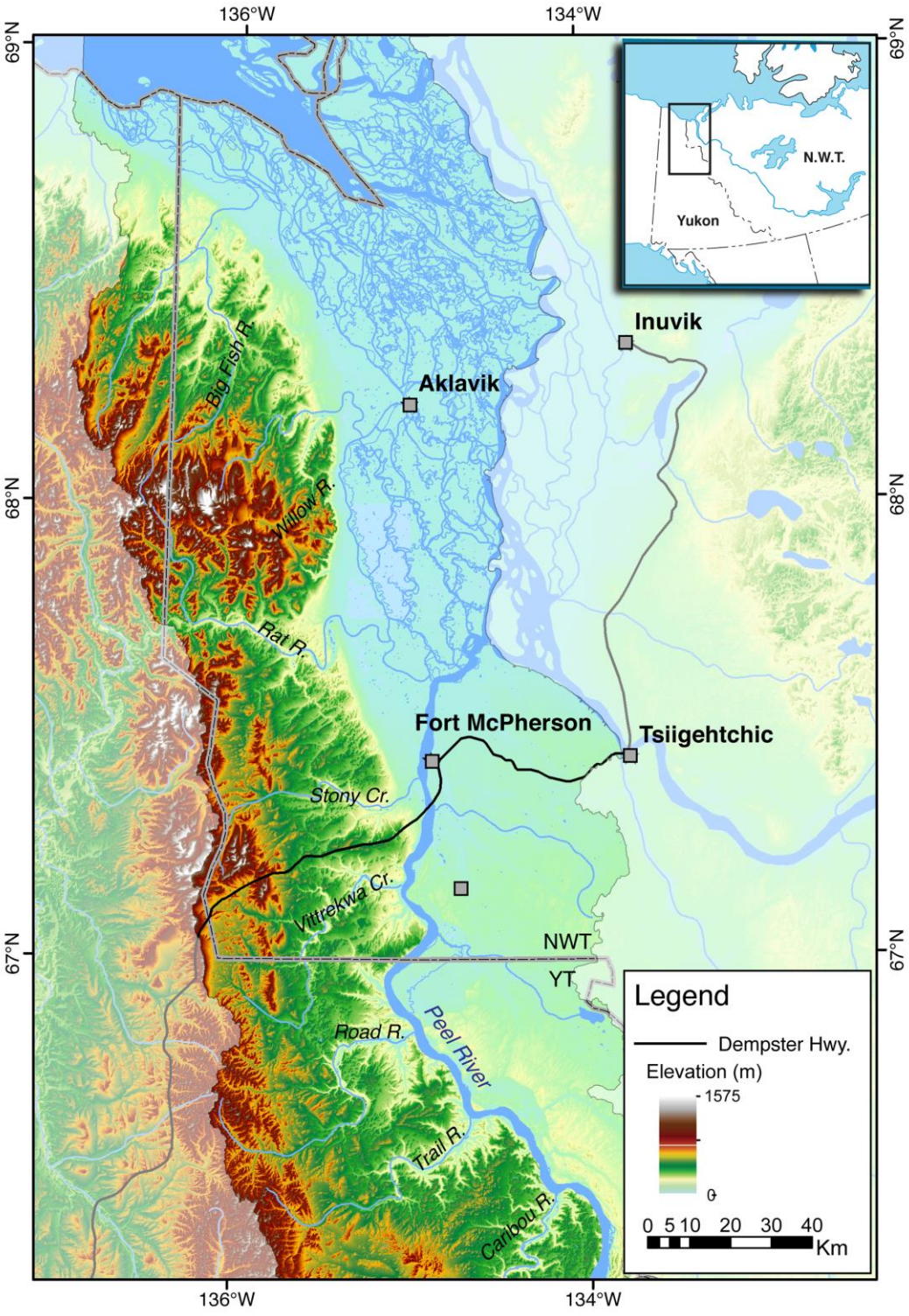

Figure 1. Map showing the extent of the study area (non-shaded region) within the Lower Peel River basin, northwestern Canada.

1.4 Literature Review

In this section, fundamental aspects of thermokarst, hydrogeochemistry of streams, and hydrologic units are discussed. First, permafrost, its classification and active layer will be discussed. Secondly, retrogressive thaw slumps, their morphology, formation and growth will be discussed. Next, the hydrogeochemistry of streams impacted by thermokarst processes will be touched on. Finally, the terminology and identification of the different scales of hydrologic units will be explored.

1.4.1 Permafrost

Permafrost is defined as ground (soil, rock and organic material) that remains at or below 0°C for at least two consecutive years (Muller, 1943; Van Everdingen, 1976). This definition is based on the ground's temperature and not on the state of water in the ground. Permafrost distribution can be classified based on the proportion of land underlain by permafrost (Heginbottom et al., 1995; Fig. 2). Permafrost distribution can be divided into continuous permafrost, with more than 90% of the landscape occupied by permafrost and discontinuous permafrost (<90%). The discontinuous permafrost is sub-divided into two zones, the extensive discontinuous permafrost (50-90%) and sporadic discontinuous permafrost (<50%).

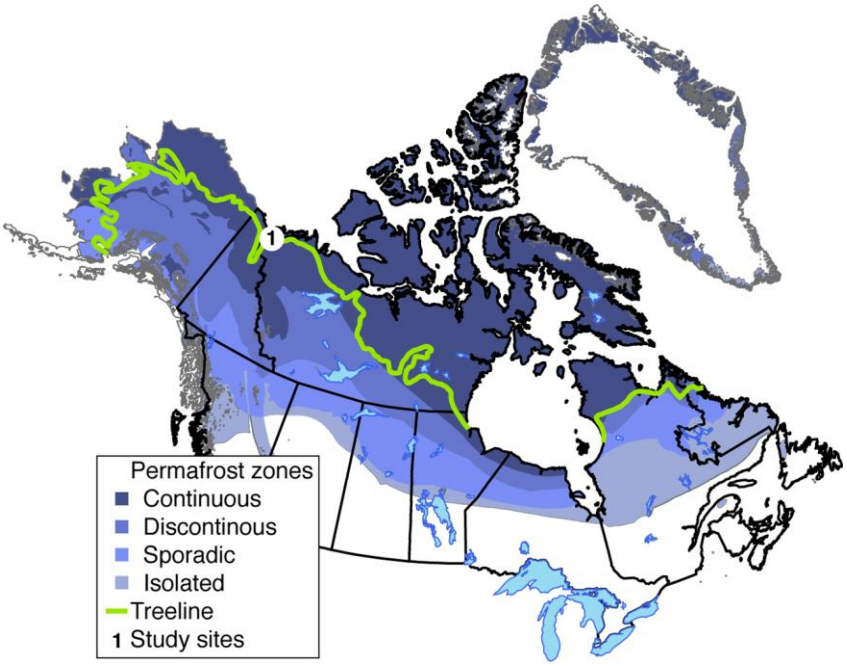

Figure 2.Left: Permafrost distribution and treeline limit in Canada. The study area, indicated by the number 1, is situated within the continuous permafrost zone near the treeline boundary.

1.4.2 Active layer

The active layer is the uppermost layer of soil that experiences either seasonal thawing and freezing, or temperature above 0°C (Heginbottom et al., 1995; Burn, 1998). The contrast between the two definitions lies in the state of water (liquid and ice), or whether the ground remains cryotic (<0C°) (Fig. 3). The depth of seasonal thaw can be estimated from the thermal conductivity of the soil and latent heat of water in soils. Gold and Lachenbruch (1973) provided the following equation to predict the thickness of the active layer (x):

[1] $$x\ (cm) = \sqrt{(\alpha \frac{P}{\pi} loge\ \{Ao/To)}$$

where, □ is the soil thermal diffusivity, P is the period of temperature cycle, A_0 is the surface temperature amplitude and T_0 is the mean annual surface temperature.

A simplified model commonly used to estimate the active layer thickness (z) is the Stephan equation, where:

[2] $$z\ (cm) = \sqrt{bI}$$

where, b summarizes soil thermal properties (thermal conductivity and volumetric latent heat) and I is the thaw degree-days.

The simplicity of Equation 2 is practical because, if we assume that soil thermal properties remain unchanged over time, then annual changes in the thickness of active layer can be estimated from the calculation of thaw degree-days, a climate index of summer temperature intensity.

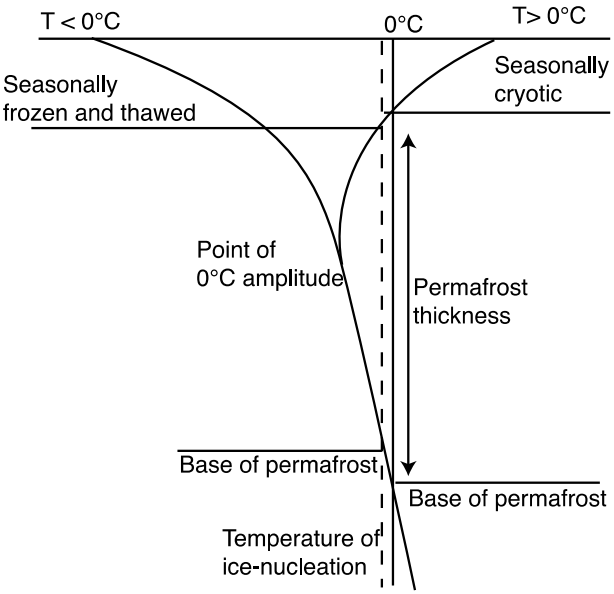

Figure 3. Schematic diagram showing permafrost related terminology. From French (2007).

1.4.3 Historical changes in active layer thickness and environmental impacts

Over the last few decades, air temperatures in Arctic have increased by 1-2°C (ACIA, 2004). Inter-annual variability in active layer thickness is a result of different factors, primarily variations in snow cover and surface air temperature (French, 2007). However, persistent increased temperatures and/or more severe disturbances, (e.g. alterations in vegetation cover, forest fires, physical and thermal characteristics of overlying soil, moisture content), can lead to deepening of the active layer and thermokarst (Brown et al., 2000; French, 2007). Figure 4 shows the annual changes in active layer thickness for various sites across the Canadian Arctic. The thickness of the active layer at any respective site shows high inter-annual variability, but a

slight increasing trend in active layer thickness is observed between 1990 and 2012 for most sites.

Several studies (Lamoureux and Lafrenière, 2009, Keller et al., 2007; 2010, Kokelj and Burn, 2005b) have shown that active layer deepening can lead to significant disturbance with a wide range of physical and geochemical impacts on the environment. Recent studies from Alaska have observed an increase in stream solutes and attributed it to a thickening active layer (Keller et al., 2007; 2010). This was based on the conclusions of Kokelj and Burn (2005b) who suggested that the ice-rich zone immediately below the active layer (i.e., the transient layer) was a sink for soluble material that could ultimately be released upon thawing of permafrost. Keller et al. (2007) demonstrated increasing calcite content as well as significantly higher concentrations of two important nutrients, P and K, in the permafrost as opposed to their concentrations in the active layer. It was proposed by Keller et al. (2010) that geochemical tracers (Ca/Na and Ca/Ba) could be used to monitor of active layer deepening due to the increasing concentrations of carbonate weathering products that could be dissolved in late summer streamwater.

Mass movements of soils along the top of permafrost (or the base of the active layer) are named active layer detachment slides. These disturbances occur when saturated and overburdened soil slides over the frozen substrate. The saturation can be caused by ground ice melt during a deep thaw, snow bank melting or rainfall contributions (Lamoureux and Lafrenière, 2009). The result is a downslope travel of material up to hundreds of meters over low slope angles (Lewkowicz, 2007). These detachment's short-term impacts include abrupt, short-termed increases in river turbidity, sediment transport pulses and possible river damming. In the long-term, they can cause a more gradual increase in discharge and overall turbidity and prolonged increases in sediment transport due to further erosion of unstable material (Lamoureux and Lafrenière, 2009).

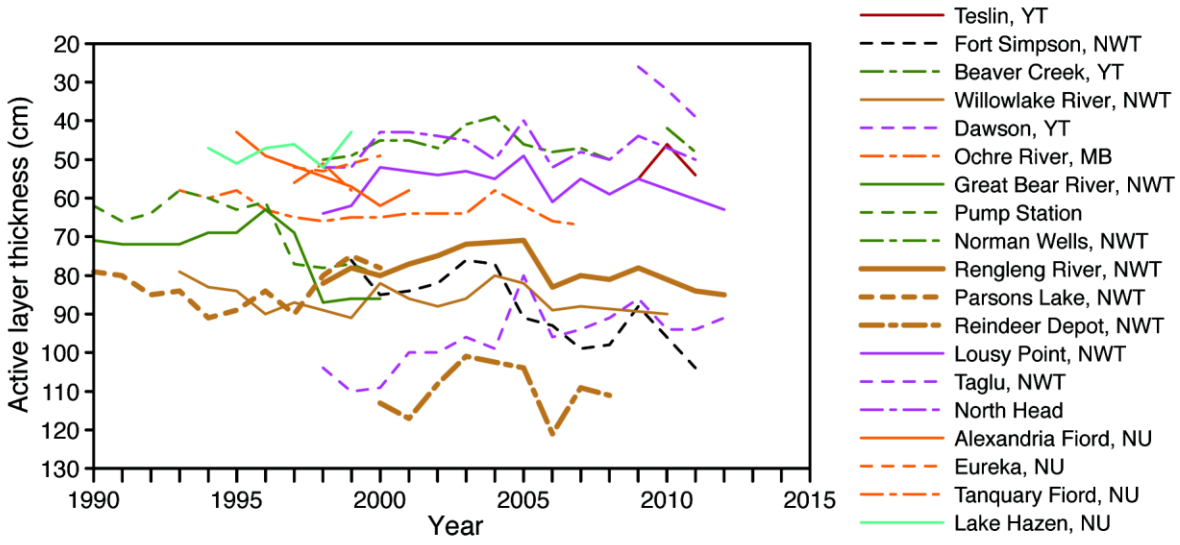

Figure 4. Historical changes in active layer thickness for sites across Arctic Canada. Data is from the Circum-Polar Active Layer Monitoring program.

1.4.4 Retrogressive thaw slumps

Thermokarst describes thermo-erosional processes in areas of ice-rich permafrost. The term thermokarst suggests the alteration of ground's surface due to thawing of ground ice in the permaforst (Murton, 1996). According to Kokelj et al. (2009a) "Thermokarst processes are of geomorphic and ecologic significance because thawing of ice-rich ground affects terrain stability, hydrology, and the chemical composition of soils and surface waters and can alter terrestrial and aquatic ecosystems''.

Retrogressive thaw slumps are one of the most dynamic thermokarst features found in permafrost environment. Thaw slumps form because of thawing of exposed ice-rich permafrost (Burn and Lewkowicz, 1990). A single thaw slump can thaw across several hectares of permafrost terrain in a single year (Kokelj et al. 2005a). In the Canadian Arctic, retrogressive thaw slumps are mostly found along the western Beaufort Sea coastline, along the shorelines of lakes and rivers, and along hillslopes (Burn, 2000; Lantuit and Pollard, 2008; Lantz and Kokelj, 2008; Lacelle et al., 2010). Retrogressive thaw slumps situated along the shorelines of waterbodies are often initiated by fluvial or thermal erosion due to the movements of waves and currents that erodes and exposes ice-rich sediments (Lantuit et al. 2012; Kokelj et al. 2009b), whereas for those situated along hillslopes, active layer detachments, forest fires and intense

precipitation have been advanced as potential slump triggering mechanisms (Lacelle et al., 2010).

Slump morphology

Thaw slumps are composed of two main elements (Fig. 5): 1) a near-vertical headwall that includes the active layer overlaying ice-rich permafrost, 2) a slump floor, or scar zone, of low gradient (2-10°) consisting of wet to dry sediments. For slumps along hillslope, a steeply sloping evacuation channel connects the slump floor to valley bottoms (Murton, 2001; Lacelle et al., 2010). The headwalls of thaw slump can often expose 10-20m of massive ground ice or ice-rich sediments; and their height can sometime exceed 40m (Lacelle et al., 2010; Kokelj et al., 2013).

Slump formation, growth and stabilization

Thaw slumps develop by ablation of the ground ice exposed in the headwall (Lewkowicz, 1987; Burn, 2000; Murton, 2001). The backwasting of the headwall can liberate considerable amount of soil and melted ground ice in the environment. For example, Lantuit and Pollard (2008) documented an average headwall retreat rate of 9.6m/yr for thaw slumps along the coast of Hershel Island, YT, values comparable to other areas in western Canadian Arctic (Lacelle et al., in review). Sediments released during ablation of the headwall are deposited by falls and slides at the base of the headwall, and are then transported away from the base of the headwall by debris flows, meltwater and sub-slump melt-out (Murton, 2001). If the slump floor is not steep enough or there is not enough meltwater generated from the thawing of the ice-rich permafrost, the sediments will accumulate at the base of the headwall, eventually covering the exposed ice-rich permafrost headwall, thus preventing further thaw and stabilizing the slump. Once a slump has been stabilized, it may re-active following removal of the surface sediments (Kokelj et al., 2009; Lantuit et al., 2012). Unlike active layer disturbances (i.e., deepening of active layer, detachment slides), thaw slumps can expose the top several tens of meters of permafrost to thaw across an area up to a kilometer wide (Malone et al., 2013).

Figure 5. Anatomy of a thaw slump: Left: Near vertical headwall exposing ice-rich permafrost, right: low-gradient slump floor flowing towards a local stream or river.

Slump distribution

Several factors influence the distribution of retrogressive thaw slumps within a given area. In the Richardson Mountains and Peel Plateau region, Brooker (2014) established certain trends in the distribution of thaw slumps. First, all identified slumps are situated within the limits of the last glacial maximum, while a larger number (68.5%) were more precisely located between the limits of the last glacial maximum and the Tuetsia recessional phase. Second, the distribution of slumps is tightly linked to the ground ice content in the region. Higher ground ice is needed for the initiation and development of slumps. Third, it was concluded that the type of surface sediment impacts the distribution of slumps. Most of the thaw slumps were found in fine-grained material, while relatively few were found in coarser-grained material. This could also be linked to the conditions necessary for the generation of ice-rich permafrost, as segregated-intrusive ice is typically found within finer-grained material (French, 2007, Mackay and Dallimore, 1992). Lastly, while thaw slumps are found on slopes of all aspects, they are predominantly found on north-east facing slopes (with an average of 60°). The identified slumps were found ranging in elevation from 0 to 765m above sea-level.

1.4.5 Identification of thaw slumps with remote sensing techniques

Thaw slumps are recognizable in the landscape by their arcuate-shape imprints. Identifying active thaw slumps is easily done using air photographs and satellite images because thaw slumps typically display a light-coloured slump floor due to reduced or absent vegetation cover (Fig. 6). It is also possible to identify evidence of stabilized thaw slumps because of a

stark contrast in vegetation with the surrounding landscape. However, after a few decades, the surface of stable thaw slumps will begin to resemble that of the surrounding landscape (Burn and Friele, 1989).

Brooker (2014) used a novel approach to identify the level of activity of thaw slumps (active or stable): the Tasseled Cap linear trend analysis of a Landsat image stack. The method "uses a dense stack of Landsat images (derived from images acquired annually, when possible) for a given area, applies the Tasseled Cap transformations to each Landsat scene and then calculates the trends in the change over time of the three Tasseled Cap transformations for each pixel. The images were acquired between 1985 and 2011, with a resolution of 30m. The three Tasseled Cap transformations were brightness (sensitive to changes in total reflectance), greenness (most capable at displaying green vegetation) and wetness (used to capture soil and plant moisture). A linear trend image was then created by combining the slope value of these three transformations. Figure 7 compares the same area using air photos, older and more recent Landsat imagery, Ikonos (high-resolution satellite) imagery and the Tasseled Cap transformed images.

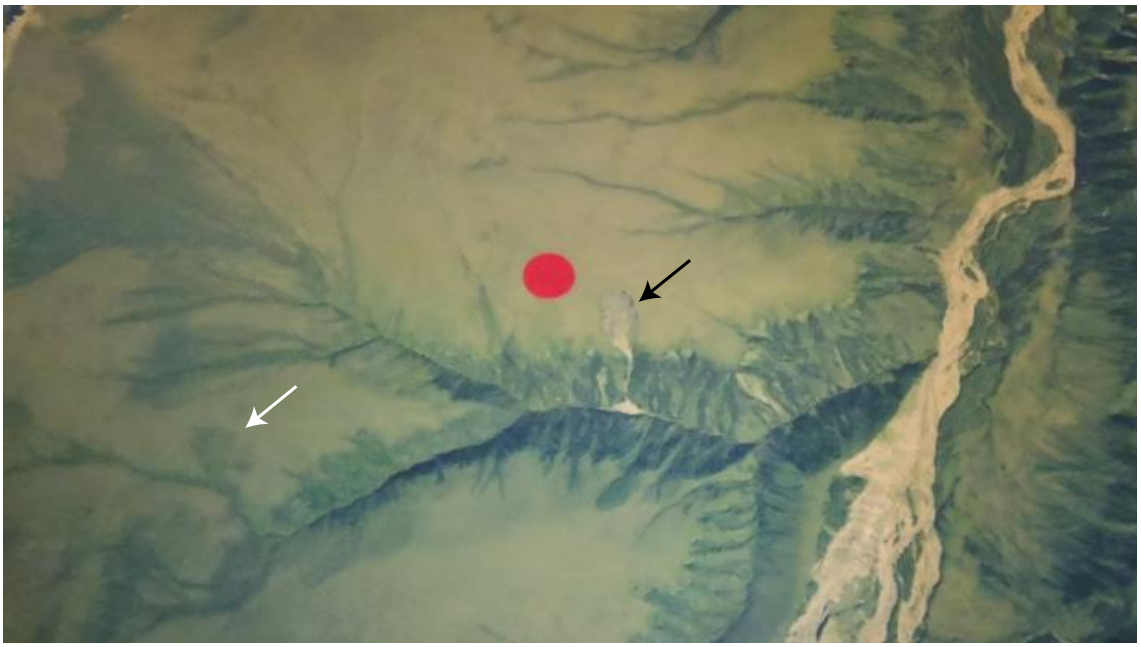

Figure 6. Example of an identified active slump (identified with black arrow) and stable thaw slump (identified with white arrow) on air photograph A31873-160, photograph taken 04-08-22.

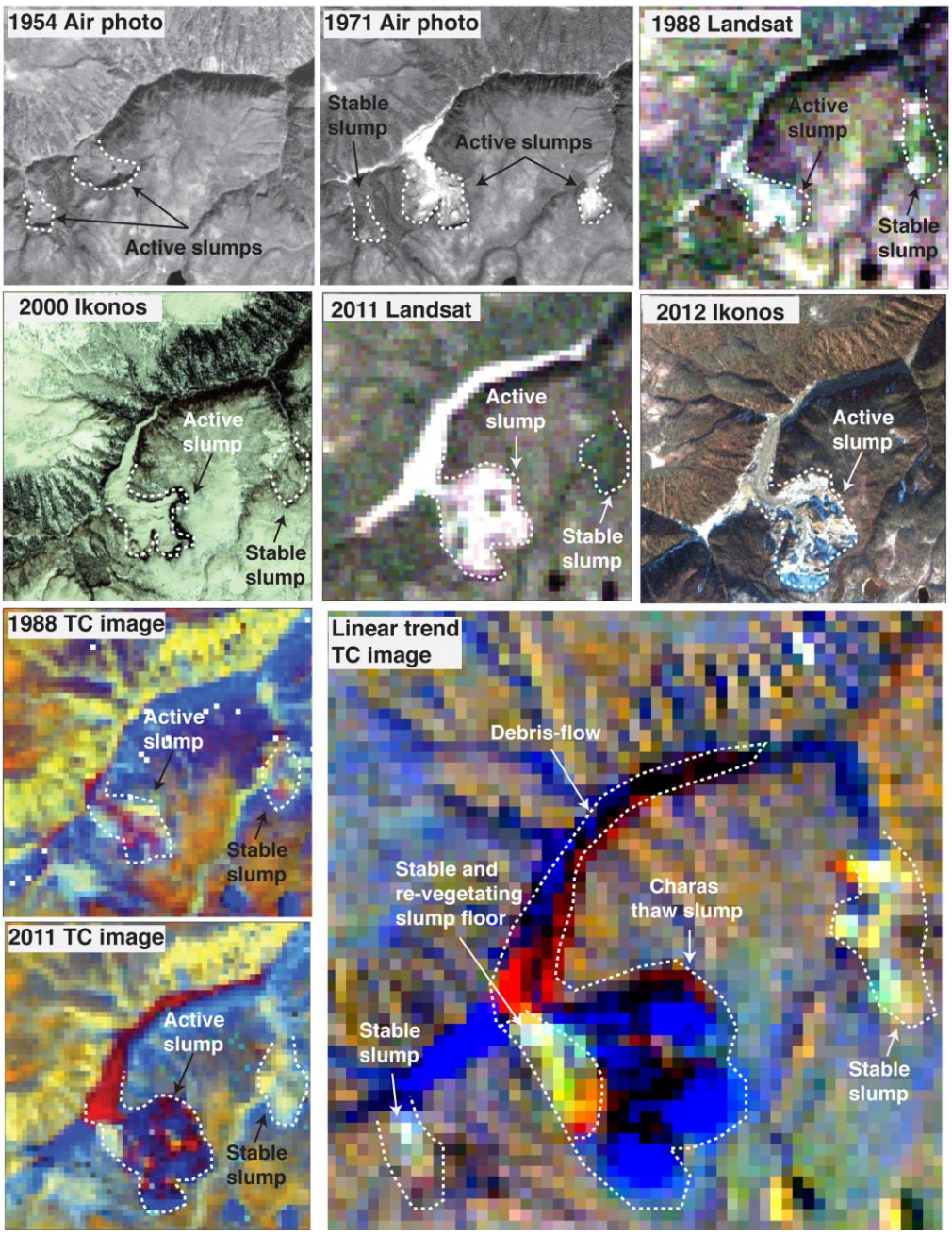

Figure 7. Air photographs (1954 and 1971), Landsat natural colors images (1988 and 2011), Ikonos images (2000 and 2012), single-date Tasseled Cap transformation images (1988 and 2011) and linear trend Tasseled Cap image showing the development of Charas mega-slump and its debris flow, and two other smaller slumps in the Stony Creek sub-basin. (From Brooker, 2014)

1.4.6 Hydrogeochemistry of streams affected by thermokarst

Thus far, little work has been done to understand the spatial extent of impacts of thermokarst features on geochemical composition of streams in western Arctic Canada. Lamoureux and Lafrenière (2009) tracked the fluvial impacts of active layer detachments along stream reaches on Melville Island, Nunavut. Immediate impacts were abrupt rises in turbidity with a more gradual increase in discharge and overall turbidity. The increased sediment load corresponded to an estimated 18% of the seasonal yield.

Kokelj et al. (2005 and 2009a) have shown that thermokarst features, including retrogressive thaw slumps, can affect the water quality in lakes in the Mackenzie Delta. In 2005, 22 lakes were studied (11 impacted by thaw slumps and 11 being pristine) and in 2009 the study was expanded to include an assessment of water chemistry of 34 thaw slumps affected lakes and 39 undisturbed lakes (total of 73) in the region. It was found that permafrost degradation and slumping were the main reason for variation in water quality, while characteristics such as surficial geology and proximity to the treeline or coast were of secondary importance. Lakes with thaw slumps along their shorelines had higher ionic concentrations (mainly Ca^{2+}, Mg^{2+} and SO_4^{2-}) when compared to undisturbed lakes. Slumping did not impact total organic carbon (TOC) concentrations. Surficial deposits were responsible for TOC concentration variations in undisturbed lakes. Finally, it was found that thermokarst features affecting as little as 2% of the catchment area can modify the chemistry of a lake for several decades after the stabilization of thaw slumps (Kokelj et al., 2005 and 2009a).

Following a study of the impact of retrogressive thaw slumps on streams in the Stony Creek sub-basin (Peel Plateau, NWT), Malone (2013) demonstrated that the concentrations of dissolved ions (SO_4^{2-}, Ca^{2+}, Mg^{2+}) in streams with large thaw slumps were significantly higher than in undisturbed streams. An important finding of the Malone et al. (2013) study was the documentation of the importance of the early Holocene thaw unconformity in relation to the ionic concentration in permafrost. The permafrost below the early Holocene thaw unconformity had solute concentrations nearly 100 times higher than the soil measured in the top 1m. Therefore, larger slumps whose headwalls extend below the early Holocene thaw unconformity can have greater impact on the geochemical composition of streams evacuating the slump's material. This sharp contrast is observed because near-surface permafrost (found above the thaw unconformity) has experienced more frequent thawing which would lead to increased leaching

from infiltrating precipitation and removal of higher solute concentration by surface runoff, in contrast to the permafrost found below the thaw unconformity. Malone et al. (2013) suggested that large thaw slumps significantly impacts the geochemistry of streams, and do so by increasing their ionic concentrations well above that of unimpacted streams. The variations of ionic concentration within a slump impacted stream likely depend on the density of slumps along that particular reach. Malone et al. (2013) has also shown that the SO_4/Cl molar ratio can be used as an effective tracer for impacted streams as there is a positive correlation between the two. The SO_4/Cl values of impacted streams can be orders of magnitude higher than non-impacted streams making them useful in the delineation of the extent of a slump impact in streams. The study also found that slumps have much larger reaching impacts than do active layer detachment slides; however, disturbed streams have a different geochemical response than disturbed lakes: the dissolved ions in affected streams are much lower than in disturbed lakes which can be due to environmental conditions. Kokelj et al. (2013) suggested that the impacts of slumps on water geochemistry can be observed at the $10^6 km^2$ watershed scale while active layer detachment slides impact watershed at the $10km^2$ scale.

It is important to note however that to date, very few studies exist that have explored the geochemical impacts of active layer disturbances, slumps and permafrost degradation at larger (sub-watershed, watershed of sub-basin) scales. Most studies (i.e., Lamoureux and Lafrenière, 2009, Kokelj et al., 2005 and 2009a, Keller et al. 2007 and 2010; Malone et al., 2013) have been limited to a single stream or catchment, at most a single drainage site. A larger scope of study is important to display the spatial dimension of the hydrological impacts of thaw slumps in the environment in order to present to and inform stakeholders and policy makers.

1.4.7 Canadian chemical standards for aquatic life

The reactions and processes when water comes into contact with soils determine the kind and amount of chemical constituents found within a stream. Within a hydrologic unit, the main inputs of chemical constituents are from precipitation, weathering of rock and biological inputs (Brooks et al. 2003). Calcium is abundant in water because it is a major constituent of many rock types. Magnesium is abundant in igneous and carbonate rocks (i.e. limestone and dolomite) and is therefore found in higher concentration in water when these rocks form the landscape. Sodium is abundant in igneous and sedimentary rocks and can be leached to surface and groundwater

systems. Sulfur occurs naturally in water from the leaching of gypsum and other common igneous and sedimentary rocks. Weathering leads to the creation of oxidized sulfate ions (SO_4^-) that are soluble in water (Brooks et al., 2003).

Previous studies have shown that the growth of thaw slumps generates significantly higher dissolved solutes when compared to unimpacted streams (Kokelj et al., 2013, Malone et al. 2013). While this is recognized, it is still unknown if these higher ionic concentrations values would impact the water quality of aquatic ecosystems. As such, this study seeks to compare measured ionic concentration values in slump impacted and pristine streams to the established standards needed for healthy aquatic ecosystems.

The standards established by the Canadian Council of Ministers of the Environment (CCME) are shown in Table 1. They represent water quality indexes identified as maximum levels of concentrations acceptable for aquatic life. Many of the dissolved chemical constituents do not appear to have concentration limits that would be harmful to fish or other aquatic wildlife. Such is the case for calcium. Sodium is only considered dangerous when both sodium and potassium concentrations exceed 85mg/L (Brooks et al, 2003). Absolute long-term and short-term exposures can vary by study. The CCME Canadian Environmental Quality Guidelines' Glossary define long-term exposure as contact to a contaminant, lasting from several weeks to years, often encompassing the reproductive cycle or lifecycle of the organism. It can also be referred to as chronic exposure. Short-term exposure is defined as contact to a contaminant for a time period that is small compared to the life span of the test organism. Exposure is usually severe enough to rapidly induce an effect. It can often be referred to as acute exposure.

Few guidelines exist as to conductivity values (total dissolved solutes) for fresh water. Conductivity is primarily impacted by the geology of the area where the stream flows. The conductivity standards shown in Table 2 were adapted from the United States Environmental Protection Agency.

Table 1 Long and short term water quality indexes (Adapted from CCME's Canadian Environmental Quality Guidelines, Brooks et al. 2003; Lumb et al., 2006).

Parameters	Long-term max. (mg/L) (weeks to years)	Short-term max. (mg/L) (days to weeks)
pH	9 (minimum =6.5)	
NO3	13	550
Cl	250	640
SO_4	500	
Al	pH>6.5: 0.01 pH<6.5: 0.005	pH>6.5: 0.05
As	0.005	
Ca	Not specified	
Fe	0.3	1
K	Not specified	
Mg	>100-400	
Na	Not specified	
S	Not specified	
Zn	0.03	0.1

Table 2. Conductivity threshold values and possible effects on the environment, USEPA.

Conductivity (µS/cm)	Classification	Effects
<50	Very low	May not be suitable for some species of fish and macroinvertebrates
50-150	Lower than ideal, but not unusual	
150-500	Ideal	Ideal for diverse aquatic life in inland fresh waters
500-1500	High than ideal, but not unusual	May not be suitable for some species of fish and macroinvertebrates
>1500	Very high	

1.4.8 Terminology and spatial extent of hydrologic units

Hydrological processes can be examined at various spatial scales, or hydrologic units. A hydrologic unit is a contiguous area of land, water, and biota within the confine of a drainage divide which drains to a single outlet. The drainage divide is the ridge line that separates two adjacent units which then drains into two separate outlets (Bedient, Huber and Vieux, 2008; NRCS-USDA, 2007). Runoff within the hydrologic unit will flow from higher elevation areas towards lower elevation areas perpendicularly to contour lines.

A hydrologic unit can include multiple waterways and cover thousands of kilometers or it can be small and represent a single tributary within a larger system (NRCS-USDA, 2007). The National Resources Conservation Service of the United States Department of Agriculture (NRCS-USDA) has established standards of the delineation of hydrologic unit boundaries based on their relative size, with eight levels of classification identified (Table 3). The spatial dimension at which hydrological processes are examined is important. The smaller 6th level sub-watersheds (up to 40,000acres) are useful when used as a tool for water-resource management and planning activities, particularly for site-specific and localized studies requiring a level of detail provided by large-scale map information (NRCS-Iowa, 2008). This classification will be used in this thesis (Fig. 8 and 9).

Table 3 Classification of various hydrologic units in the landscape (from NRCS-USDA, 2007; McCammon, 2012)

Level	Drainage unit
1st level	Region
2nd level	Sub-region
3rd level	Basin
4th level	Sub-basin
5th level	Watershed
6th level	Sub-watershed
7th level	Drainage site
8th level	Level site

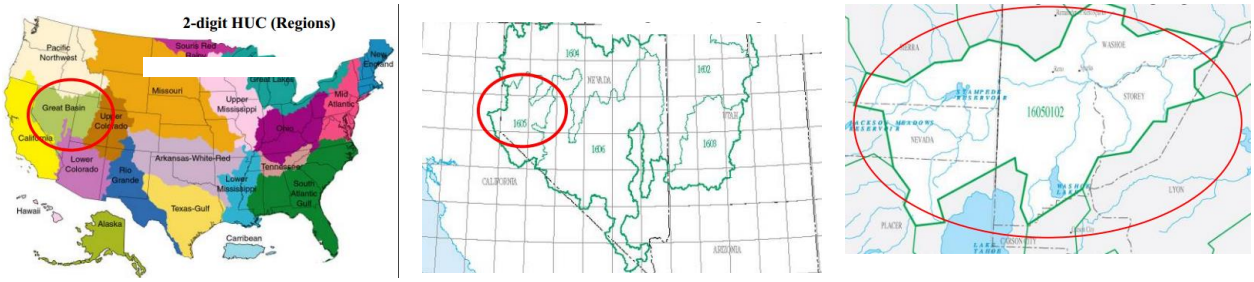

Figure 8. Examples of scales at which watersheds can be analyzed. A) 1st level region, B) 2nd level subregion, C) 4th level, sub-basin, NRCS-USDA, 2007

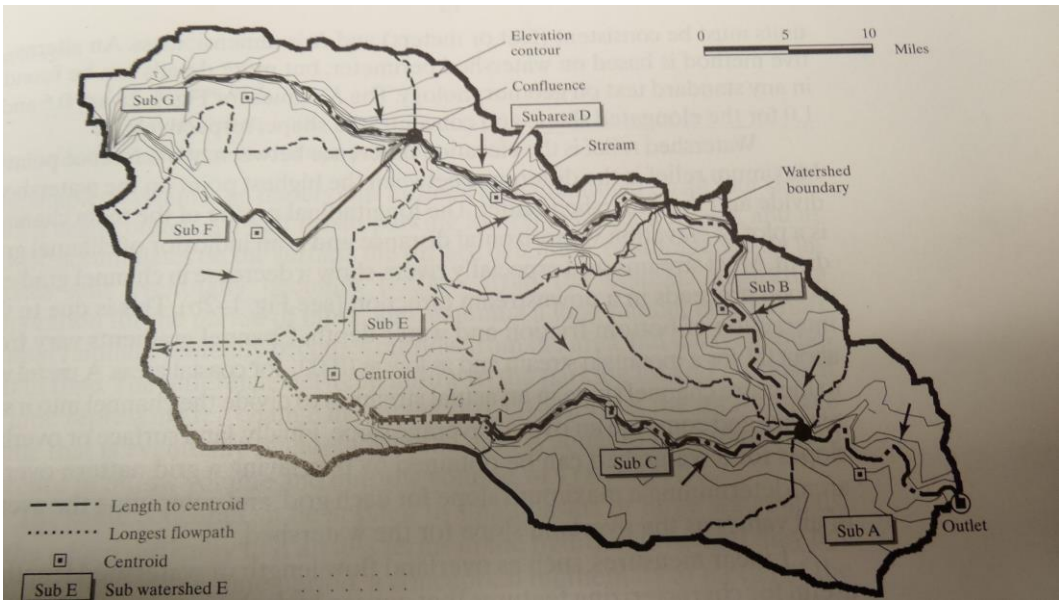

Figure 9. Example of scales at which watersheds can be analysed. The figure shows a 5th level watershed divided by 6th level sub-watersheds (A to G), (Bedient, Huber and Vieux, 2008).

Chapter 2. Study Area

The study area encompasses the Richardson Mountains and Peel Plateau region in northwestern Canada (Fig. 1). In the Richardson Mountains, elevation is typically more than 500m, the lowest point being Summit Lake in McDougall Pass (320m) and the highest point is Mount Sittichinli (1575m). The Peel Plateau is situated in the southern and eastern foothills of the Richardson Mountains and occupies the Lower Peel River basin. This region consists of a broad, gently eastward-sloping plateau with elevation ranging from 100m to 650m (Catto, 1996). The area is dominated by alpine and arctic tundra with subalpine and subarctic woodlands and forests in the southern valleys and arctic shrub lands in the northern valleys (Ecosystems Classification Group, 2010).

2.1 Sub-basins in the Richardson Mountains – Peel Plateau region

According to the National Hydro Network, the rivers and streams draining the east and south slopes of the Richardson Mountains are part to the Lower Peel River basin. At the more local scale, the study area is divided into 12 sub-basins (Fig. 10). The 12 major sub-basins range in size from the largest (Big Fish River, 2935.54km^2) to the smallest (Unnamed sub-basin #2, 99.36km^2) (Table 4). The main channels in each sub-basin share certain physical characteristics such as stream size and type. Braided streams travelling around vegetated and un-vegetated sand bars (varying from a few meters to dozens of meters in length and a few meters to a dozen or so meters in width) were observed in every sub-basin. Canyon-like and V-shaped valleys dissect the landscape (Fig. 11).

Table 4 Name and surface areas of the sub-basins in the Lower Peel River and Western Mackenzie basin.

Sub-basin	Surface area (km^2)
Big Fish River	2935.54
Unnamed sub-basin #1	404.8
Willow River	808.77
Unnamed sub-basin #2	99.36
Rat River	2692.94
Stony Creek	1224.46
Unnamed sub-basin #3	341.86
Vittrekwa River	1979.11
Road River	1545.54
Unnamed sub-basin #4	155.18
Trail River	1281.29
Caribou River	2227.77

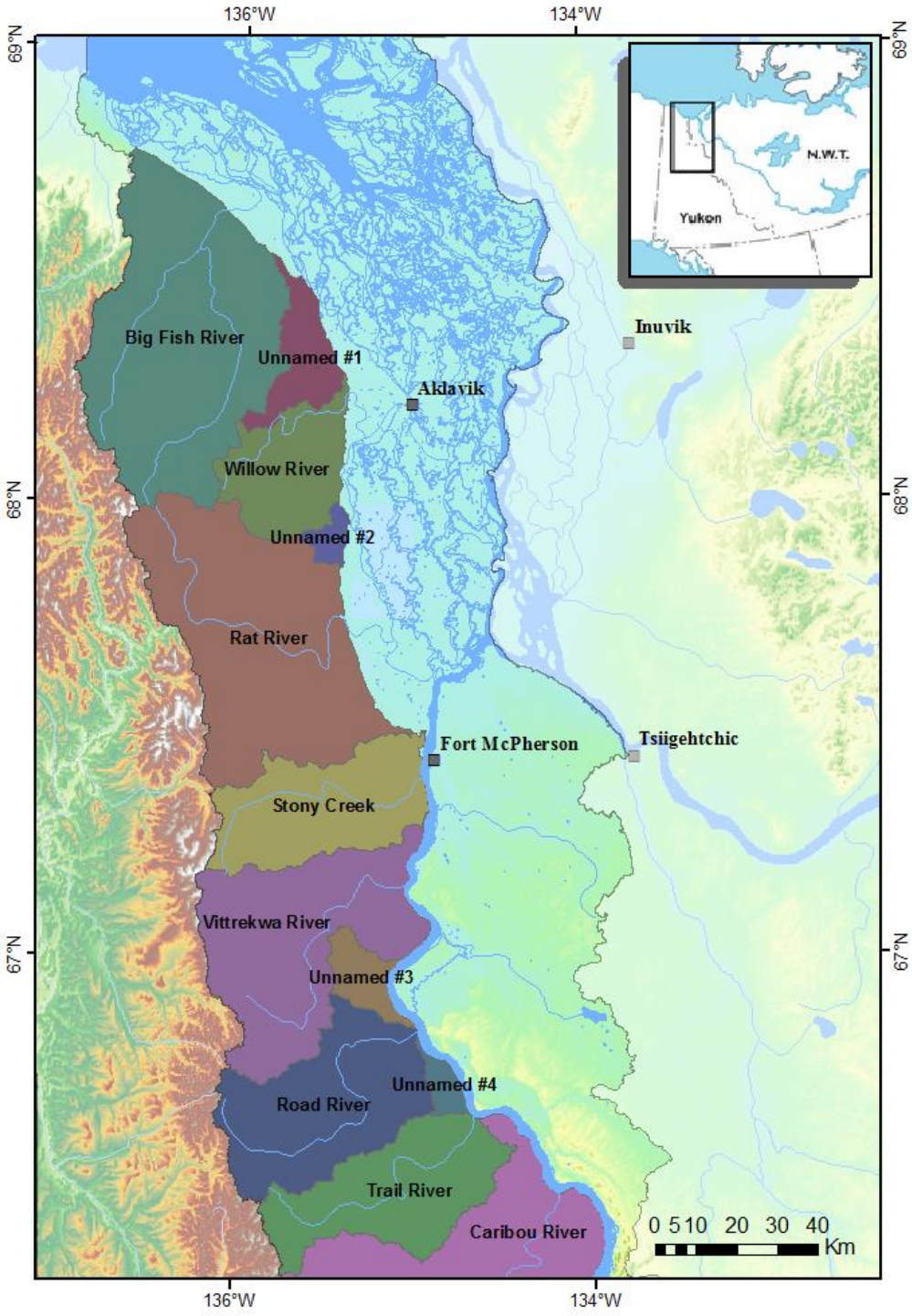

Figure 10. Names of the major sub-basins in the Richardson Mountains-Peel Plateau region, northwestern Canada.

2.2 Glacial history

The study area is situated at the maximum western limit of the Laurentide ice sheet and as such the Richardson Mountains consist of unglaciated mountainous terrain adjoining a glaciated plateau covered by till (Lamirande et al. 1999; Lacelle et al. 2010). The Laurentide Ice Sheet reached the eastern foothills of the Richardson Mountains at about 18,000 cal yr BP and the glacial advance was short-lived with the recessional Tutsieta stage dated to 15,000 cal yr BP (Dyke et al., 2002; Zazula et al., 2009; Lacelle et al., 2013). The stagnating ice sheet along the eastern foothills of the Richardson Mountains allowed for the development of hummocky/rolling moraine terrain, up to 60 m thick (Rampton, 1982).

Following deglaciation, a series of post-glacially incised river and stream valleys dissected the Richardson Mountains (Big Fish, Willow and Rat rivers) and Peel Plateau (Stony, Vittrekwa, Road, Trail and Caribou rivers) with parts of the modern rivers and streams occupying sections of the paleo-meltwater channels. The fluvial incision has resulted in a dendritic network characterized by V-shaped valleys in the uplands with relief less than few meters that evolve to canyon-type valleys with relief of ca. 350m near the confluence with the Mackenzie and Peel rivers (Fig. 11). Based on ^{14}C ages from ancient fluvial terrace along Bonnet Plume Creek in the Willow River sub-basin, the rate of fluvial incision was higher during the early Holocene, and is still ongoing, although at a much slower rate (i.e., Lacelle et al., 2010).

Figure 11. Main streams in Stony Creek (left) and Trail River (right) sub-basins (photo by Paquette, 2013).

2.3 Geology and surface sediments

Figure 12 shows the surface sediments in the study area. The majority of the area is covered by glacial deposits that consist of unsorted silt, sand and clay as well as coarser clasts. These sediments were deposited following the retreat of the Laurentide Ice Sheet. The deposits shown in green (morainal) indicate a terrain of broad hummocks and low hills of 10-20m of relief and characterized by coarse till up to 20m thick. The area is also characterized by a moraine plain with flat to gently sloping terrain overlain by till 3-20m thick. The surficial geology in the Mackenzie River Delta consists of alluvial deposits including sand, silt and minor gravel found within a modern drainage system. Some areas have coarser sand and gravel while others also have thermokarst depressions. Found near rivers and streams are slope complexes which can consist of various undivided deposits. The unglaciated portions of the Richardson Mountains are covered by colluvial and sheetwash deposits such as diamicton and rubble derived from weathering of bedrock and surficial materials. Some areas are characterized by a discontinuous till veneer 0-2m thick overlying the bedrock. The mountains also have smaller pockets of pediment deposits. These are silty gravel 1-2m thick overlain by <1m of silt.

The bedrock geology in the Richardson Mountains and Peel Plateau region is varied due the thrusting and faulting during the formation of the mountains (Fig. 13). Much of the area is underlain by the Lower Cretaceous Arctic Red formation and Rat River formation, which have a marine origin and is composed of shales and sandstones. In the Richardson Mountains the Mount Goodenough and Martin Creek formations (both of the Lower Cretaceous) and the Husky and Bug Creek formations (of the Jurassic and Cretaceous) are encountered.

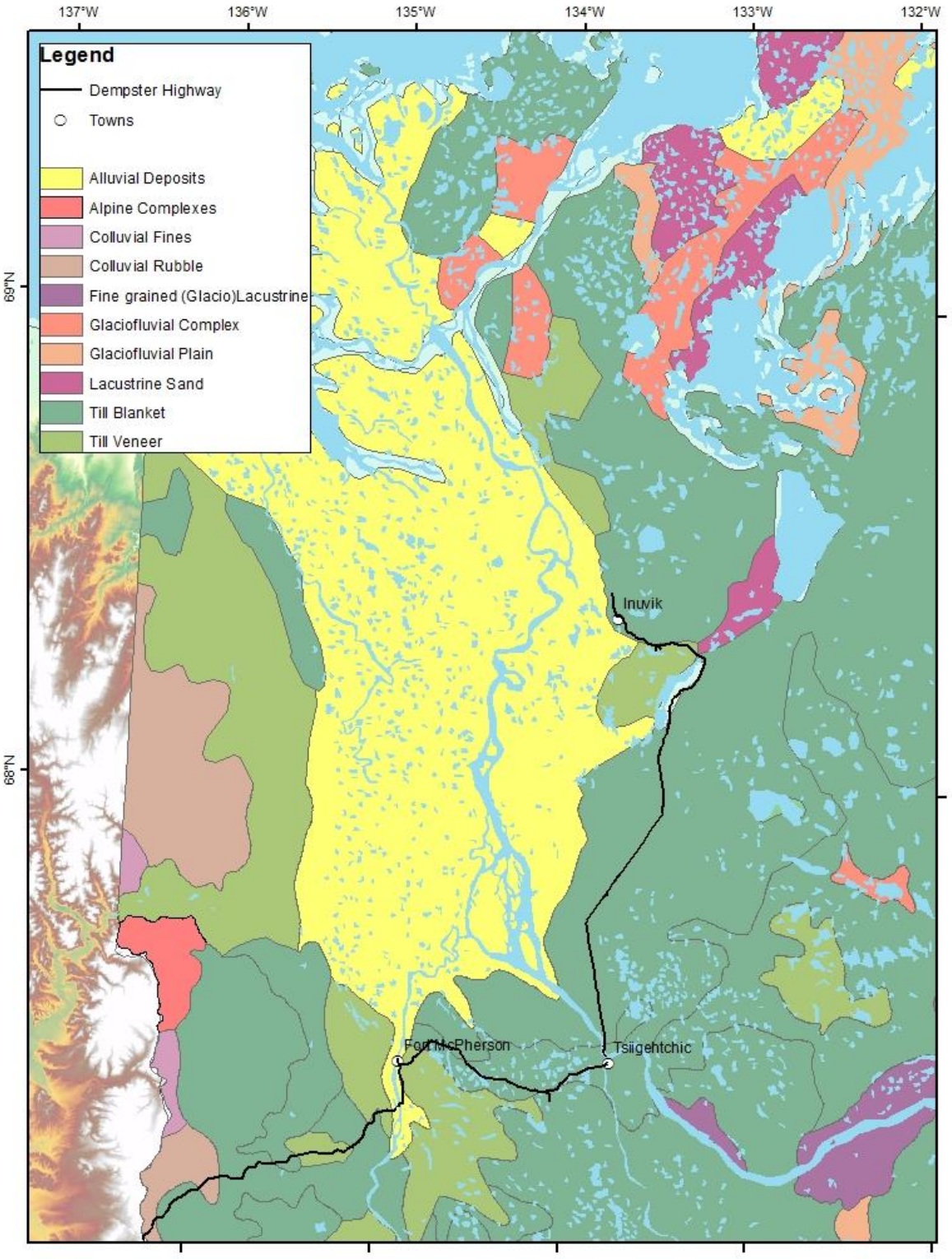

Figure 12. Map showing the surficial geology in the Richardson Mountains-Peel Plateau area.

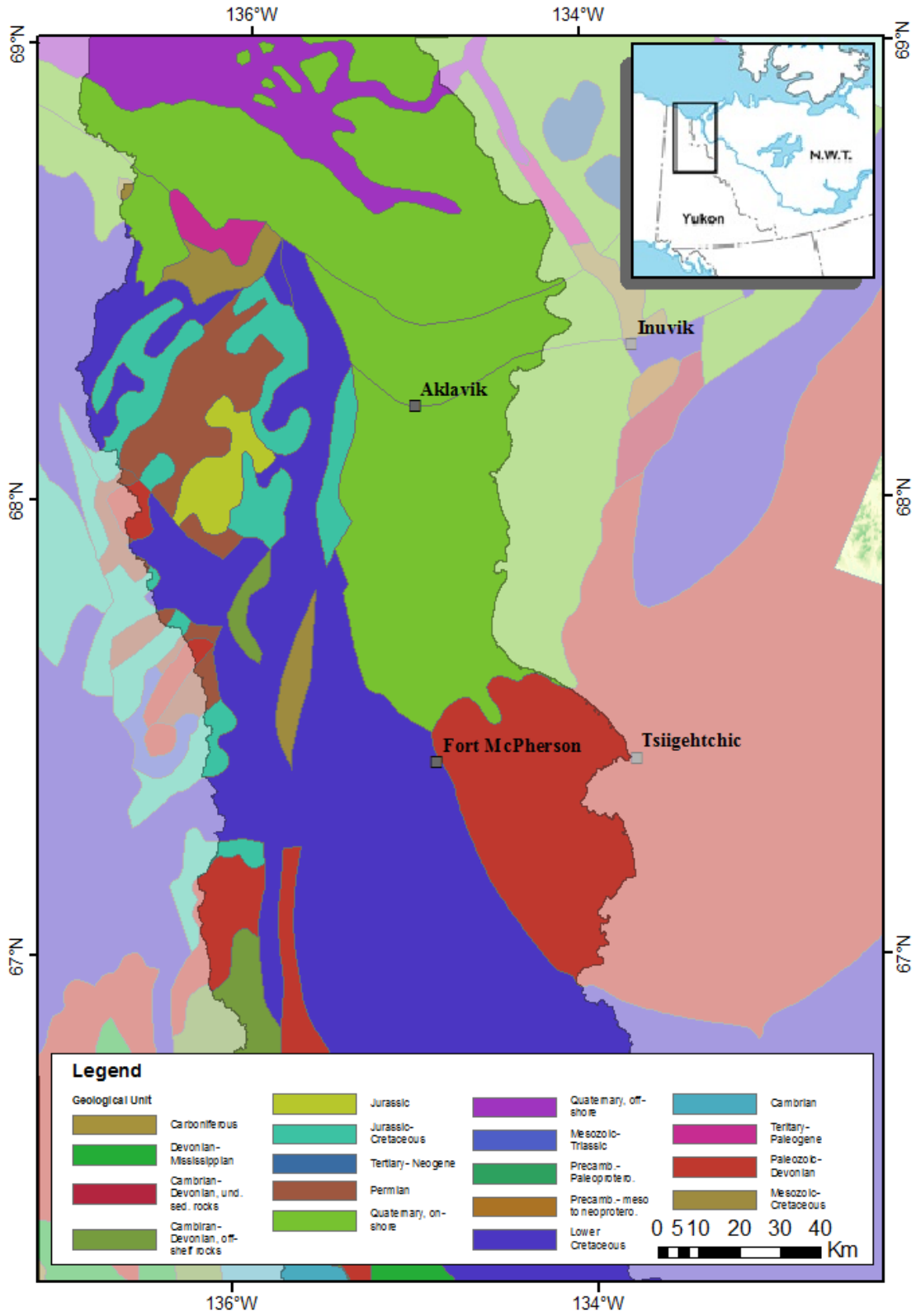

Figure 13. Map showing bedrock geology in the Richardson Mountains and Peel Plateau region, northwestern Canada (modified from the Geological Survey of Canada, Norris, 1991).

2.4 Soils and Vegetation

According to the Ecosystem Classification Group (2010), the Richardson Mountains and Peel Plateau region is dominated by cryosols found under sedge-cottongrass tussock tundra where permafrost is continuous. Regosols and poorly developed brunisols are found in the warmer valley slopes and river terraces.

The study area's vegetation is dominated by alpine and arctic tundra communities characterized by sedge and cottongrass tussocks, black crowberry, northern Labrador tea and a few herbs. Trees are found in river valleys and include krummholz black spruce islands, wet black spruce-shrub-lichen woodlands in the south, white spruce forests with birch and balsam poplar, tall willow, green alder and dwarf birch thickets found in valleys and can extend north into the treeless Low Arctic.

2.5 Regional climate

The western Canadian Arctic is characterized by a continental-type climate regime, with long cold winters and short cool summers (Burn and Kokelj, 2009). In the study area, the closest communities with meteorological stations operated by Environment Canada are situated in Inuvik and Fort McPherson, NWT. The Inuvik climate record begins in 1960, whereas the one in Fort McPherson starts in 1986.

Air temperatures

Figure 14 shows the mean annual air temperature (MAAT), mean summer air temperature (MSAT) and mean winter air temperature (MWAT) and thaw degree-days (TDD) for both Inuvik and Fort McPherson.

The MAAT for Inuvik between 1960 and 2012 averages -8.7 ± 1.6°C, with a MSAT average of 11.9 ± 1.2°C, and MWAT average of -26.5 ± 3.1°C. Between 1960 and 2012, the MAAT varies from –11.9°C to –3.7°C, and has been increasing at a statistically significant rate of 0.068°C yr^{-1}. The increase in MAAT is largely attributed to increasing mean winter air temperature, which has been increasing at a statistically significant rate of 0.117°C yr^{-1}. Conversely, the mean summer air temperature increased at a much slower rate of 0.029°C yr^{-1}. Table 5 shows the MAAT, MAST and MWAT calculated for each decade since 1960.

The trends seen in the available climatic data from Inuvik are not as obvious in the Fort McPherson data. The earliest data is from 1986 thus limiting the possibility of identifying longer-term trends. However, as it is possible to observe, there are significant variations from year to year. The average MAAT for 1986-2010 (excluding 2009 where the data was not available) is -6.9 ± 1.6°C, the average MSAT was 13.5 ± 1.3°C and the average MWAT was -25.6 ± 2.4°C. The MAAT varies from -8.9°C to -3.7°C, and increases by 0.06°C yr^{-1}. The MSAT varies from 11.3°C to 16.3°C showing no observable trend (an increase of only 0.002°C yr^{-1}. Finally the MWAT varies from -31.3°C to -21.7°C, with increases of 0.01°C yr^{-1}. Table5 shows very little decadal trends in the Fort McPherson air temperature record.

The number of thaw degree days in Inuvik is increasing between 1960-2012, as shown by the steep trend line. The TDD varies from a minimum of 938 (in 1959) to a maximum of 1822 (in 1998) with an average of 1316. The number of TDD in Fort McPherson corresponds well with that in Inuvik. The TDD varies from a minimum of 1007 (in 2005, where data for the month of August was missing) to a maximum of 1932 (in 1998).

Table 5 Decadal averages of MAAT, MSAT and MWAT for Inuvik and Fort McPherson, NWT.

Decadal averages	MAAT	MSAT	MWAT
Inuvik, NWT			
1960-1969	-10.02	11.05	-28.86
1970-1979	-9.50	11.70	-28.17
1980-1989	-8.96	12.07	-26.07
1990-1999	-7.64	12.69	-26.25
2000-2009	-7.80	11.88	-23.90
2010 - 2012	-6.29	12.83	-24.01
1960-2012	-8.69	11.91	-26.5
Fort McPherson, NWT			
1986-1989	-7.39	14.13	-23.93
1990-1999	-6.99	13.51	-26.88
2000-2010	-6.55	13.34	-25.01
1986-2010	-6.87	13.54	-25.61

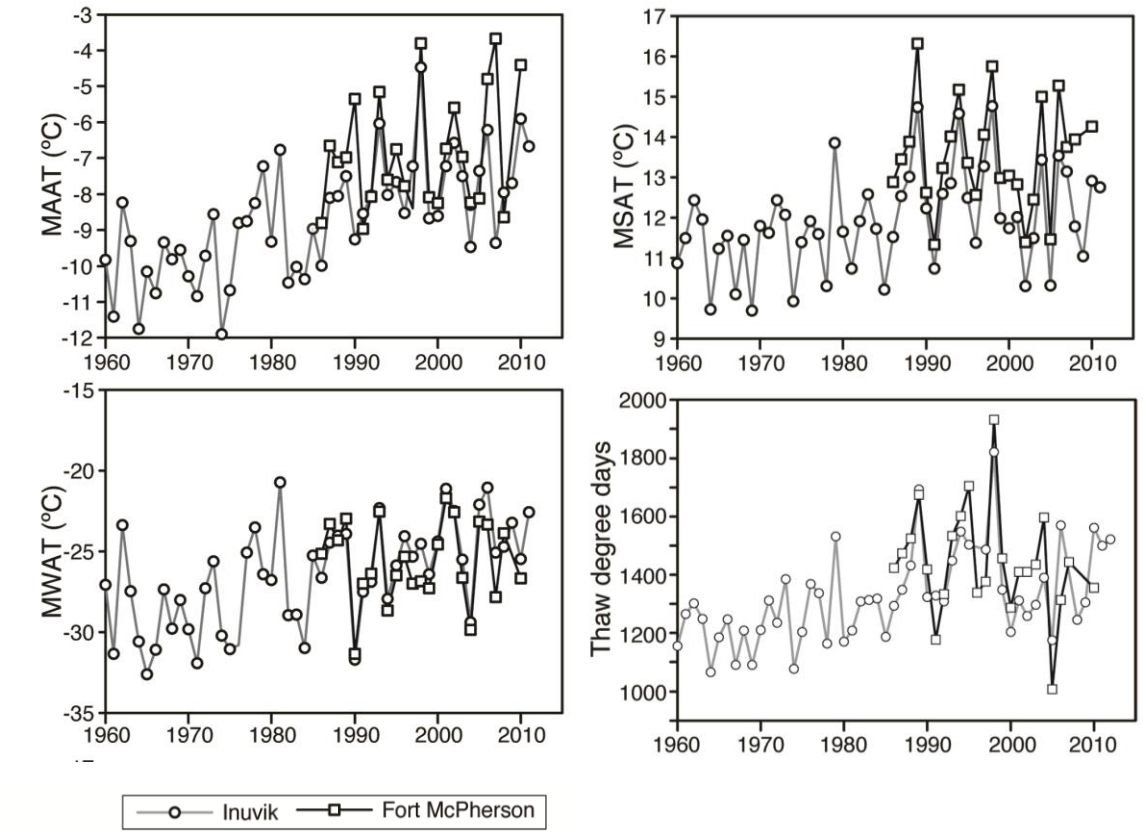

Figure 14. Top left: Mean Annual Air Temperature (MAAT); Top right: Mean Winter Air Temperature (MWAT); Bottom left: Mean Summer Air Temperature (MSAT); Bottom right: Thawing degree days between 1960 and 2012 in Inuvik and 1986-2010 in Fort McPherson, NWT, meteorological stations.

Precipitation

The total amount of precipitation (rain and snow) received at Inuvik and Fort McPherson is shown in Figure 15 (top left and right). The amount of annual precipitation received at Inuvik is decreasing at a statistically significant rate. By contrast, the amount of annual rainfall received at Fort McPherson has been increasing. The last decade also saw a shift in the frequency of high intensity rainfall events (>20 mm). At Inuvik, 7 of the 12 highest daily rainfall events since 1960 occurring over the last decade, whereas at Fort McPherson, the 8 highest rainfall events occurred over the last 20 years. Rainfall recurrence interval for 20mm rain events is 3 years, whereas it reaches 43 years for 40mm rain events (Fig. 15, bottom left and right)

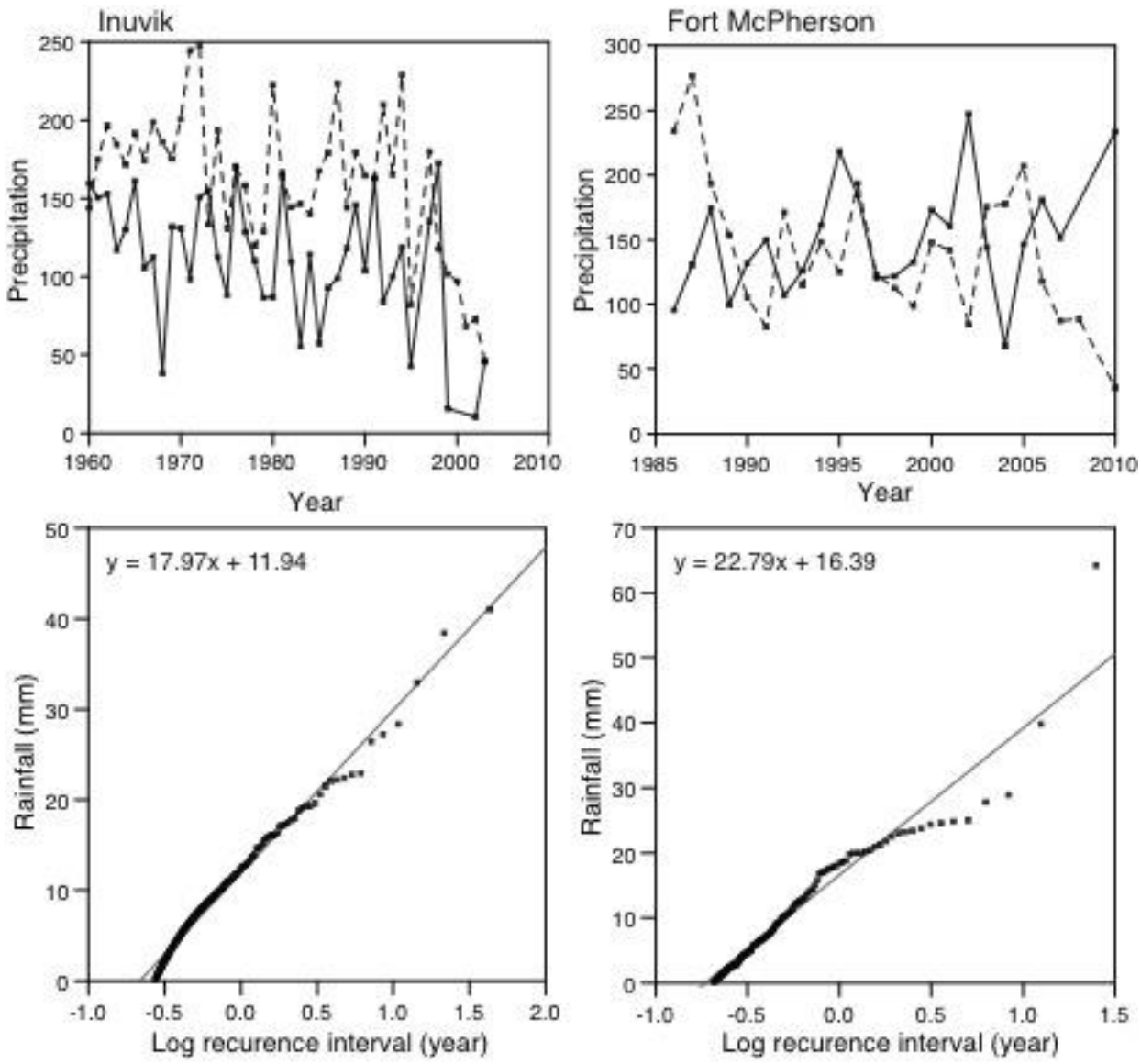

Figure 15. Annual snow and rain totals for both Inuvik and Fort McPherson since beginning of recording (Top left and right). Frequency of rainfall events (Bottom left and right).

Holocene climate

The regional climate history in the western Canadian Arctic and associated geomorphic changes is synthesized in Table 6. The regional climate during the early Holocene was warm and dry (Lauriol et al., 2002a), as the Northern Hemisphere was receiving maximum solar insolation due to Milankovitch variations (Ritchie et al., 1983). Due to the presence of continental ice sheets at this time, sea level was considerably lower than today, resulting in the coastline in northern Yukon and adjacent NWT to be ca. 100 km north of today's shoreline (Hill et al.,

1985). This increased distance from the coast gave the Tuktoyaktuk Peninsula and interior NWT a more continental climate. During the early Holocene, mean summer air temperatures were 3 – 8°C higher than present (Clark et al., 2004; Kauffmann et al., 2004). The warmer summer air temperatures resulted in active layer depths being roughly 1.5 to 2 times deeper than today and led to the development of thaw lakes (Mackay and Dallimore, 1992; Burn, 1997). Maximum active layer depths were reached around 8000 years ago (Burn, 1997), at which point climate conditions changed from warm and dry to cool and wet, due to a shift in atmospheric circulation (Lauriol et al., 2002; 2009). The dry climate of the early Holocene is thought to have been due strong anticyclonic activity from the northeast Pacific, resulting in northwestern Canada being dominated by westerly winds, while the warmth is due to increased solar insolation as a result of Milankovitch variations (Ritchie et al., 1983). The cooler and wetter climate of the mid-Holocene is attributed to increased sea-level from the recession of the ice sheets, giving this area a more maritime climate (Burn, 1997).

Table 6 Synthesis of the regional Holocene climatic history reported by various studies. The radiocarbon age limits provide only rough dates for environmental change as these changes were gradual. (modified from Lauriol et al., 2002).

Years BP	Regional Holocene climate history
0-4000	Climate similar to present with some minor fluctuations
4000-8000	Climatic cooling until temperatures reached values close to present.
	Retreat of tree-line and thinning of the thickness of the active layer.
8000-12,000	Summer temperatures were 3-7C higher than present.
	Climate was very dry between 10,000 and 9000 BP.
	Active layer was ~1.5 times thicker than today.
15,000-18,000	Gradual warming.
	Glacial retreat in the Richardson Mountains.

2.6 Permafrost and ground ice conditions

The Richardson Mountains and Peel Plateau region is situated in the continuous permafrost zone (Fig. 2). Permafrost is almost 500 m thick along the Beaufort Sea and decreases southward, measuring 300 m in the Richardson Mountains and 100m near Inuvik (Smith et al. 2010). Permafrost temperature measurements from the nearby Mackenzie Valley region indicate that the mean annual ground temperature varies between –1°C and –5°C (Smith et al., 2010). Since

1945, permafrost temperature measured at the Norman Wells station (discontinuous permafrost zone) showed an increase in MAGT from –8°C to –3°C (Smith et al., 2010). The main periglacial landforms in the study area include patterned ground, solifluction and polygonal peat plateaus (Ecosystem Classification Group, 2010).

According to the circum-Arctic permafrost and ground ice conditions map (Fig. 16 and 17), the relative abundance of ground ice content in the study area is classified as low-to-medium ice content (<20%vol). However, based on measurements from the headwalls of thaw slumps in the Willow River and Stony Creek sub-basins, ground ice content ranges from 50%vol to tabular bodies of massive ground ice (Lacelle et al., 2004; 2010; Malone et al., 2013).

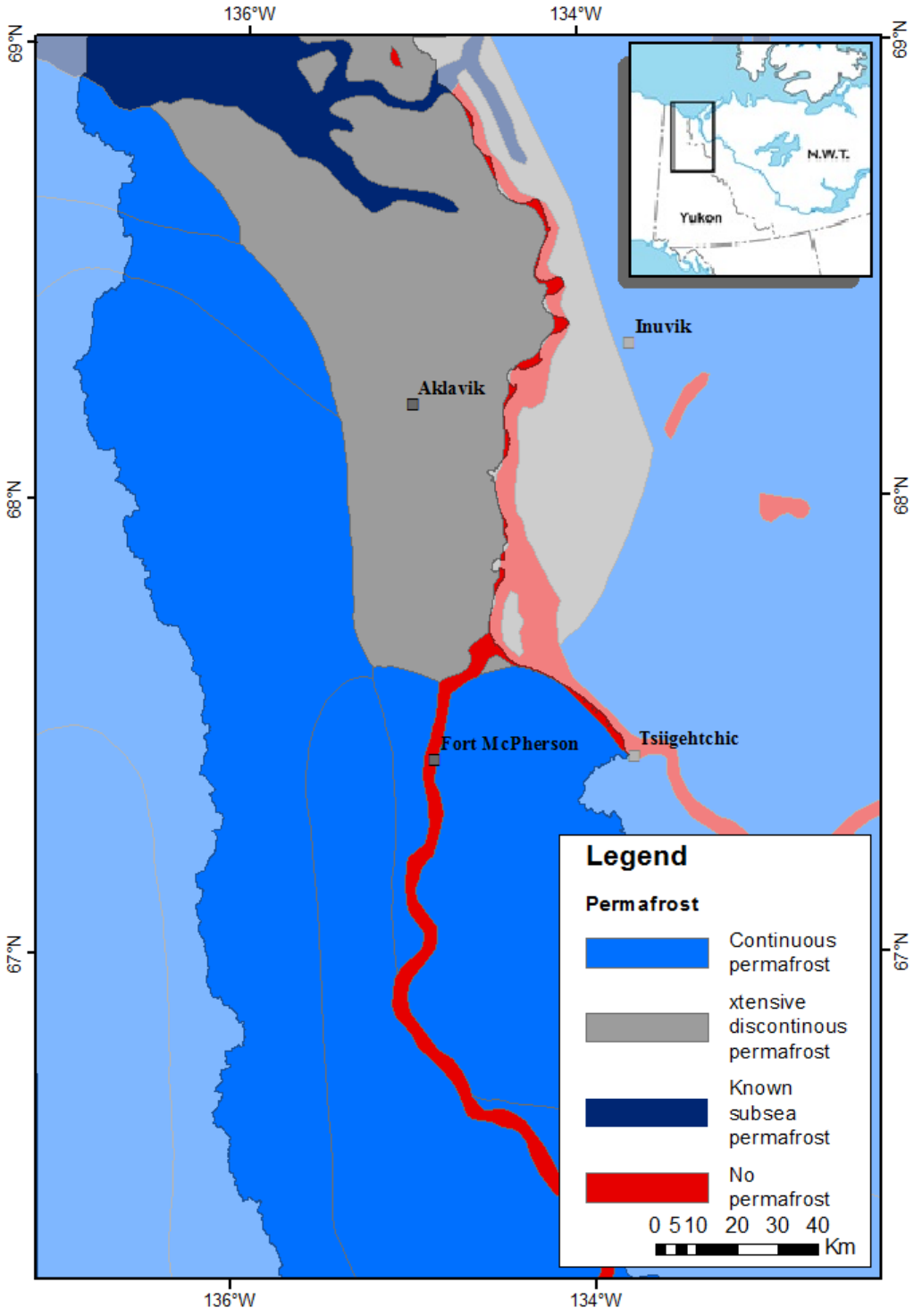

Figure 16. Classification of permafrost conditions in the Richardson Mountains and Peel Plateau, northwestern Canada (from Brown, 1998).

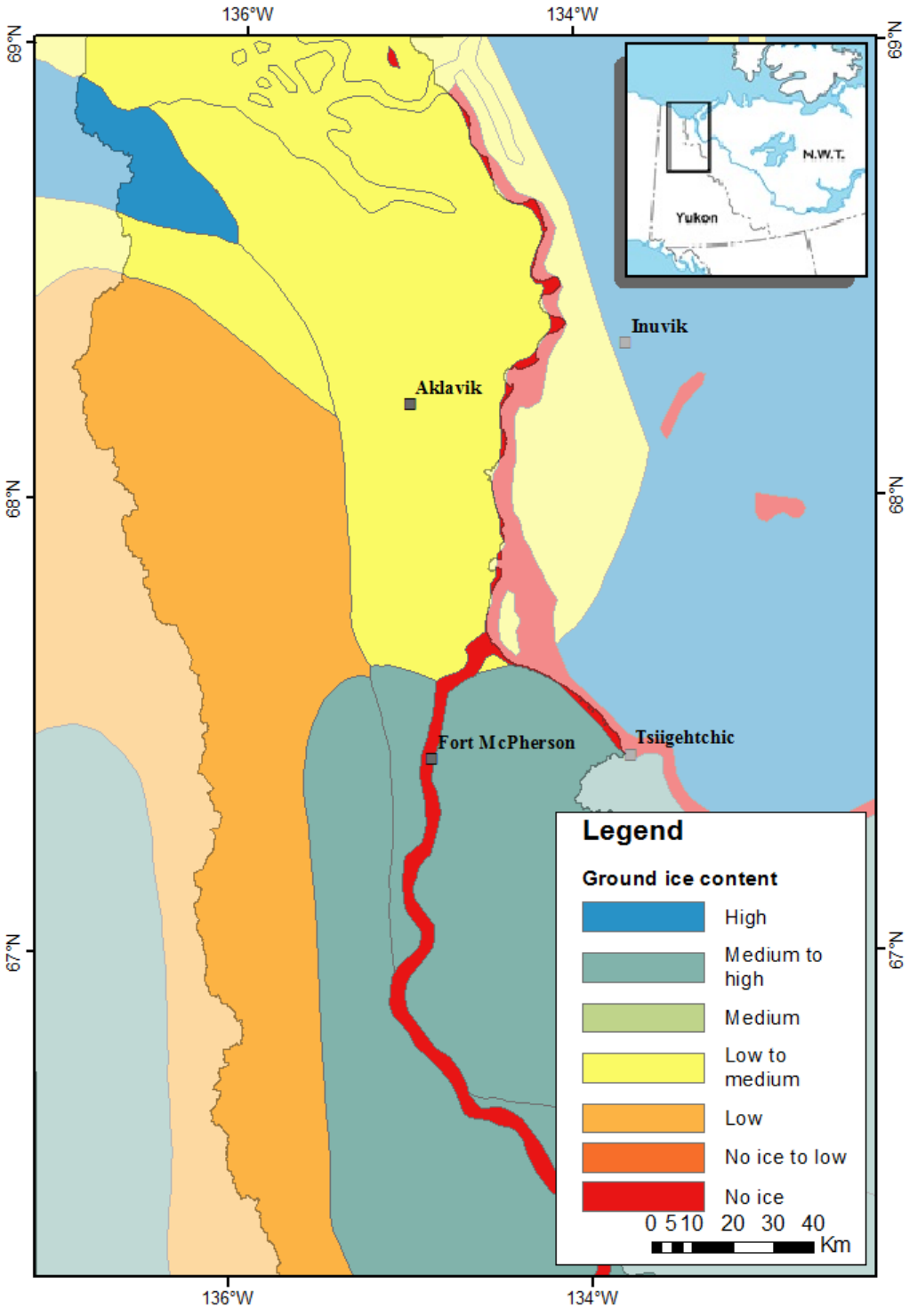

Figure 17. Classification of ground ice conditions in the Richardson Mountains and Peel Plateau region, northwestern Canada (from Brown, 1998).

Chapter 3. Methodologies

The objective of this study is to quantify the effect of thaw slumps on the geochemistry of streams in the Richardson Mountains and Peel Plateau region, northwestern Canada, using various hydrological units as a framework. Below, the methodologies required to achieve this objective are described: 1) a slump database was created in order to assess their distribution within the Richardson Mountains-Peel Plateau region at a variety of scales; 2) a geochemical database of streams was compiled and assessed based on certain standards for quality aquatic ecosystems; 3) the slump and geochemistry databases were analysed together to understand their spatial relationships.

3.1 Hydrography of the Richardson Mountains – Peel Plateau region

Extraction of drainage basin

The hydrological units in the Richardson Mountains and Peel Plateau region were extracted from the Canadian Digital Elevation Data digital elevation model (CDED DEM) through a series of processing steps using ArcHydro tools, an ArcGIS-based suite of tools designed for water resources applications (ESRI, 2012). Using the CDED DEM, the ArcHydro tools generate raster grids of adjusted elevation, flow direction, flow accumulation, stream definition, stream segmentation, sub-basins, watersheds and sub-watersheds delineation, from which the vector representation of the drainage basins and network are obtained. If prior vector data of the drainage network are available, the first step is to recondition the surface of the DEM using the AGREE surface reconditioning system. This algorithm adjusts the surface elevation to be consistent with the vector data by dropping/raising the elevation of the cells within a given buffer distance of the identified streams to ensure drainage continuity in flat areas (Carrière, 2008). This method was improved from previous methods, such as "burning in the streams", that only decreased the elevation of the cell directly identified as a stream. As a result of the buffer distance, the AGREE method allows for discrepancies between the vector data and the exact location of the streams on the DEM. The smooth distance specifies the elevation drop over the specified range of cells within the buffer distance of the stream vector whereas the sharp distance specifies the elevation drop of the cell containing the stream vector. The third step is to compute the flow direction grid using the D8 algorithm. The flow from a particular cell is directed to a single downslope neighbour (one of eight surrounding cells). The flow direction is determined

based on the direction of the largest distance weighted drop, calculated by taking the difference in elevation values and dividing by $\sqrt{2}$ for a diagonal cell and 1 for a non-diagonal cell. As a result, each cell is assigned one of 8 possible flow directions values: East = 1; Southeast = 2; South = 4; Southwest = 8; West = 16; Northwest = 32; North = 64; Northeast = 128.

The fourth step is to compute the flow accumulation grid. Flow accumulation is simply the total number of cells that drain into a given cell, as determined from the flow direction grid. Finally, a threshold value is chosen from the flow accumulation grid such that cells with flow accumulation above the threshold are defined as belonging to a stream. The threshold is thus the minimum flow required to initiate a stream. Once the drainage network is delineated, drainage catchments are identified as the contributing area draining to each stream segment. Whereas the default threshold value is set to 1% of the maximum flow accumulation, a choice of a smaller threshold will result in the production of drainage networks with higher drainage densities and a greater number of catchments. Once the steps were completed, a polygon shapefile was created for 4th to 6th level units. The sub-basins, watersheds and sub-watersheds shapefiles will be used as the reference unit, or platform, on which to portray the distribution of thaw slumps and geochemical composition of streams. Thaw slump density map (number of slumps per sub-drainage area) will be created as well as the average geochemical composition of streams (acquired during field work) within each hydrologic unit. This will allow the evaluation of the spatial dimension of the hydro-geochemical impacts of thaw slumps in the Richardson Mountains.

The physical characteristics of the hydrological units in the Richardson Mountains and Peel Plateau region are described in terms of catchment shape. For the latter, the area (*A*), perimeter (*P*) and length (*L*) of each catchment was determined using basic ArcGIS functionality and then used to compute the circularity and elongation indices:

Circularity:

$$[5] \qquad C = \frac{A}{A_C(P)} = \frac{4\pi A}{P^2}$$

The circularity of a basin is the ratio of the area of the basin slice to the area of a circle of perimeter *P*. Thus, for a circular basin, *C* equals 1.

Elongation:

[6] $$E = \frac{d_C(A)}{L} = \frac{2\sqrt{A}}{L\sqrt{\pi}}$$

The elongation of a basin is the ratio of the diameter of a circle of area *A* to the basin length (the distance from the mouth to the most distant point on the perimeter). Thus for a circular basin, *E* equals 1.

3.2 Distribution of thaw slumps in the Richardson Mountains – Peel Plateau region

There are two main data sources that can be used to identify retrogressive thaw slumps: aerial photographs and satellite imagery. The area covered by the 1954, 1970, 1992 and 2004 sets of aerial photographs within the Richardson Mountains-Peel Plateau region is insufficient to gather data across this region (Fig. 18). For example, the photographs taken in 1954 cover 4990km^2 while the photos acquired in 2004 only cover 343km^2. Though photographs are available for different time periods, their spatial coverage is too small to be used in this study.

The distribution of thaw slumps in the Richardson Mountains and Peel Plateau region was thus mapped using Landsat Thematic Mapper (TM) and Enhanced Thematic Mapper (ETM) images covering the 1985 to 2012 period. The mapping of slump distribution was done by Alex Brooker (2014). Using the Landsat images, the three Tasseled Cap (TC) transformations were calculated (greenness, wetness and brightness) from which a TC linear trend image was created. Integer versions of the TC trend (slope) images were then derived for easier visualization by applying a scaling factor of 1000. The three TC index trends were combined into a single RGB image (i.e. brightness slope=red, greenness slope=green, wetness slope=blue) to generate a color image representing the three-dimensional TC trajectory, the linear trend TC image (Brooker, 2014).

The linear trend TC image can identify the level of activity of a thaw slump (active or stable features) and ground-truthing allowed the interpretation of the color scheme of the linear trend TC image (Fig. 7). Blue colors (representing increasing TC wetness) are associated with the wet and active portion of the slump floor and debris flow and red colors (representing increasing TC brightness) are associated with dry and un-vegetated surfaces of the debris flow. The teal and yellow colors (representing increasing TC greenness) correspond to portion of the slump floor that is stable and undergoing regrowth by colonizing vegetation.

Using the linear trend TC image, the distribution of active and stable thaw slumps in the Richardson Mountains – Peel Plateau region was mapped by Lacelle et al. (in review). The identification of thaw slumps is limited to the pixel resolution of the Landsat images (30m), as such features less than 2x2 pixels are likely not identified (<0.36ha). The distribution of slumps identified using this method was then analysed within hydrological framework, and broken down using a variety of parameters (number of slumps, density, total surface area and average surface area) at the three studied hydrological scales.

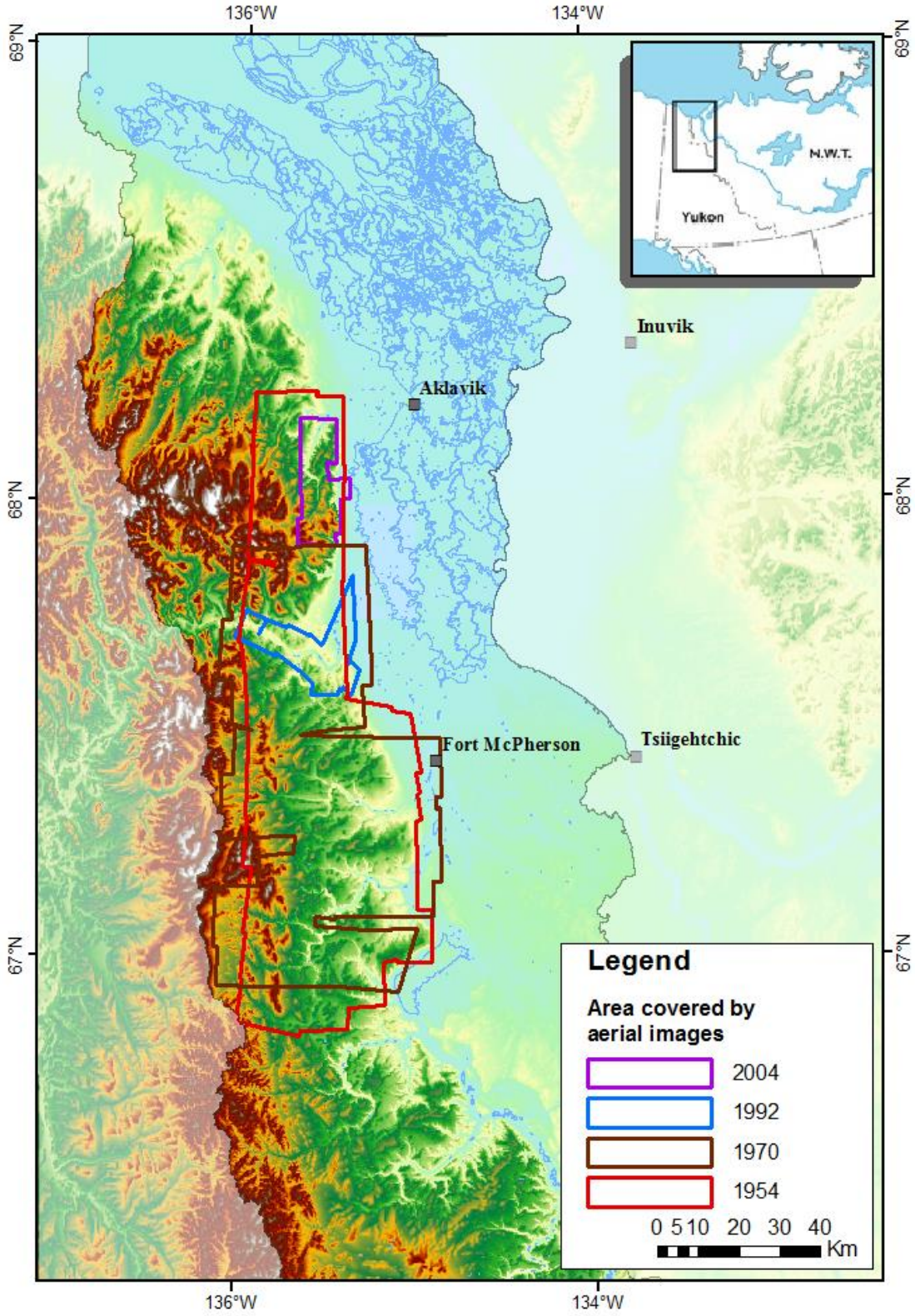

Figure 18. Area covered by aerial images by year the photographs were taken, in the Richardson Mountain-Peel Plateau region, Canada.

3.3 Geochemical composition of streams in the Richardson Mountains – Peel Plateau region

The regional geochemistry of streams in the Richardson Mountains – Peel Plateau is derived from two existing databases. In areas for which little to no information exists, field sampling of streams was performed in summer 2013 to complete the existing databases. The existing stream geochemistry databases were obtained from Geological Survey of Canada Open File 4670 (Day et al., 2005) as well as a database collected in 2011 and 2012 by Malone (2013) (Fig. 19). Day et al. (2005) conducted a geochemical survey of streams in the Richardson Mountains in the early 2000s for mineral exploration purposes. The area in which streams were sampled ranged from the latitude of Aklavik to that of Fort McPherson. The water samples were analyzed for conductivity, major ions and trace metals (Ca^{2+}, Mg^{2+}, Na^{+}, K^{+}, Fe_{tot}, Al_{tot}, As_{tot}, S, Zn^{2+}, SO_4^{2-}, NO_3^{-} and Cl^{-}). In 2011 and 2012, Malone (2013) sampled streams in the Stony Creek sub-basin and analyzed their conductivity and determined the concentration of major ions. Malone's study (2013) was done to investigate the effect of retrogressive thaw slumps along two streams (Poor Man's Creek and the lower reach of Stony Creek).

During fieldwork performed in August 2013, water samples from streams in the Rat River, Stony Creek, Vittrekwa River and Trail River sub-basins were collected using helicopter support. Sample sites were chosen to add to the existing databases in order to expand the geographical area covered. For this reason many of sites are of a significant distance from one another (>500m). Therefore it is difficult to compare nearby values between datasets to assess data consistency and quality. In total, 37 stream locations were sampled. At each sampling site, pH (0.2 unit accuracy) and conductivity (0.1 µS/cm accuracy) was measured *in situ* using a YSI Professional Plus handheld meter. Water samples were collected in 30ml pre-rinsed amber polyethylene bottles after rinsing with the local water. Samples were filtered in the field when possible through 0.45µm pore diameter filters. Otherwise, the samples were filtered in the evening back at camp.

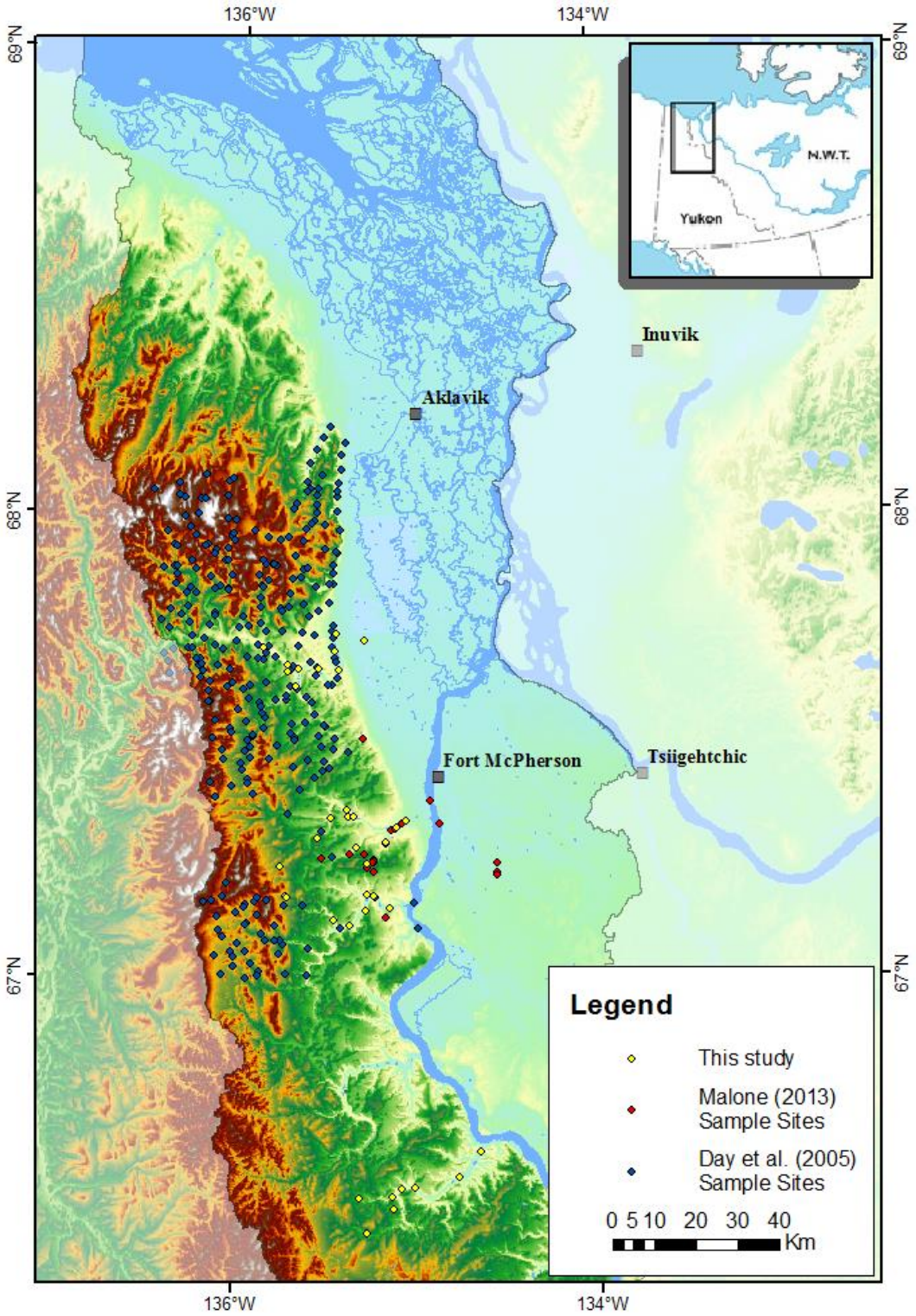

Figure 19. Sites of samples taken in the Richardson Mountains and Peel Plateau region, northwestern Canada (Malone, 2013 and Day et al. 2005).

3.4 Geochemical analysis

The stream water samples collected in August 2013 were analysed for major ions that have been described as the dominant ions in the region. Cation (Ca^{2+}, Mg^{2+}, Na^{+}, K^{+}, Fe_{tot}, Al_{tot}, As_{tot}, S, Zn^{2+}) concentrations were determined by first adding 100µl of acid (HNO_3) to 10ml of each sample. The acidified samples were then analysed using a Vista-Pro simultaneous charge coupled device (CCD) detector Inductively Coupled Plasma Optical Emission Spectrometer (ICP-OES) at the University of Ottawa's Geochemistry Laboratory in the Department of Earth Sciences. Anion (SO_4^{2-}, NO_3^{-} and Cl^{-}) concentrations were determined by first diluting the samples in distilled water using an auto-diluter. To 1ml of sample water was added 10ml of distilled water.

All data identified as being below detection thresholds were removed from the dataset. In the Day et al. (2005) data these were expressed with negative signs (-). The samples analyzed in this study (summer 2013) with values below detection thresholds were identified by the laboratory technicians, and removed from analysis. For consistency purposes, all geochemical data was initially displayed in ppm (parts per million). Some of the Day et al. (2005) data were published expressed in ppb (parts per billion) due to the lower concentrations of certain ions (i.e Al, As, NO_3, SO_4 and Zn). The ppb values were converted to ppm (ppb/1000=ppm). Once this was done, all usable ppm values (i.e those above minimal detection limit) were also expressed in milliequivalents per litre of sample (mEq/L; see equations 7 and 8). Molar ratios and other small calculations were then performed and added as fields in the dataset, such SO_4/Cl, Na/Cl and Ca+Mg.

[7] $\frac{mmoles}{L} = \frac{ppm}{gfw}$,where gfw = gram formula weight

[8] $\frac{mEq}{L} = \frac{ppm}{gfw} \times valence\ (z)$

3.5 Geospatial and statistical analyses

The geochemical data used in this study is derived from 417 single stream sampling point (Fig. 19). Not all sample points had measurable values of each parameter (i.e. due to values lower than measuring threshold). In order to create a more visual representation of the geochemical characteristics within hydrological units, joins were created between point data

(hydro-geochemistry and slumps) and polygons (sub-basins, watersheds and sub-watersheds) shapefiles (Fig. 20). This creates a new polygon shapefile where descriptive statistics of specific geochemical properties are displayed within the 4th to 6th level units. This process was also done with the distribution of thaw slump point shapefile.

To be able to compare geochemical characteristics of hydrological units with slump properties (density, number, average size, etc.), both new shapefiles were joined together. This creates a new layer where each record (each individual 4th, 5th and 6th level polygon) has the geochemical information of sites within its limits and has information on slumps found within its limits.

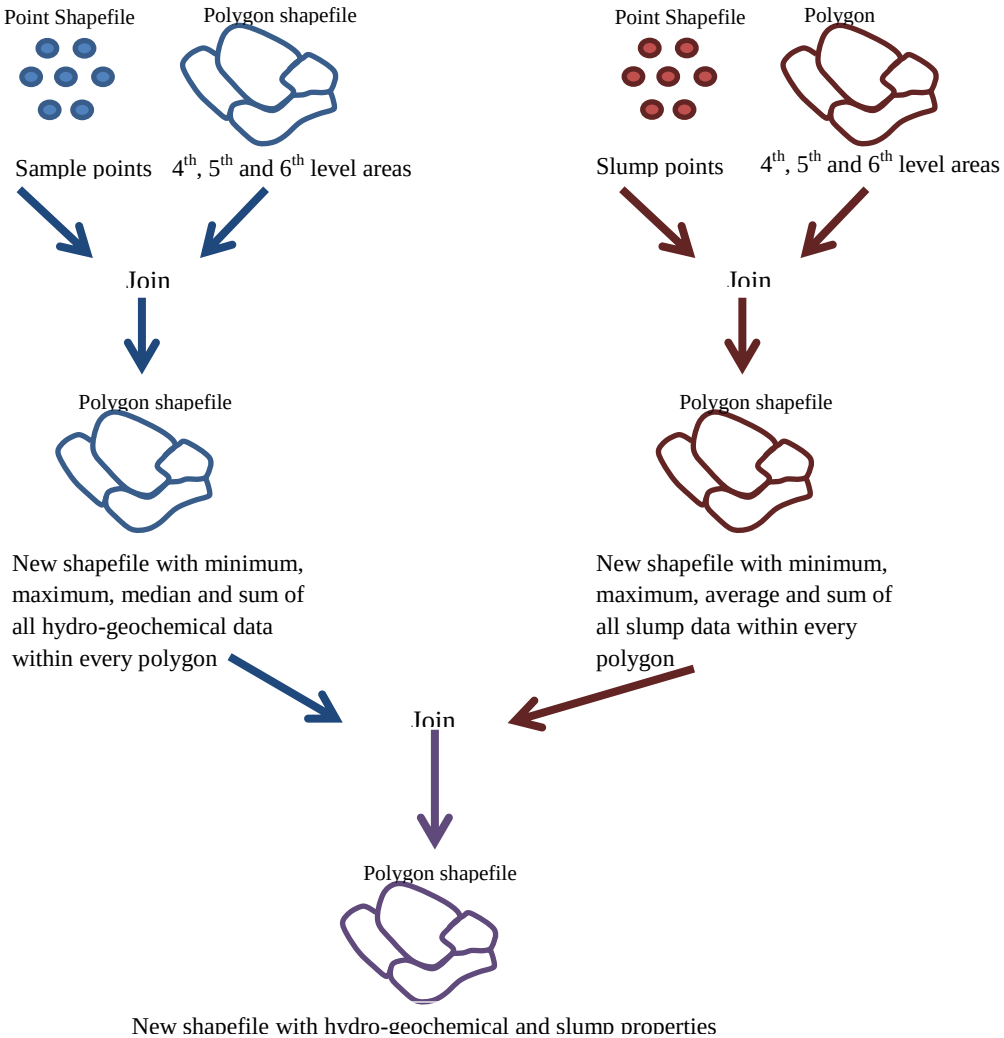

Figure 20 Process to create shapefiles combining watershed, hydro-geochemical and slump information for analysis in ArcGIS.

The analysis of results was done in three steps. First, the distribution of slumps at the 4th, 5th, and 6th level hydrologic units was accomplished by looking at factors such as number of slump per unit, slump density, total surface area of slumps and average surface area of slumps. Second, the same was done for the geochemical composition of streams. Lastly, the relationship between the two (slump distribution and hydro-geochemistry) was assessed with a correlation analysis.

The CCME standards were used to appropriately display the average value for each parameter in each hydrologic unit (usually in relation to short and long term maximums). Where no previously established standards existed (i.e. density of slumps), classes were built using the spread of variables (maximum value-minimum value) and using Sturges table to determine an approximate number of classes (Simard, 2008).

3.6 Potential environmental impacts

Slumping activity could have an impact on the water quality of drinking water for the communities within the Richardson Mountains-Peel Plateau region. Stream water in the Willow and Rat river sub-basins, part of the larger Lower Peel basin, is being used as drinking water source in communities such as Aklavik (Fig. 21). As such, the potential impact of thaw slumps on water quality in these sub-basins will be closely explored. Change in water quality could lead to modifying steps needed to dispatch drinking water to local communities.

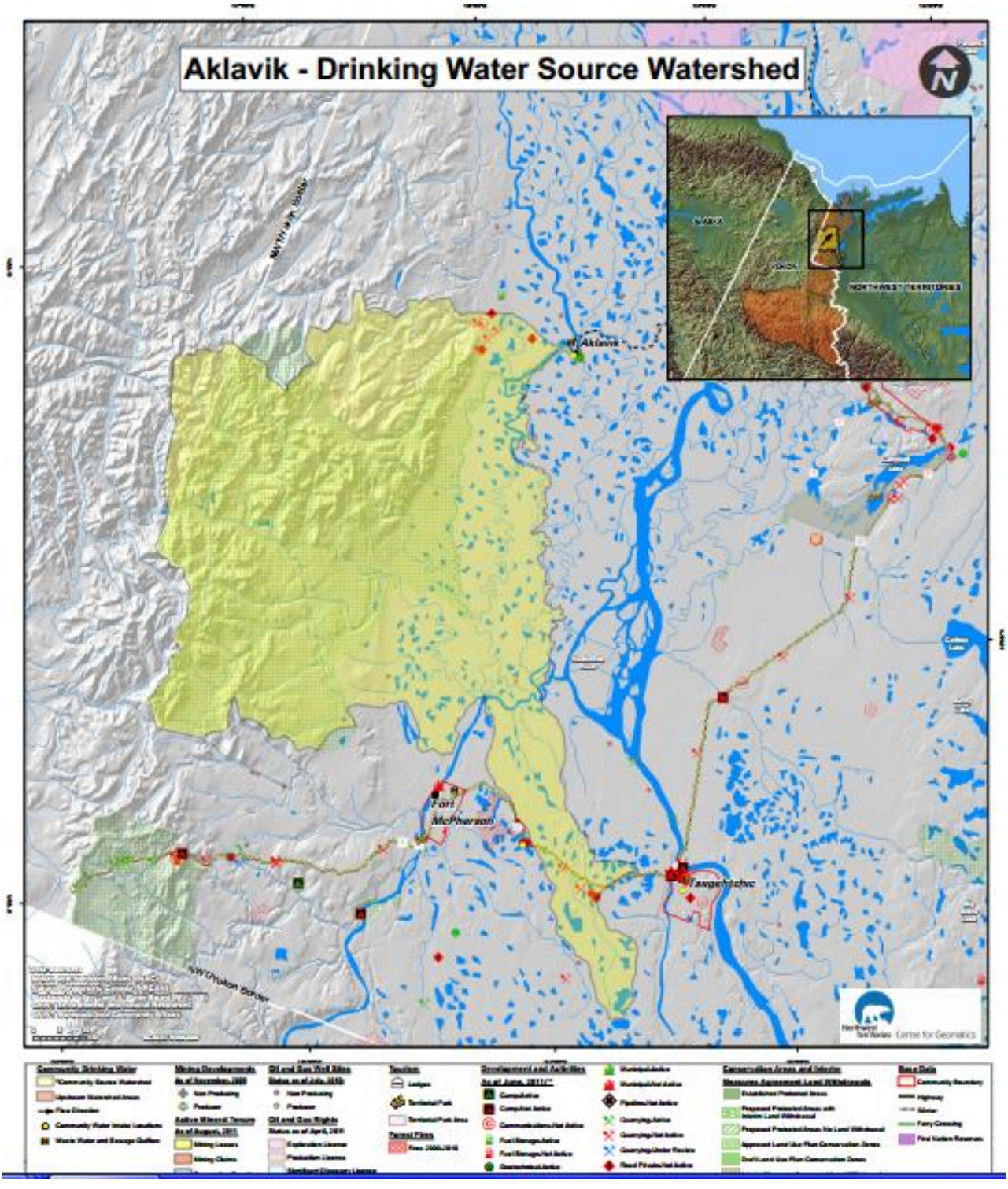

Figure 21 Area used as a source for drinking water in Aklavik (portions of the Willow and Rat river sub-basins, within the Lower-Peel basin) (NWT Centre for Geomatics, GNWT, 2011)

Chapter 4 - Results

4.1 Hydrography of the Richardson Mountains – Peel Plateau, NWT

The eastern slopes of the Richardson Mountains and the Peel Plateau are occupied by the Lower Peel River basin, which covers a surface area of 31,678 km^2. The main rivers in this basin are the Big Fish River, Willow River and Rat River, Stony Creek, Vittrekwa Creek, Road River, Trail River and Caribou River (Fig. 10). With a surface area of 2935.5 km^2, the Big Fish River sub-basin is the largest one in the study area, while the Willow River sub-basin is the smallest named one (808.7km^2). In order to display the spatial dimension of the hydrological impacts of thaw slumps in the environment, 5th and 6th level watershed and sub-watershed were created with the ArcHydro tool in ArcGIS for each of the 8 sub-basins in the study area (Fig. 22). In the study area, 50 5^{th} level watersheds units are identified and have an average surface area of 313.4km^2. A total of 177 6^{th} level sub-watersheds are counted in the area, and they have an average surface area of 86.5km^2. The largest one spans 489.0km^2 in the Big Fish sub-basin. Table 7 presents the physical characteristics of each sub-basins. Based on these results there is little congruence between the elongation and the circularity values. The elongation values are all relatively high (>0.6) indicating that the sub-basins are mostly circular. However, the circularity values are less than 0.5, suggesting that the sub-basins are more elongated in nature.

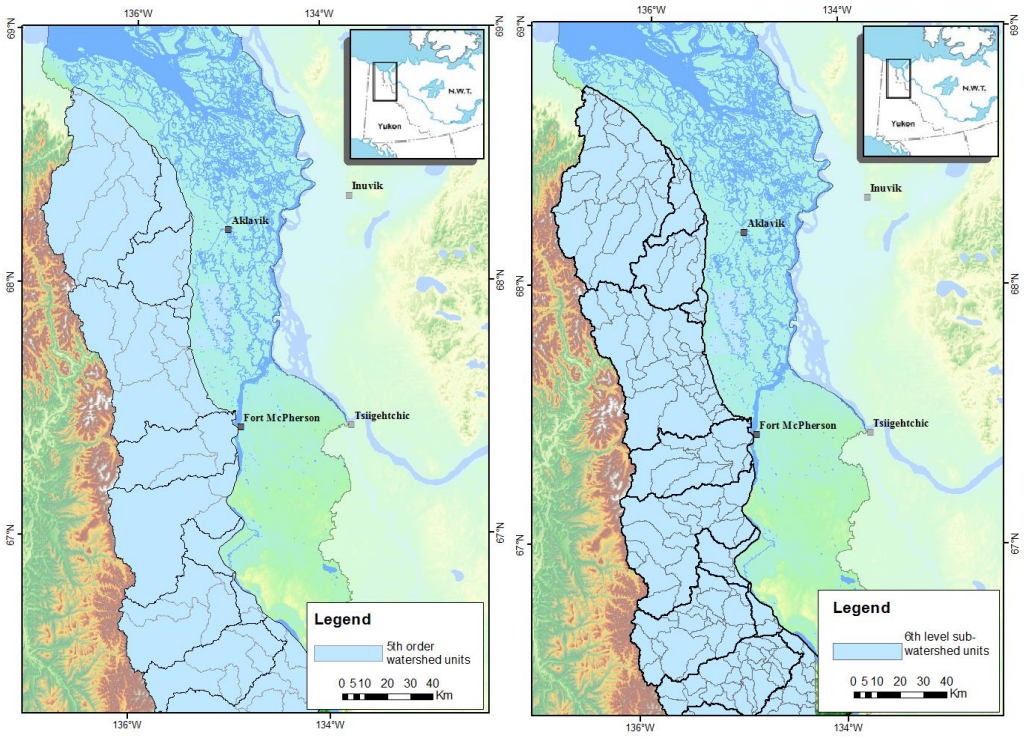

Figure 22. (Left) 5th level watershed ArcHydro delineations with 4th lever sub-basin delineations in thicker lines, in the Richardson Mountains-Peel Plateau region.; Right) 6th level sub-watershed ArcHydro delineations with 4th level sub-basin delineations in thicker lines, in the Richardson Mountains-Peel Plateau region.

Table 7 Physical characteristics of 4th level sub-basins.

Name	Surface area (km2)	Longest stream (km)	Elongation	Circularity
Big Fish	2935.5	92	0.68	0.44
Unnamed #1	404.8	37	0.62	0.26
Willow River	808.7	52	0.71	0.43
Unnamed #2	99.4	7.1	0.71	0.45
Rat River	2692.9	90	0.85	0.37
Stony Creek	1224.5	57	0.77	0.37
Vittrekwa	1979.1	95	0.79	0.30
Unnamed #3	341.8	15	0.65	0.26
Unnamed #4	155.2	8.5	0.62	0.38
Road River	1545.5	90	0.87	0.37
Trail River	1281.3	76	0.68	0.31
Caribou River	2227.7	100	0.69	0.27
Average	1308.1	60	0.72	0.35

4.2 Distribution of thaw slumps in the Richardson Mountains – Peel Plateau, NWT

In the Richardson Mountains and Peel Plateau region, 212 slumps were identified, of which 189 were classified as active (Fig. 24; Lacelle et al., in review). The surface area of the slumps ranges from 0.4ha (the minimum size identifiable with Landsat satellite imagery) to 52ha (with an average of 5ha) (Fig.23 and 24). The surface area of thaw slumps that fall outside the normal distribution curve are here classified as mega-slumps (>25ha). Out of the 212 slumps identified, 7 mega-slumps are distributed in the Stony Creek (2), Vittrekwa Creek (2), Trail (2) and Caribou (1) sub-basins. The mega-slumps are all active and the sum of their surface area accounts for 22% of the surface area of all other mapped active slumps.

Willow River, Stony Creek and Vittrekwa River sub-basins contain the highest number and density of slumps (Fig. 25). Together, these three sub-basins account for nearly 60% of all slumps in the study area. The number of thaw slumps is generally higher in the northern sub-basins, with the Willow River sub-basin contains the highest number and density of slumps. However, the thaw slumps in the Richardson Mountains (Big Fish and Willow rivers sub-basins, further north) are generally much smaller in surface area (<15ha) than those on the Peel Plateau) (Fig. 26). The largest slumps (>20ha) are found within the Stony Creek, Vittrekwa Creek, Trail River and Road River sub-basins. With these trends, the Willow River, Stony Creek, Vittrekwa Creek and Trail River sub-basins are most impacted by thaw slumps, all containing cumulative slump surface area > 200ha (Fig. 26).

At the scale of the entire study area, it seems that latitude plays of a role when it comes to slump size and their distribution (Fig. 24-27). Latitude has somewhat of an impact on the number of slumps within a single sub-basin. As seen in the top left of figure 27, there are fewer slumps in the southern sub-basins (i.e Caribou and Road Rivers), whereas there are generally more slumps in the northern sub-basins (i.e Willow), with the exception of the Big Fish sub-basin. The density of slumps follows this trend as well, with the sub-basins with higher densities generally found further north, and the sub-basins with lower densities found further south (Fig. 27, top right). There is a negative correlation between average slump surface area and latitude. The sub-basins with higher average slump surface area are found further south (i.e. Caribou and Trail) while the sub-basins with smaller average slump sizes are found further north (Willow and Big Fish) (Fig.27, bottom left). This indicated that the larger slumps are found further south and

smaller slumps are generally found further north. Finally, there seems to be no identifiable trends between total slump surface area of slumps in sub-basins and latitude.

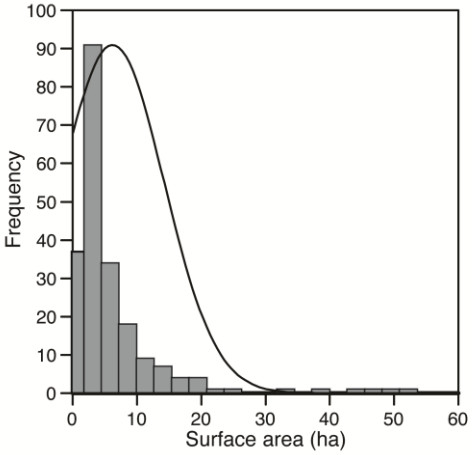

Figure 23 Frequency distribution of all identified thaw slumps, by size.

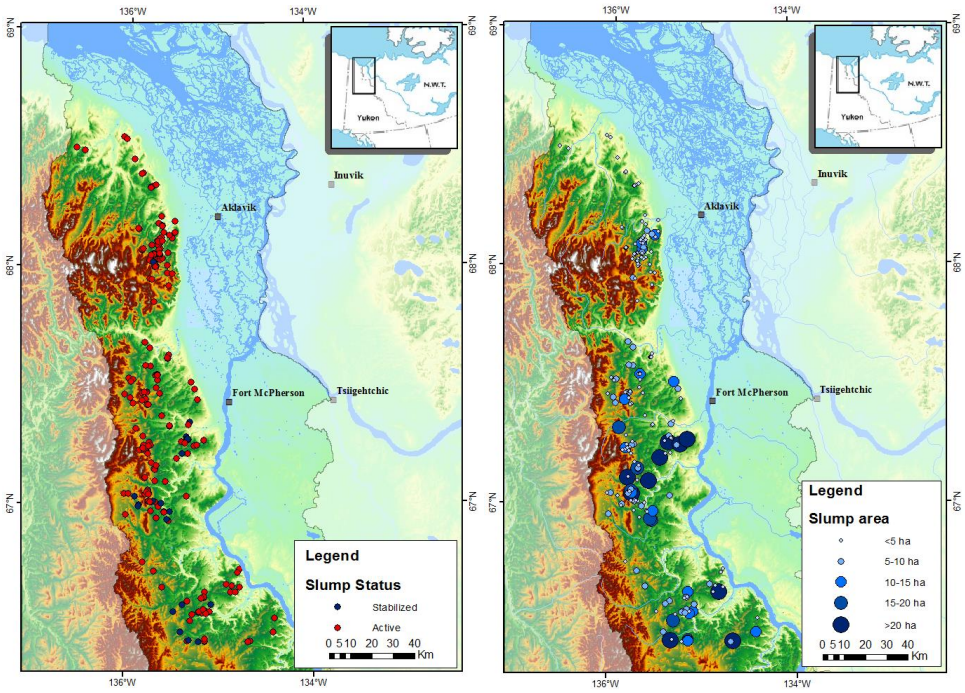

Figure 24 Left) Distribution of all identified slumps within the study area, classified as active or stabilized at time of identification, in the Richardson Mountains-Peel Plateau region (data source Brooker, 2014). Right) Distribution of all identified active thaw slumps within the study area, classified by surface area (ha), in the Richardson Mountains-Peel Plateau region (data source from Brooker, 2014).

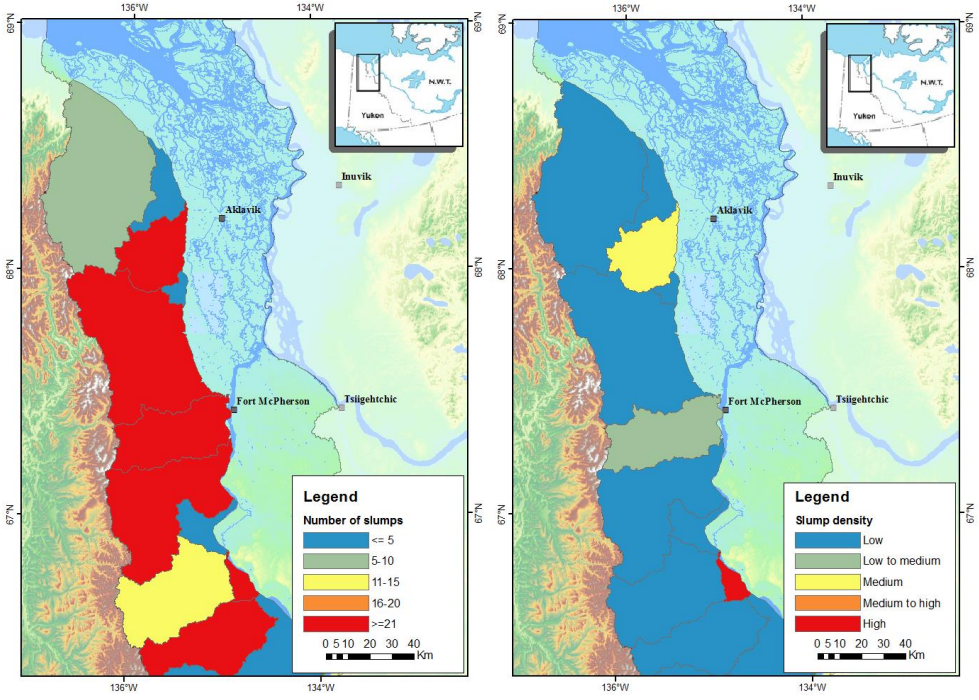

Figure 25. Left) Number of slumps in each 4th level sub-basin in the Richardson Mountains-Peel Plateau region, Right) Density of slumps in each 4th level sub-basin in the Richardson Mountains-Peel Plateau region: Low density:< 30 slumps/1000 km2, Low to medium density: 30-58 slumps/1000 km2, Medium density: 59-88 slumps/1000 km2, Medium to high density: 89-117 slumps/1000 km2, High density: 118-148 slumps/1000 km2.

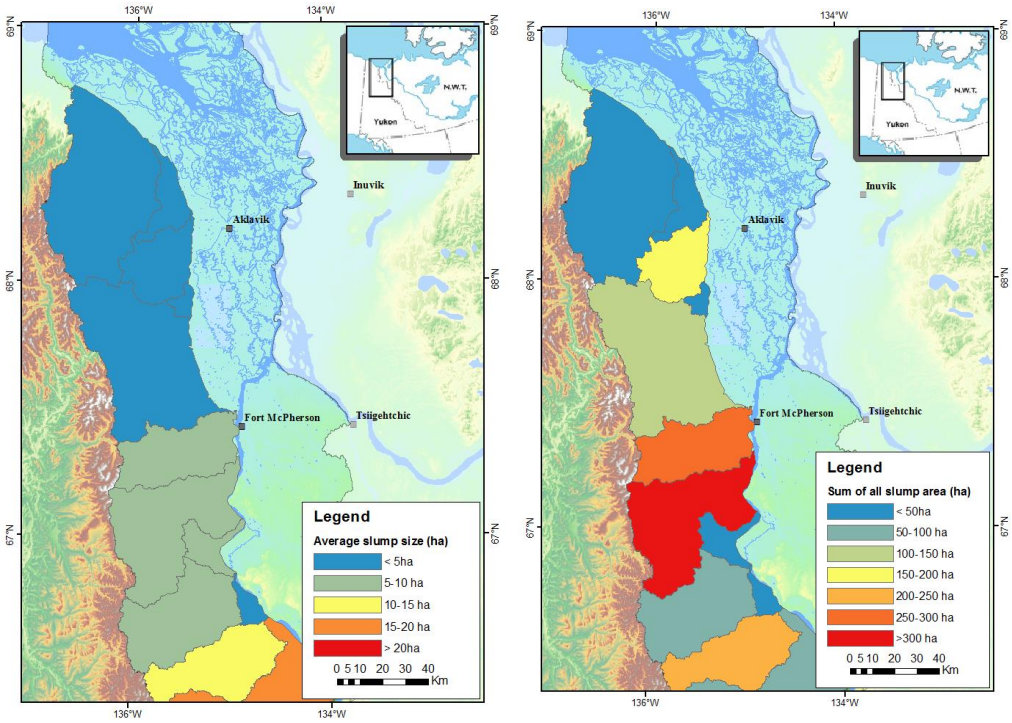

Figure 26. Left) Average slumps size in each 4th level sub-basin in the Richardson Mountains-Peel Plateau region, Right) Total area covered by slumps in each 4th level sub-basin in the Richardson Mountains-Peel Plateau region.

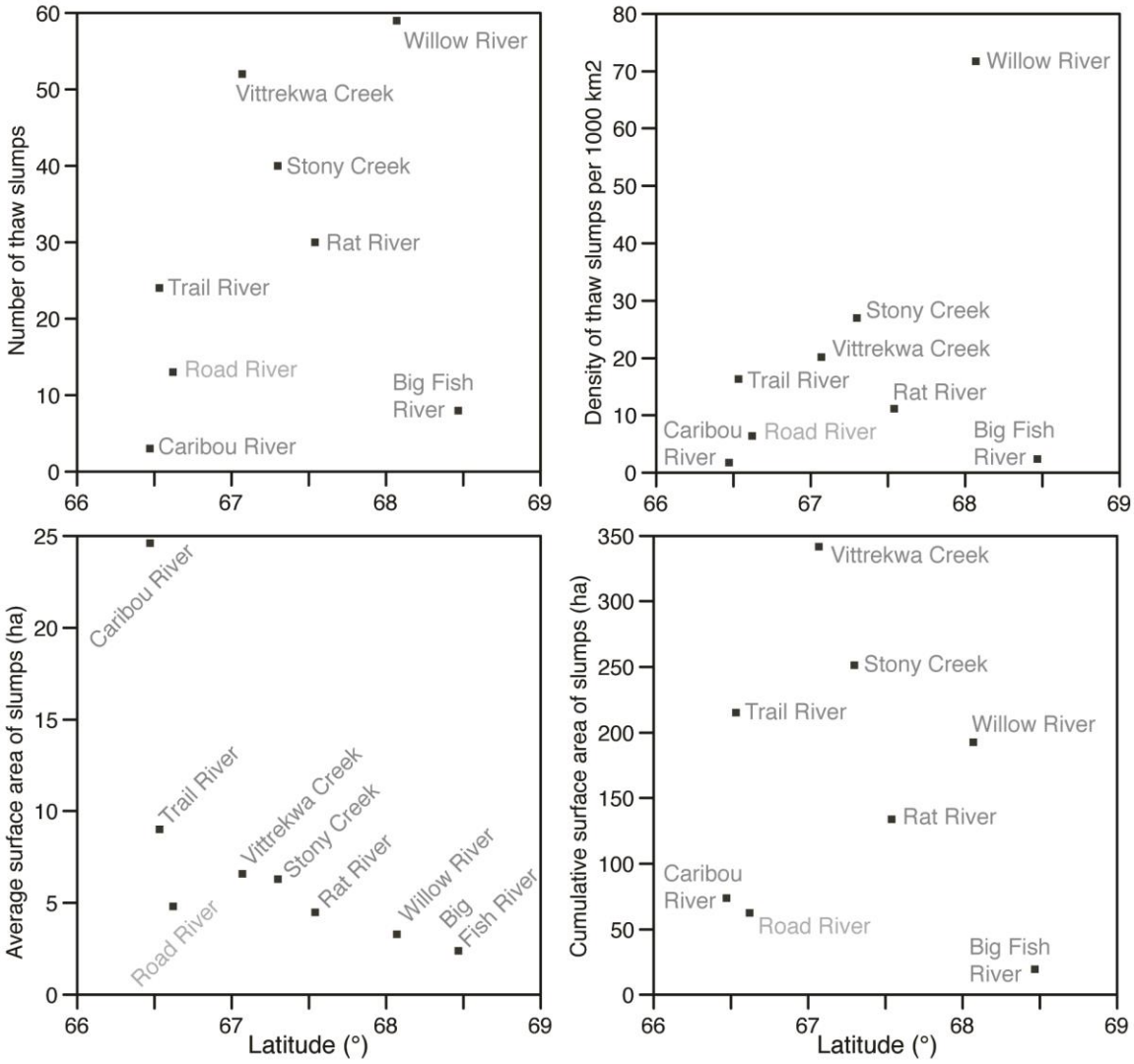

Figure 27 Top left: Number of slumps per 4th level sub-basin by latitude; Top right: Density of thaw slumps (number of slumps per 1000km^2) per 4th level sub-basin, by latitude; Bottom left: Average surface area of individual slumps (ha) per 4th level sub-basin, by latitude; Bottom right: Cumulative surface area of slumps (ha) per 4th level sub-basin, by latitude, all in the Richardson Mountains-Peel Plateau region.

4.2.1 Distribution of thaw slumps in the 5th level watershed units

Based on figure 28, 26 of 50 watershed units (52%) are occupied by thaw slumps. Of these, 17 (34%) have 5 or fewer slumps, one has between 6 and 10 slumps, two contain between 11 and 15 slumps, and four have over 20 slumps (21, 21, 48 and 50 slumps each respectively) (Fig. 28 and 30). These four watersheds containing the highest number of slumps are found within the Vittrekwa, Stony Creek, Willow and Rat rivers sub-basins and host 74% of all active slumps. The average slump density is 9.37 slumps per 1000km^2. The units with the highest densities are found within the Willow, Stony Creek and Rat river sub-basins (Fig. 28 and 30).

At the watershed scale, the average total slump surface area per unit is 26.3ha, with a maximum of 341.9ha (Fig. 29). The watersheds with the highest total slump areas are found in the Willow, Stony and Vittrekwa sub-basins. The mean average slump area is 3.53ha. The units with the highest average slump area are found in the Caribou, Trail and Stony sub-basins (Fig. 29).

Figure 30 show the number of slumps and surface area of slumps plotted against the latitude of the watersheds. Though there are no trends relating to the frequency of slumps with latitude, it is possible to discern trends relating to slump size. As Figure 30 shows, the watersheds in the more southern latitudes have considerably higher average slump surface areas. The watersheds above 68°N all have average slump areas below 5ha. This once again indicated that the larger slumps are found further south in the Lower Peel basin.

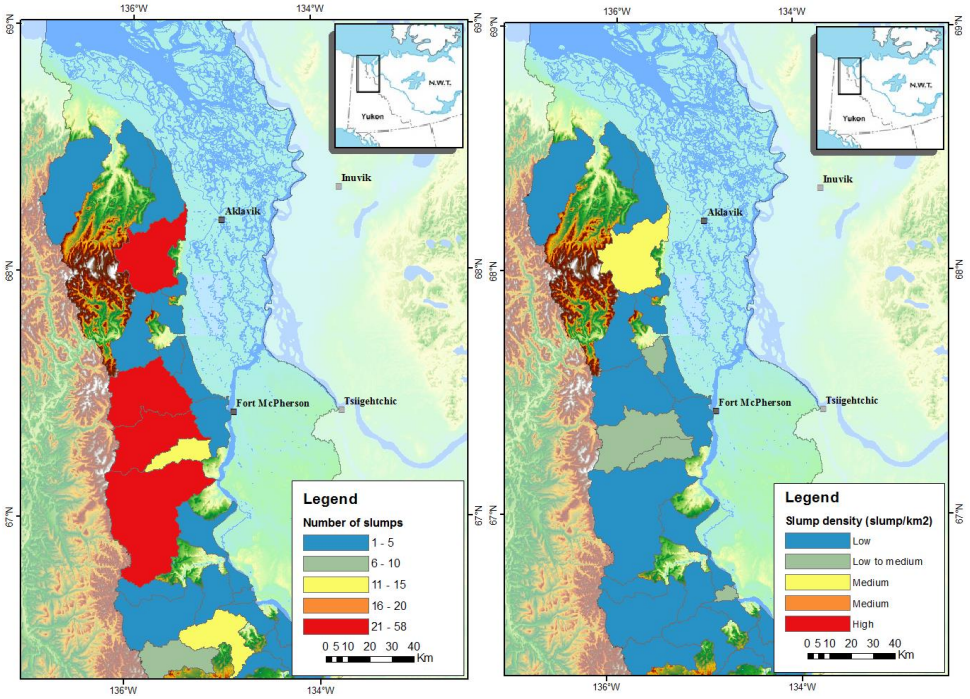

Figure 28. Left) Number of slumps in each 5th level watershed unit, in the Richardson Mountains-Peel Plateau region.; Right) Density of slumps in each 5th level watershed unit in the Richardson Mountains-Peel Plateau region: Low density:< 30 slumps/1000 km2; Low to medium density: 30-58 slumps/1000 km2; Medium density: 59-88 slumps/1000 km2; Medium to high density: 89-117 slumps/1000 km2; High density: 118-148 slumps/1000 km2.

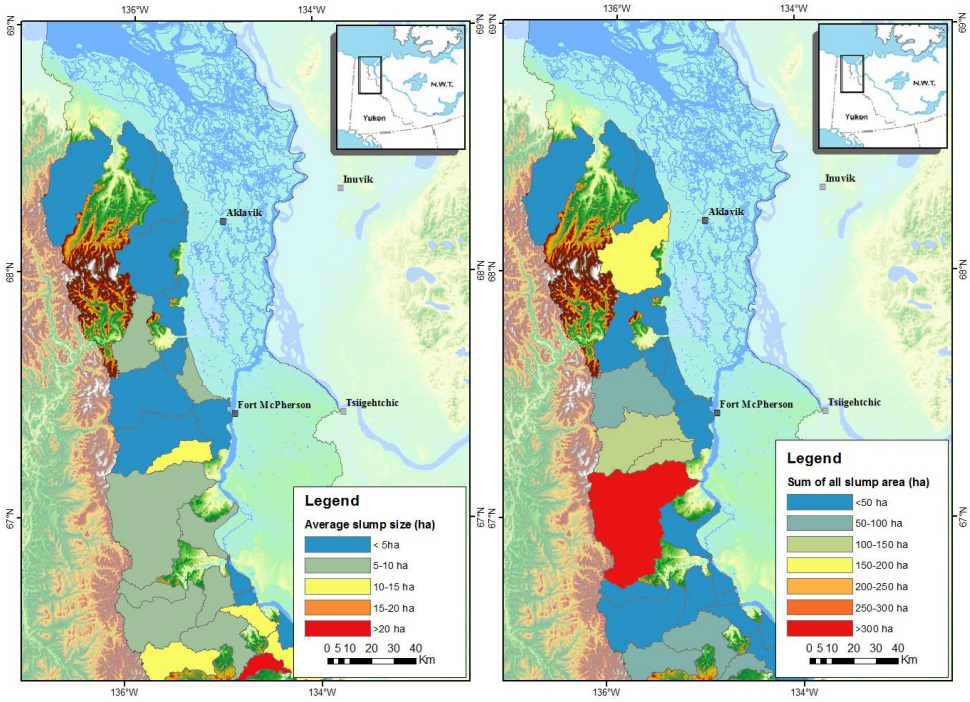

Figure 29 Left) Average slump size in each 5th order watershed in the Richardson Mountains-Peel Plateau region, Right) Total surface area covered by slumps (ha) in each 5th level watershed units, in the Richardson Mountains-Peel Plateau region.

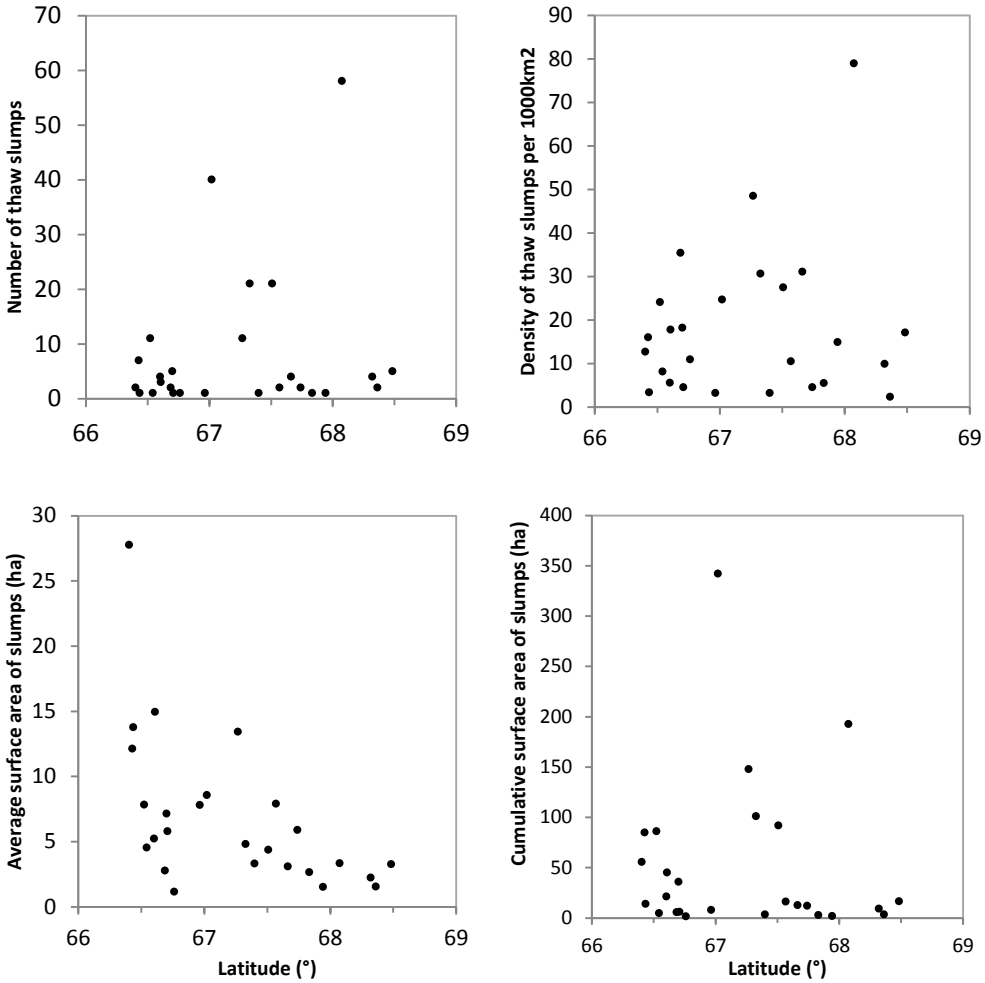

Figure 30. Top left: Number of slumps in each 5th level watershed, by latitude; Top right: Density of thaw slumps (number of slumps per 1000km^2) per 5th level watershed, by latitude; Bottom left: Average surface area of individual slumps (ha) per 5th level watershed, by latitude; Bottom right: Cumulative surface area of slumps (ha) per 5th order watershed, by latitude, all in the Richardson Mountains-Peel Plateau region.

4.2.2 Distribution of thaw slumps in the 6th level sub-watershed units

As seen in figure 31, 54 of the 180 sub-watershed units (30%) are occupied by thaw slumps. Of these, 44 units (24.4%) have 5 of fewer slumps, 7 (3.9%) have 6-10 slumps, 2 (1.1%) contain 11-15 slumps, and one (0.6%) has more than 25 slumps. The two units with more than 10 slumps (13 and 14 respectively) are found in the Stony Creek and Rat river sub-basins, whereas the sub-watershed that contains the highest number of slumps is found in the Willow sub-basin. Together, they contain almost half of all slumps.

At the sub-watershed scale, the average slump density is 11.45 slumps per 1000km^2. The sub-watersheds with the highest slump density (>100 slumps by 1000km^2) are found in the Caribou, Rat, Willow and Trail sub-basins (Fig. 31). The average total slump area per sub-watershed unit is 7.43ha, with a maximum of 165.4ha. The two sub-watersheds with total slump areas over 100ha are situated in the Vittrekwa and Willow sub-basins, which is consistent with the observations at other scales (Fig. 32). The average slump surface area is 2.16ha. Four sub-watershed units, found within the Stony, Vittrekwa, Trail and Caribou sub-basins, have average surface areas of over 20ha (Fig. 32). Figure 33 plots these parameters against latitude. This, once again supports the observations at smaller hydrological scales that the more southern portions of the study area are home to the larger slumps. The sub-watersheds with higher slump numbers seem to be found in the centre of the study area, between the 67th and 68th degrees. The average slump size trend observed at other hydrological scales is also observable here. The sub-watershed units with higher average slump surface areas are found further south, indicating that larger slumps develop in the southern portion of the Lower Peel River basin.

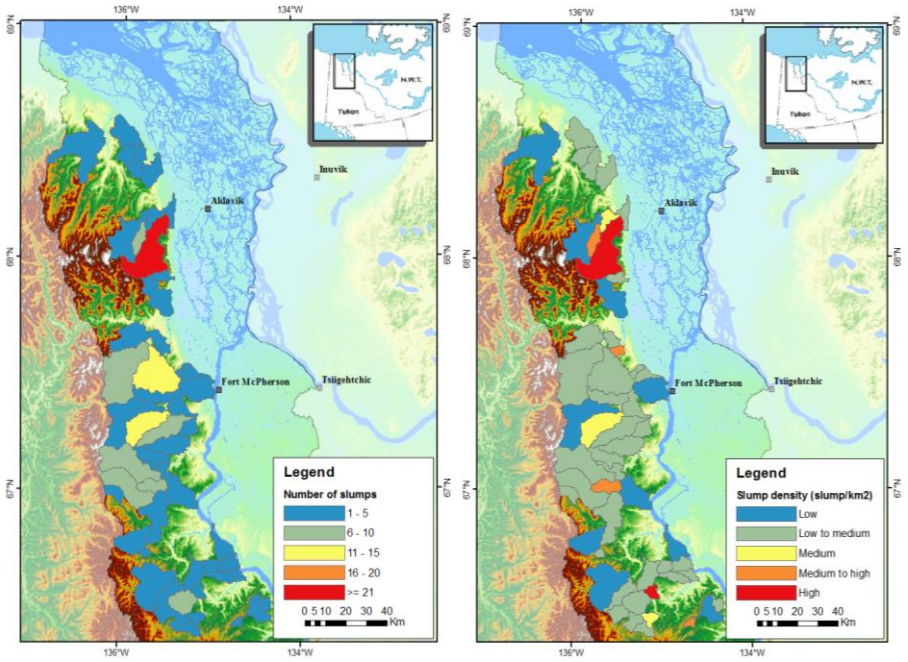

Figure 31. Left) Number of slumps in each 6th level sub-watershed unit, in the Richardson Mountains-Peel Plateau region. Right) Density of slumps in each 6th level unit, in the Richardson Mountains-Peel Plateau region: Low density:< 30 slumps/1000 km2; Low to medium density 30-58 slumps/1000 km2; Medium density59-88 slumps/1000 km2; Medium to high density: 89-117slumps/1000 km2; High density: 118-148 slumps/1000 km2.

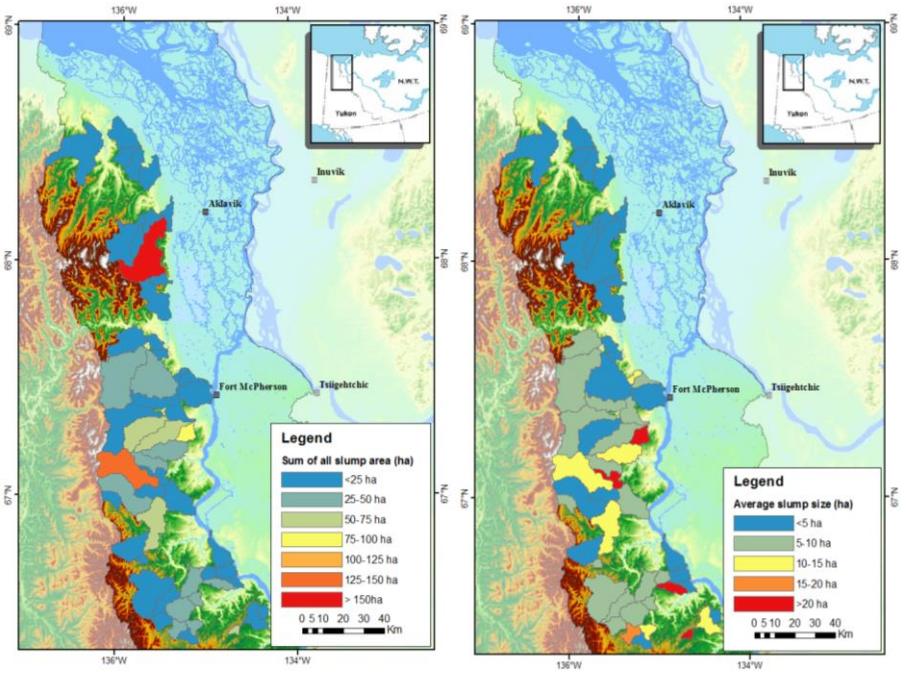

Figure 32 Left) Average slump size in each 6th order sub-watersheds in the Richardson Mountains-Peel Plateau region, Right) Total surface area covered by slumps (ha) in each 6th level sub- watershed units, in the Richardson Mountains-Peel Plateau region.

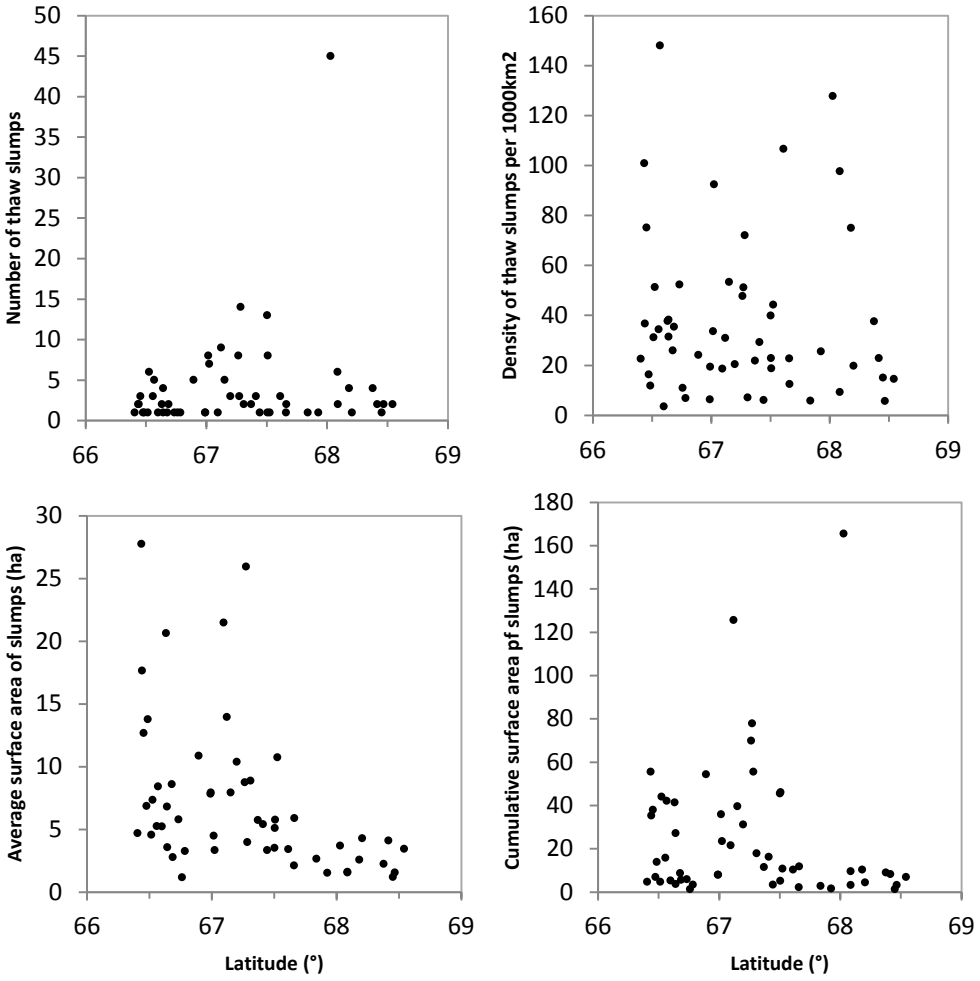

Figure 33. Top left: Number of slumps in each 6th level sub-watershed, by latitude; Top right: Density of thaw slumps (number of slumps per 1000km^2) in each 6th level sub-watershed, by latitude; Bottom left: Average surface area of individual slumps (ha) in each 6th level sub-watershed, by latitude; Bottom right: Cumulative surface area of slumps (ha) in each 6th level sub-watershed by latitude.

4.3 Geochemical composition of streams in the Richardson Mountains – Peel Plateau, NWT

The distribution of values of conductivity, pH, and concentration of major and trace ions (SO_4, Cl, Na, Ca, Mg, Fe and Zn) are shown in figure 34. The distribution of these data is not normal. For this reason, the analysis of the geochemical composition of streams is done using median values for each unit of analysis. Table 8 shows the results of a Shapiro-Wilk's test for normality, allowing the statement with 95% confidence that the data does not fit the normal distribution.

Table 8 Shapiro-Wilk's Test for Normality results (α=0.10), within the Lower Peel River basin.

Variable	Mean	Std. Dev.	Skewness	Kurtosis	W	p	Normality?
SO4	2.71861	5.84117	5.37427	32.3997	0.399076	<0.0001	No
Ca	1.18516	1.45037	3.53106	15.0153	0.617683	<0.0001	No
Mg	1.2621	2.14375	4.2219	20.7918	0.517939	<0.0001	No
Na	0.283287	0.832496	7.049	52.4532	0.270955	<0.0001	No
Fe	0.27037	7.96722	7.74333	59.9214	0.115282	<0.0001	No
Cond.	243.5	316.65	3.78806	17.6993	0.60489	<0.0001	No

In the Lower Peel River basin, the streams are characterized by a Ca(Mg)-SO_4 geochemical facies (Fig. 35). The processes responsible for the geochemical composition of slump runoff and streams can be assessed by examining the ionic relations. Figure 36 examines the potential of halite (NaCl), gypsum ($CaSO_4$ 2 H_2O), anhydrite ($CaSO_4$), $MgSO_4$, dolomite dissolution and pyrite oxidation as contributing processes. For example, the dissolution of gypsum can be expressed by the following equation:

[7] $CaSO_4 2H_2O \rightarrow Ca^{2+} + SO_4^{2-} + 2H_2O$:

Assuming that Ca^{2+} and SO_{42-} in the waters originate from the dissolution of gypsum, their concentration (expressed in equivalent units) should plot close to the 1:1 line. Figure 36 show linear relations between various measured ions. A 1:1 relation is observed between SO_4^{2-} and Ca^{2+} and SO_4^{2-} and Ca^{2+}+$Mg2^{+}$ (Fig. 36, top and bottom right), suggesting that the SO_4 and Ca in the stream waters originates from the dissolution of sulfate salts. The same trends were observed by Malone et al. (2013) who examined slump-impacted and pristine streams in the Stony Creek sub-basin.

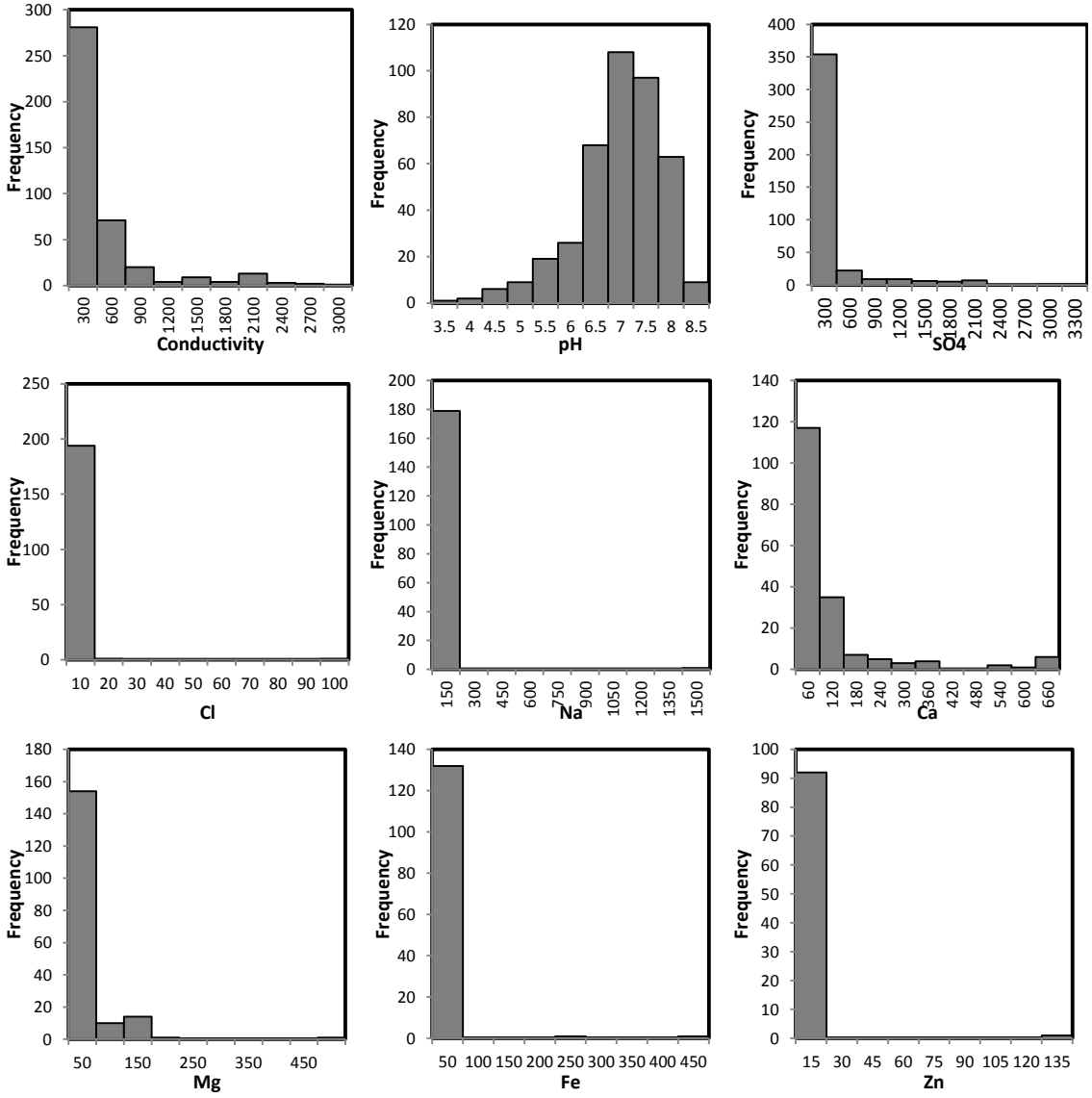

Figure 34. Histogram of values of measured parameters in the Lower Peel River basin. Top left: log(conductivity); Top middle: log(pH); Top right: log(SO4); Middle left: log(Cl); Middle middle: log(Na); Middle right: log(Ca); Bottom left: log(Mg); Bottom middle: log(Fe); Bottom right: log(Zn).

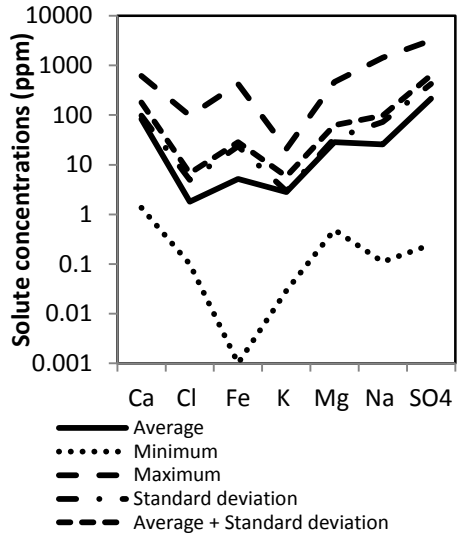

.

Figure 35. Schoeller diagram of geochemical composition stream samples, in the Richardson Mountains-Peel Plateau region.

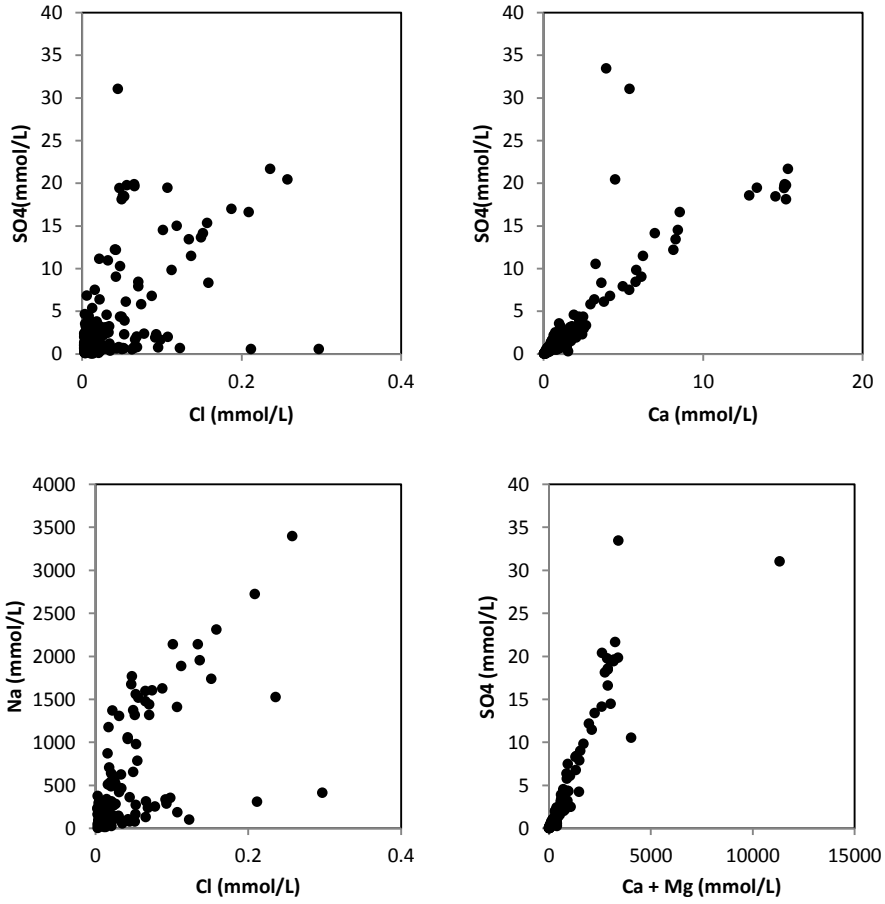

Figure 36. Scatter plots exploring the relationship between values of various measured and analysed ions, in the Richardson Mountains-Peel Plateau region.

4.3.1 Geochemical composition of streams represented at different hydrologic scales

The geochemical composition of streams in the Lower Peel River basin was examined for the following parameters (conductivity, SO_4^{2-}, Cl^-, Ca^{2+}, pH, Fe_{tot} and Zn). For each parameter, four maps were created. The first map shows the samples points and their range of values, the second shows the median stream geochemical composition at the sub-basin scale (4^{th} level), the third shows the median stream geochemical composition at the watershed scale (5^{th} level) and the fourth shows the median of the characteristic at the sub-watershed scale (6^{th} level). The measured ionic concentrations and their median values were then classified based on the CCME and US-EPA standards for freshwater aquatic life (Tables 1, 2 and 3).

Conductivity in the Lower Peel River basin

Of the 408 stream water sample points, 54 (13.2%) have very low conductivity (<50µS/cm), 116 (28.4%) have lower than what is usually ideal, but not unusual (50-150 µS/cm), 160 (39.2%) have ideal conductivity for diverse aquatic life (150-500 µS/cm), 55 (13.5%) have higher than ideal though not unusual conductivity (500-1500 µS/cm), and finally 23 (4.5%) have very high conductivity (>1500 µS/cm) (Fig. 37). The lowest measured conductivity value was 10 µS/cm (measured 11 times), and was found in the centre-south and in the south-west sections of the Rat sub-basin. The highest measured conductivity value was 2893 µS/cm, measured in the Stony Creek sub-basin.

Figure 37 also shows the median water conductivity at the sub-basin scale. Of the 7 sub-basin units, none have very low or very high conductivity averages. The Big Fish River and Rat sub-basins are labelled as lower than ideal though not unusual, the Vittrekwa, Stony Creek and Willow sub-basins are labelled as ideal for diverse aquatic life while teo sub-basins (Unnamed #2 and Trail) had higher than ideal though not unusual median conductivity values. The sub-basin with the lowest median conductivity is the Big Fish River while the sub-basin with the highest median conductivity is the unnamed sub-basin #2.

Figure 38 shows the median water conductivity at the watershed scale. Of the 21 watershed units, one was characterized as being very low (found in the Rat sub-basin), 4 (19%) had lower than ideal but not unusual conductivity values, 11 (52.4%) had ideal for diverse aquatic life conductivity values, 4 (19%) higher than ideal though not unusual values and 1 was characterized as being very high conductivity values. The lowest median conductivity value at

the watershed scale was 40µS/cm, found in the Rat River sub-basin. The highest median conductivity value was 1872 µS/cm in the Willow River sub-basin.

Figure 38 also shows the median water conductivity at the sub-watershed scale. Of the 51 sub-watershed units, 3 (5.9%) had very low conductivity values, all of which were in the Rat River sub-basin. 12 of the 6th level units (23.5%) have median conductivity values between 50 and 150 µS/cm, which is defined as being lower than ideal but not unusual. 24 (47.1%) of the sub-watershed units have ideal median conductivity values, 10 (19.6%) have medians higher than ideal conductivity values and 3 (5.8%) have medians characterized as very high conductivity values. The lowest median conductivity values at the sub-watershed scale was 20 µS/cm, found in the Rat River sub-basin. The highest median conductivity was 1930 µS/cm, measured in the Unnamed sub-basin #2. The three units with very high median conductivity were all in the same area, the north-east section of the unnamed sub-basin #2 and in the eastern section of the Willow River sub-basin.

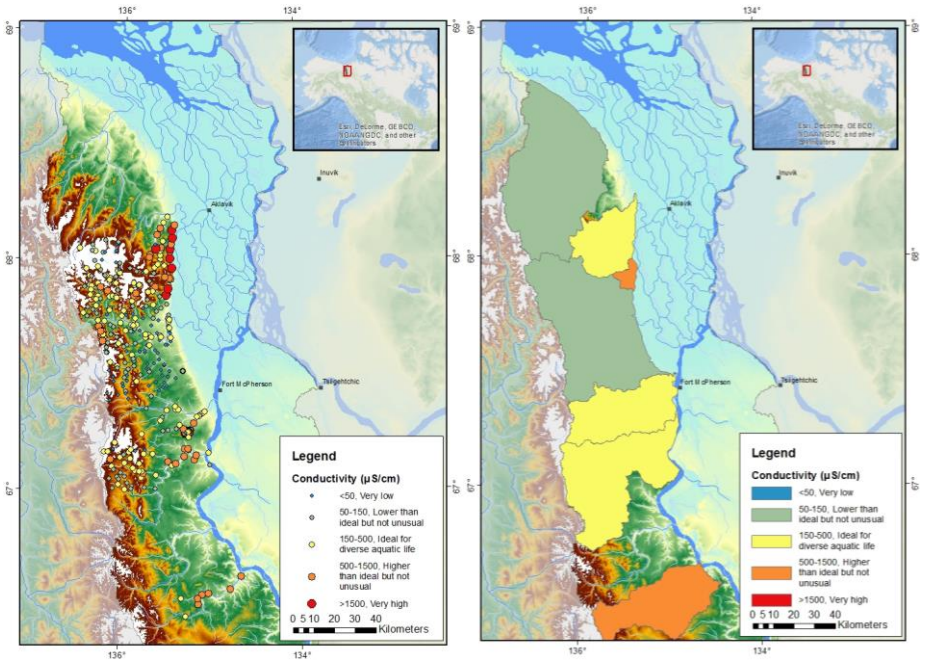

Figure 37. Left) Measured conductivity values (µS/cm), sorted based on USEPA standards for diverse freshwater aquatic life, in the Richardson Mountains-Peel Plateau region, Right) Median conductivity values (µS/cm) within 4th level sub-basins, sorted based on USEPA standards for diverse freshwater aquatic life, in the Richardson Mountains-Peel Plateau region.

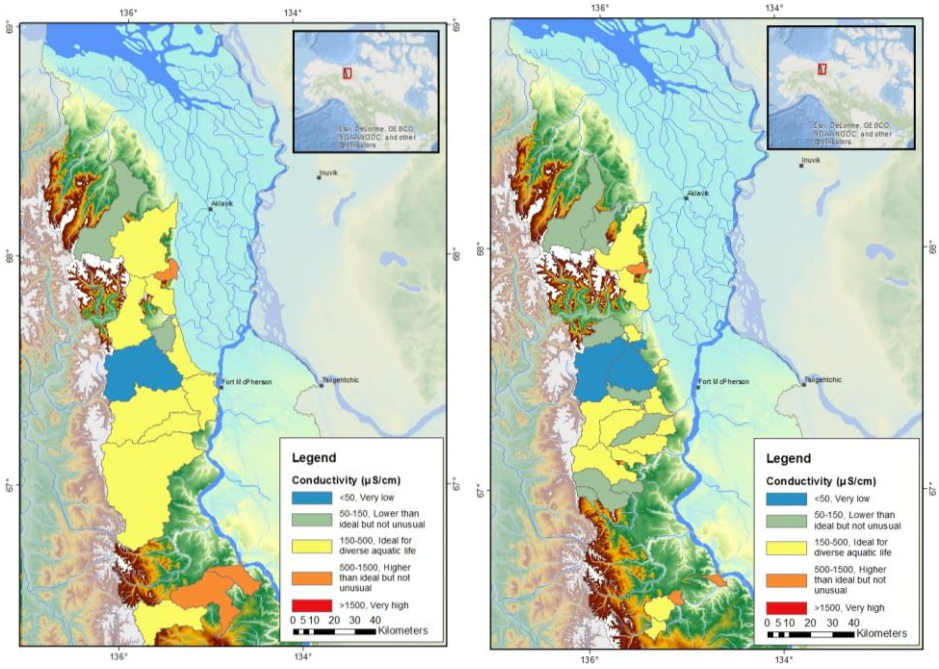

Figure 38 Left) Median conductivity values (µS/cm) within 5th level watersheds, sorted based on USEPA standards for diverse freshwater aquatic life, in the Richardson Mountains-Peel Plateau region, Right) Median conductivity values (µS/cm) within 6th level sub-watersheds, sorted based on USEPA standards for diverse freshwater aquatic life, in the Richardson Mountains-Peel Plateau region.

SO_4^{2-} concentrations in the Lower Peel River basin

Of the 414 sample points in streams in the Lower Peel River basin, 156 (37.7%) were below 50 ppm, or below the identified CCME long term maximum. 101 stream sample points (24.4%) had SO_4 concentration above 50 ppm and below 100ppm (below the identified short term CCME maximum) (Fig. 39). The remaining 157 points (37.9%) had SO_4 concentrations above 100 ppm (above all CCME standards). The highest measured value for SO_4^{2-} was 3211 ppm measured in the middle of the Willow River sub-basin, while the lowest value was 0.25 ppm measured in the middle of the Rat River sub-basin.

Figure 39 also shows the median SO_4^{2-} concentrations at the sub-basin level. Of the seven sub-basin units with stream water samples, the Big Fish River and Rat River sub-basins have median SO_4 concentrations below the long term CCME maximum of 50 ppm, the Stony Creek sub-basin has a median SO_4 concentration below the short term maximum (<100 ppm), whereas the remaining 4 units (Willow, unnamed #2, Vittrekwa and Trail rivers sub-basins) had median SO_4 concentrations all above CCME standards (>100 ppm). The lowest median SO_4^{2-} value is 34.99ppm measured in the Big Fish sub-basin and the highest median SO_4^{2-} value is 437.75ppm measured in the unnamed sub-basin #2.

Figure 40 shows the median SO_4^{2-} values at the watershed level. Of the 21 watershed units with water samples, 5 (23.8%) had SO_4 concentrations below 50 ppm, 7 (33.3%) had SO_4 concentrations between 50 and 100 ppm, whereas 9 (42.9%) had values above CCME standards for freshwater aquatic life. The highest median SO_4^{2-} value measured was 1058.3 ppm in the eastern Willow sub-basin. The lowest median SO_4^{2-} value was 23.14 ppm in the southwest Rat River sub-basin.

Finally, Figure 41 also shows the median SO_4^{2-} concentrations at the sub-watershed level. Of the 51 sub-watershed units with water samples, 16 (31.4%) had SO_4 concentrations below 50 ppm, 13 (25.5%) had SO_4 concentrations between 50 and 100 ppm, whereas 22 (43.1%) had values above 100 ppm, or above all CCME standards. The highest median SO_4^{2-} value was 1067 ppm measured in the unnamed sub-basin #2, while the lowest median SO_4^{2-} value was 1.8 ppm measured in the centre of the Rat River sub-basin.

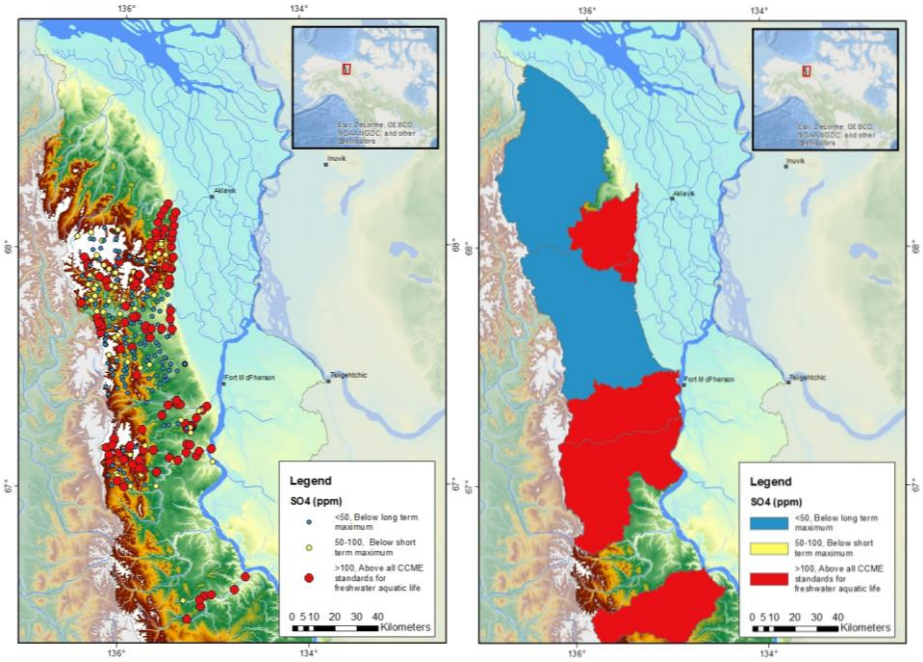

Figure 39. Left) Analysed SO_4^{2-} values, sorted based on CCME standards for long term and short term maximums for freshwater aquatic life, in the Richardson Mountains-Peel Plateau region, Right) Average SO_4^{2-} concentration within 4th level sub-basins, sorted based on CCME standards for long term and short term maximums for freshwater aquatic life, in the Richardson Mountains-Peel Plateau region.

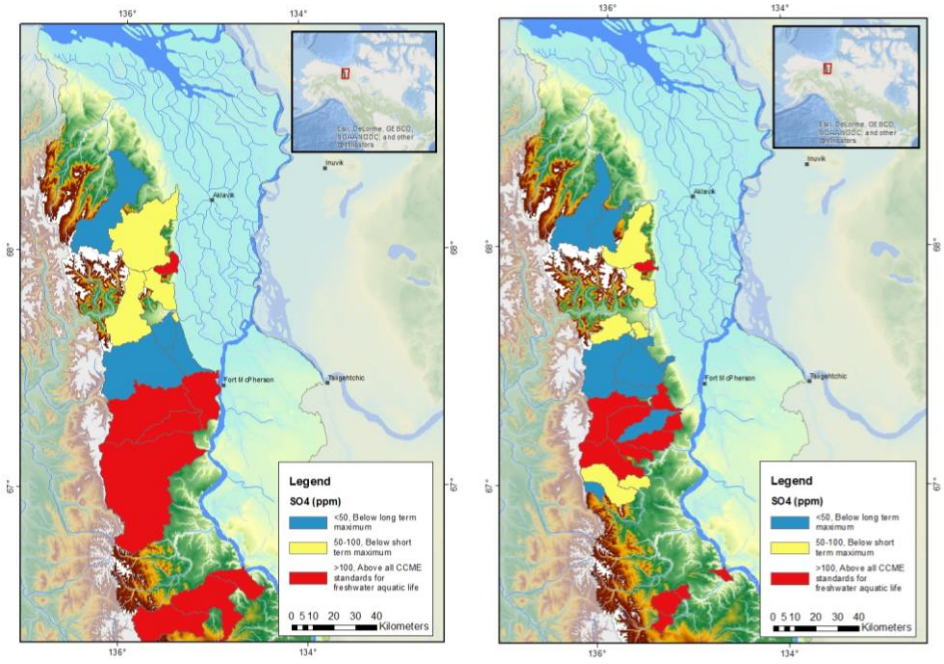

Figure 40 Left) Average SO_4^{2-} concentration within 5th level watersheds, sorted based on CCME standards for long term and short term maximums for freshwater aquatic life, in the Richardson Mountains-Peel Plateau region, Right) Average SO_4^{2-} concentration within 6th level sub-watersheds, sorted based on CCME standards for long term and short term maximums for freshwater aquatic life, in the Richardson Mountains-Peel Plateau region.

Cl^- concentrations in the Lower Peel River basin

The CCME identifies a threshold of 250ppm as a long term maximum and a threshold of 640ppm as a short term maximum for the concentration of chloride. Of the 414 stream sample sites, 218 had Cl values too low for detection. Of the 196 other samples, the maximum chloride value was 97.1ppm (measured in the Willow river), which is considerably below the thresholds identified by the CCME.

pH in the Lower Peel River basin

Of 410 stream samples sites where pH values were measured, 109 (26.6%) were below 6.5, which is identified as being below the CCME threshold (Fig. 41). The 301 other sample sites (73.4%) were measured between 6.5 and 9 on the pH scale, which is within the identified acceptable CCME threshold. The highest measured pH value was 8.5, measured twice in the Stony Creek sub-basins, whereas the lowest value was 3.3 measured in the Rat River sub-basins.

Figure 41 also shows the median pH values for the 4th level sub-basin scale. Of the 7 sub-basin units where samples were taken, the Big Fish sub-basin had a median pH value below the 6.5 threshold while the six others (Willow, unnamed #2, Rat, Stony, Vittrekwa and Trail) had median values within the 6.5-9 thresholds. The unnamed sub-basins #2 had the highest median pH value at 7.5 while the Big Fish sub-basin had the lowest median pH values at 5.5.

Figure 42 shows the average pH values for 5th level watershed scale. Of the 21 watershed units where samples were taken, four (19%) were below the 6.5 threshold, while 17 (81%) were within the 6.5-9 threshold. The highest measured median value was 8.06 in the western portion of the Trail River sub-basin. The lowest measured median value was 5.5 in the southern Big Fish sub-basin.

Figure 42 also shows the median pH values for 6th level sub-watershed scale. Of the 51 sub-watershed units where samples were taken, 15 (29.4%) were below the 6.5 threshold, while 36 (70.6%) were within the 6.5-9 threshold. The highest median value was 8.1 found in the eastern part of the Trail River sub-basin while the lowest median value was 4.5 measured in the northern part of the Willow River sub-basins.

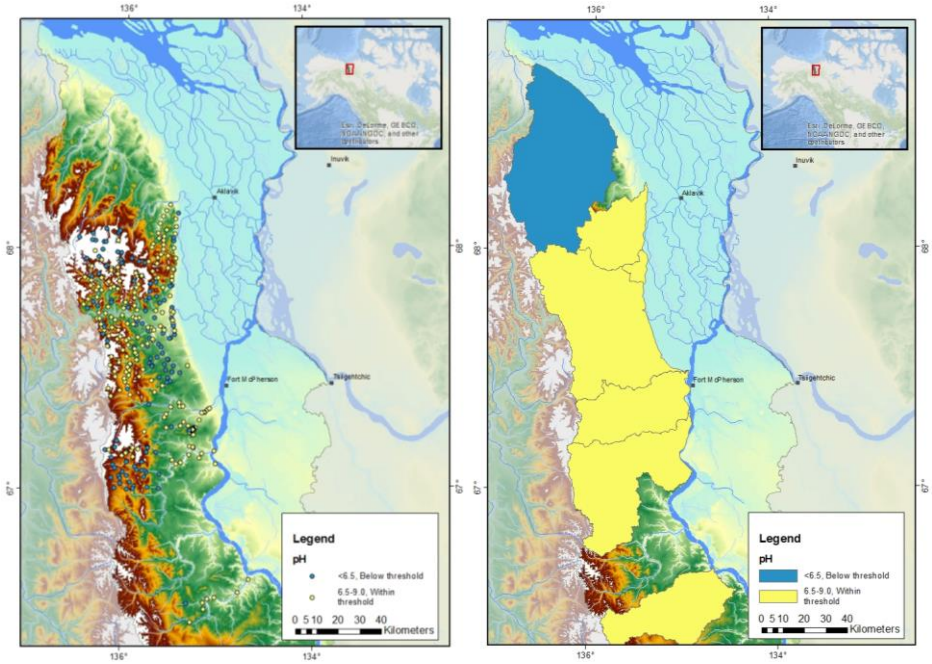

Figure 41. Left) Measured pH values sorted based on CCME standards for freshwater aquatic life, in the Richardson Mountains-Peel Plateau region, Right) Average pH values within 4th level sub-basins, sorted based on CCME standards for freshwater aquatic life, in the Richardson Mountains-Peel Plateau region.

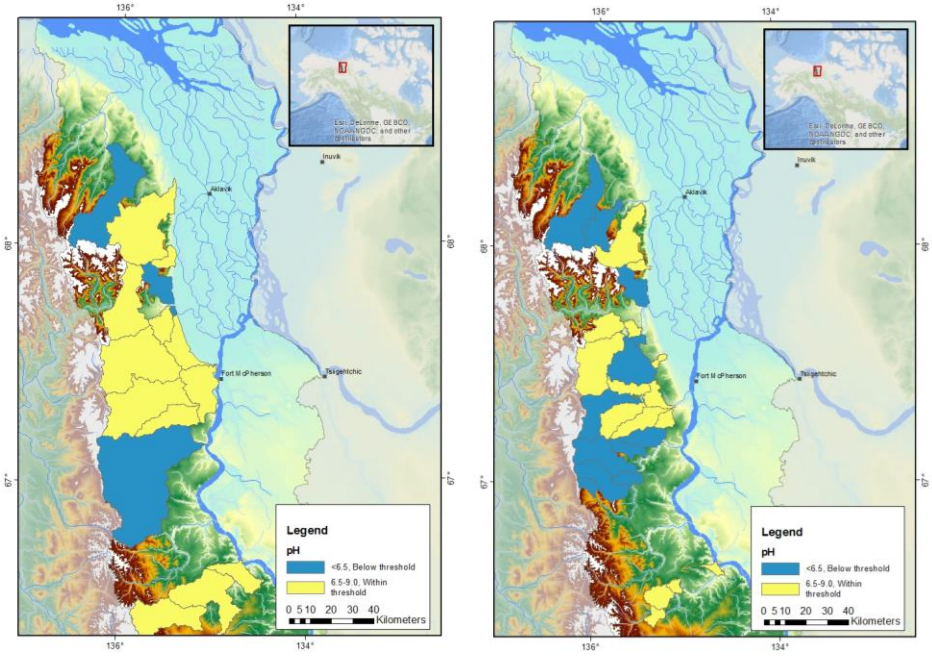

Figure 42 Left) Average pH values within 5th level watersheds, sorted based on CCME standards for freshwater aquatic life, in the Richardson Mountains-Peel Plateau region, Right) Average pH values within 6th level sub-watersheds, sorted based on CCME standards for freshwater aquatic life, in the Richardson Mountains-Peel Plateau region.

Iron in the Lower Peel River basin

According to the CCME standards, the long-term maximum iron concentration is 300ppm. Of the 134 samples sites where the Fe_{tot} levels were superior to the detection limit, only one had a value superior to 300ppm (425.86ppm, found in the Willow River sub-basins). Only one other sample site had a value above 12ppm (215.77ppm found in the Rat River sub-basin). The smallest measured value was 0.01ppm (lower limit of detection) in the Vittrekwa sub-basin.

Zinc in the Lower Peel River basin

According to the CCME standards, the maximum zinc concentration is 30ppm. Of the 93 samples sites where the measured zinc levels were superior to the detection limit, only 1 was found to be above the 30ppm threshold (123.02 ppm found in the Rat River sub-basin). Of the 93 samples, all but two were below 1ppm, with the lowest value being 0.0001ppm (lower detection limit) in the Stony Creek sub-basin.

4.4 Relations between thaw slumps parameters and geochemical composition of streams

4.4.1 Individual stream scale

This section examines the relations between the geochemical composition of streams (conductivity, SO_4, Cl, and SO_4/Cl) with respect to the distribution and surface area of thaw slumps along stream transects in the various sub-basins. The figures showing SO_4/Cl molar ratio have a shaded area below the 300 value. According to Malone et al. (2013), values above this threshold indicate streams having been impacted by slumping. Figure 43 shows the location of the examined streams.

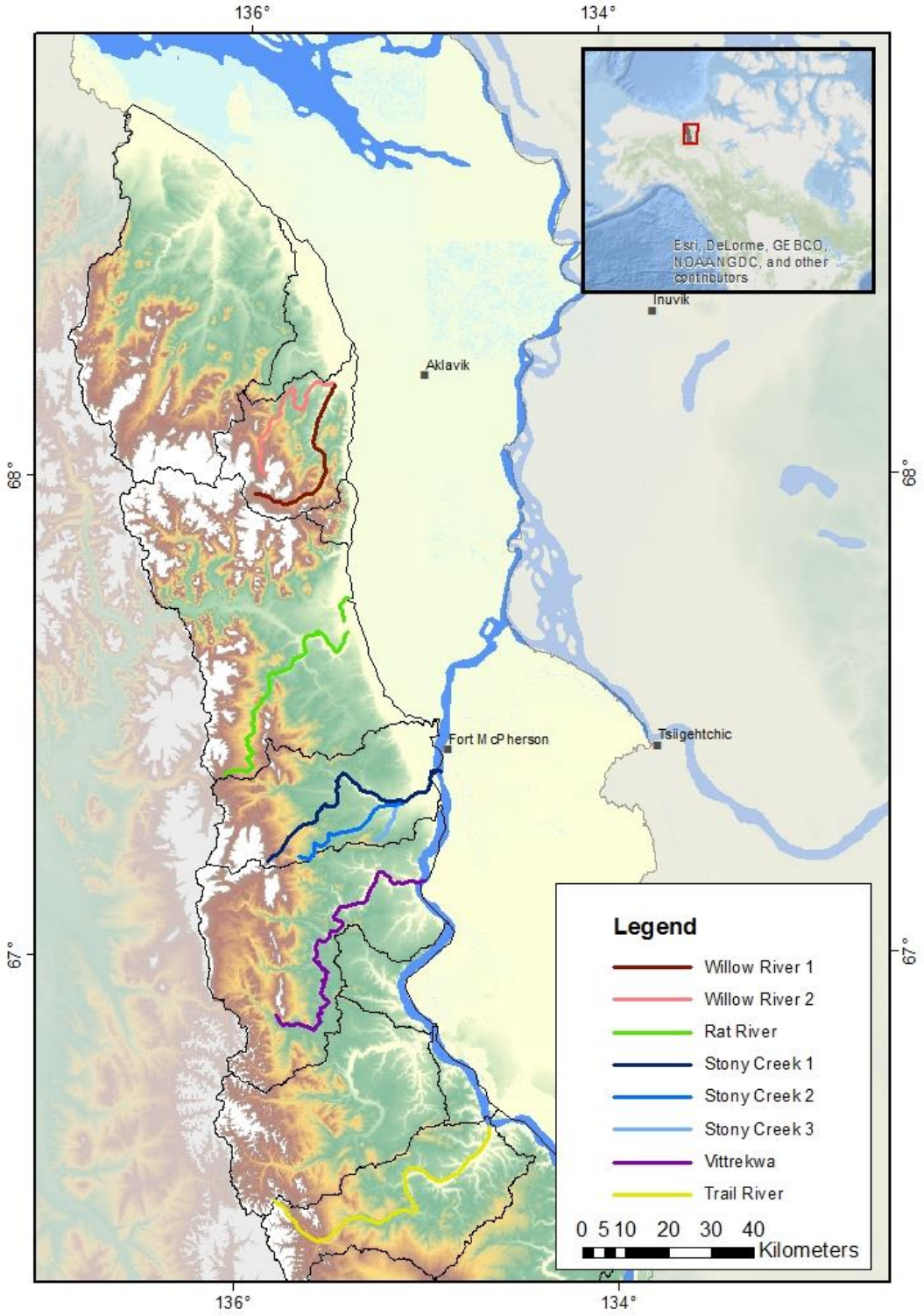

Figure 43 Location of individually assessed streams in the Richardson Mountains-Peel Plateau region.

Willow River 1 ***(figure 44, top left)***

There are 20 slumps along this stretch of the Willow River, covering on average 4.87ha each The smallest slump covers 1.14ha and the largest covers 11.96ha. Along this stretch, 13 slumps are considered small (<5ha) and 7 cover more than 5ha (two of which cover more than 10ha).

The data collected along this stretch of the Willow River indicate the importance of slump size in affecting stream geochemistry. Thaw slumps along this reach range from 1 to 12ha. Too few Cl values (which vary between 0.3 and 0.7ppm) exist to identify a trend. However, the Cl values prior to the 30km mark were below detection limits indicating negligible chloride content. The Cl values increase to detectable levels following the area of higher slump concentration (after the 20km mark).

The SO_4 and conductivity values in this stream also seem to vary in relation to areas with a high number of larger slumps. The first 20km show low SO_4 (<123.8ppm) and conductivity (<310 µS/cm) values with not slumps over 10ha. The SO_4 values quadruple in less than 2km (97.5ppm to 1310ppm of SO_4 and 270 µS/cm to 1180 µS/cm of conductivity) following a number of slumps ranging in size from 3ha to nearly 10ha.

The first few slumps (all < 8 ha) are upstream from low SO_4/Cl values (<100). Following an area of high slump density (16 slumps between 24.4km and 35.6) and the presence of much larger slumps (>10ha), the SO_4/Cl ratio increases to reach a high of over 400. As the slumps sizes decrease after the 30km mark, the SO_4/Cl values decrease as well, especially with a new stream input.

Willow River 2 ***(figure 44, top right)***

There are 8 slumps along this stretch of the Willow River, covering on average 2.27ha each. The smallest slump covers 1.23ha while the largest covers 4.65ha. All slumps along this reach are considered small (<5ha).

Though there are few slumps and stream samples points along this branch of the Willow River, the impact of slumping activity of stream geochemistry is evident in all parameters. The Cl, SO_4 and conductivity values are relatively low downstream from the first few slumps (0.6ppm, 218.3ppm and 680 µS/cm respectively). Though no samples are available, it could be deduced that their values lower as the distance to the slumps increase. The values then increase

sharply with the input from the 4.5 ha slump at the 6.8km mark (5.56ppm of Cl, 1469.1ppm of SO_4 and 1700 µS/cm of conductivity).

The SO_4/Cl values are remain below the threshold through this section of the Willow, showing limited response to slumps, which are all small in size (<5ha).

Rat River 1 ***(Figure 44, bottom left)***

There are 6 slumps along this reach, covering on average 6.33ha each. The smallest slump covers 2.1ha while the largest one covers 9.14ha. Two of the six slumps are considered small (<5ha) while the four others are of fair size (5-10ha).

Of the 25 sample points along this reach of the Rat River, only 9 had Cl values over the minimum detection limit. As with the other sub-basins, there seems to be no relation between Cl values and proximity to, and size of, slumps.

The SO_4 and conductivity values are also consistently lower than average in this stretch of the Rat River. The values are very low for the first 40km of the river, even with the presence of slumps. These slumps, however, are all small (<10ha), meaning they might not be inputting as much material into the stream. Following the 40km mark, both SO_4 and conductivity values increase. The highest SO_4 value reaches 608.73ppm (63.3km) and highest conductivity value reaches 372 µS/cm (44.5km). Both parameters show important fluctuation from the 40km mark onward. This could be due to the major stream inputs (at the 34km, 43km and 55km marks) and the several smaller stream inputs along the reach.

Due to the lack of Cl data, the SO_4/Cl values do not show the same high-fluctuating trend. The lower SO_4/Cl values (like the SO_4 and conductivity values) measured in this segment of the Rat River could be due to the smaller (<10ha) slumps and/or the distance from the slumps. The smaller values could also be due to the multiple stream inputs (16km, 26km, 34km, 43km and 55km). The first SO_4/Cl value (150) is nearly 7km downstream from the closest slumps(which is only 4ha in size). The SO_4/Cl values peak at approximately 300 at the 63km mark. This sample points is a considerable distance downstream from any slumps, indicating the probable influence of an impacted stream input.

Stony Creek 1 ***(Figure 44, bottom right)***

There are 12 slumps along this stretch of Stony Creek with an average size of 3.66ha. The smallest slump covers 1.37ha while the largest covers 6.64ha. Ten of twelve slumps along this stretch are considered small, covering less than 5ha, with the other two covering less than 7ha.

The relations between the presence and surface area of thaw slumps and Cl, SO_4, conductivity and SO_4/Cl are shown. The Cl concentrations (< 0.4ppm) are all below water quality threshold. There is no relation between Cl concentrations and the presence of slumps as the Cl values fluctuate between 0.2 and 0.4ppm, even in proximity of slumps.

The SO_4 concentrations in streams vary in relation with the presence of slumps along the reach. After the initial group of thaw slumps, the values for SO_4 increase to 145.8ppm and subsequently decrease to value of 137.6ppm at 15km then 25.9ppm at 19km along the stream reach. The SO_4 concentration in the stream then increases to values of 140ppm as other slumps are encountered along the reach.

Conductivity values follow the same response as SO_4. After the initial group of thaw slumps, conductivity values were measured at 295 µS/cm at 3.6km, and then decrease to 240. 80 µS/cm at 15km then 226 at 24km along the stream reach. The conductivity values then increase to a maximum of 286 µS/cm as other slumps are encountered.

The SO_4/Cl varies along the stream with respect to the presence of slumps. The SO_4/Cl value (180) is moderately high near the initial group of slumps along the stream. The second SO_4/Cl value (>300) follows the additional input of two larger (>5ha) slumps. The SO_4/Cl values then decrease to near 100. There is a span of several kilometers with no thaw slumps followed by the inputs of two smaller slumps which seems to lead to a slight SO_4/Cl increase. This agrees with Malone et al. (2013) that stated that less than 10km is needed for the higher ionic concentration values to decrease to near background values. In this case, the adding of material from two smaller slumps increased the ration. The lower ratio values following the slumps found just prior to the 40km distance can be attributed to the input of unimpacted water from a connecting stream.

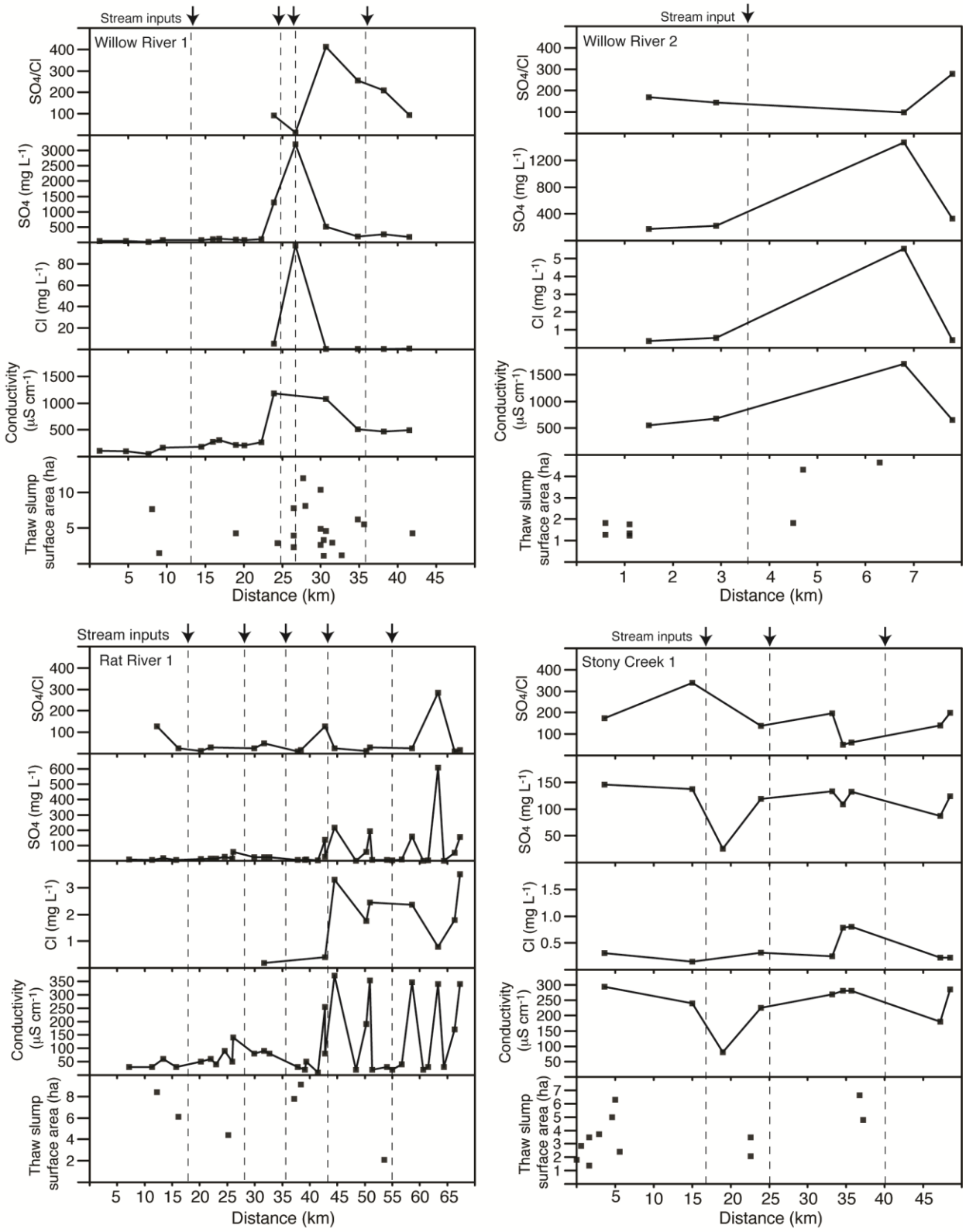

Figure 44 Relationship between the geochemical composition of streams (conductivity, SO_4, Cl, and SO_4/Cl) with respect to the distribution and surface area of thaw slumps along stream transects in the northern portion of the study area.

Stony Creek 2 ***(figure 45, top left)***

There are 7 slumps along this stretch of Stony Creek covering on average 9.59ha each. The smallest slump covers 0.99ha while the largest is extremely large, covering 52.22ha. However, 6 of the 7 slumps along this stretch are small, covering less than 6ha

The previously mentioned trend is not as obvious in the Stony Creek2 because of distance between the location of slumps and the location sampling took place (several kilometers downstream). Again, there is no relation between Cl concentrations and the presence of slumps as the values fluctuate between 0.35 and 1.87ppm, even in proximity of slumps.

The SO_4 values increase immediately after the initial group of slumps reaching 95.31ppm and increasing further to 147.47ppm at 21km. The higher values seen downstream could be due to a stream input around the 20km.

The conductivity values have the same response along this reach. Conductivity values reach 252.5µS/cm after the first group of slumps, then increase further downstream, after the new stream input and reach a maximum of 297µS/cm at the 21km mark.

The SO_4/Cl values are all very small (<100).

The high SO_4 and conductivity values measured after the 20km mark of this branch of the Stony Creek may be attributable to in stream input at approximately the 20km mark. However, they may be due to the extremely large slumps at the 8km mark covering an area of over 50ha. This slump might have a longer downstream reach than other slumps (which have an average reach of less than 10km) simply due to its significantly above average size.

Stony Creek 3 ***(figure 45, top right)***

There are only three slumps along this stretch of Stony Creek, covering an average of 25.92ha each. The smallest slump covers 9.58ha while the largest slump covers 48.09ha. The three slumps along this stretch are considered to be large.

Though there are few thaw slumps and stream sample sites along Stony Creek 3, it does contain some of the largest slumps (>10ha) and the impact of slumps on stream geochemistry can still be noticed with SO_4/Cl, SO_4 and conductivity changing to the input of slump material along this stretch. The Cl values once again do not seem to react to slump input as the highest values, 0.83ppm, is measured prior to any slump input.

The SO_4 value is 30ppm 300m into this stretch and increases to 100ppm after a 10ha slump. Further downstream, the two measured values following a 20ha slump increase to 182.76ppm and 718.11ppm respectively.

This trend is also observable when looking at conductivity. Following the smaller 10ha slump, values reach 219.6µS/cm. Further downstream and following a 20ha slump, conductivity values peak at 785µS/cm.

Prior to any slump input, SO_4/Cl value is minimal (108.63) which is well below the identified threshold for impacted streams. Following a slump of approximately 10ha the SO_4/Cl value increases to approximately 100. After the presence of two large slumps (48.09ha and 20.09ha) the ratio values remain extremely high (>400) more than 5km downstream.

Vittrekwa River 1*(figure 45, bottom left)*

There are 7 slumps along this stretch of the Vittrekwa River, covering on average 8.67ha each. The smallest slump covers 3.24ha while the largest slump covers 18.05ha. Four of these slumps are small (<5ha), while 3 are large (>10ha, two of which are larger than 15ha).

All stream sample points along this reach of the Vittrekwa River are found downstream from identified slumps. Therefore, the input of several streams and smaller branches impact the data more than the slumps themselves. There are major and minor stream inputs at the 34km, 36km, 43km (second largest stream within the Vittrekwa sub-basin), and 75km marks. The second largest stretch of the Vittrekwa is home to very large slumps (one covering over 40ha and two others covering over 10ha) and could have important impacts of hydro-geochemistry values downstream from where it joins with the main Vittrekwa reach.

The Cl values show very little variation (minimum value of 0.72ppm and maximum value of 1.2ppm) and there seems to be little relation between their values and slumps and stream inputs.

The SO_4 and conductivity values follow a similar trend. The SO_4 values increase gradually from a low of 63.62 at 35.5km, to 435.48 at 66km. The values then fluctuate greatly until the end of this reach, highlighting the impacts of several stream inputs. The conductivity values follow the same pattern, increasing from a low of 150µS/cm at 35.5km to a peak of 794µS/cm at 66km, then fluctuating with new stream inputs.

All SO4/Cl values are below 200, showing limited impact by slumps, which is to be expected as the sample points are all more than 20km downstream from slumps.

Trail River 1 ***(figure 45, bottom right)***

There are 9 slumps along this stretch of the Trail River, covering on average 8.17ha each. The smallest slump covers 4.07ha while the largest covers 18.57ha. Three of these slumps are small (<5ha), 3 cover between 5 and 10ha while 3 more cover more than 10ha.

All Cl values are low (<1.0ppm). However, they increase following the area of higher slump density to reach a maximum of 0.93ppm at approximately the 21km mark. After this point the values decrease.

The highest SO_4 and conductivity values are found closely downstream from slumps. Both of these values begin relatively small (SO_4 being 94.2ppm and conductivity being 174.3 µS/cm at the 5km mark). Both of these parameters increase following the area of higher slump concentration (between 8 and 16km) to reach at 338.72ppm of SO_4 and 588 µS/cm of conductivity. The increase in both of these measured parameters after the 30km (similarly to the SO_4/Cl value increase) could be due to the input of streams joining the main Trail River.

The SO_4/Cl values measured through this stretch are lower than the threshold (other than the first one), which could be explained by the several stream inputs as well as the downstream distance from slumps.

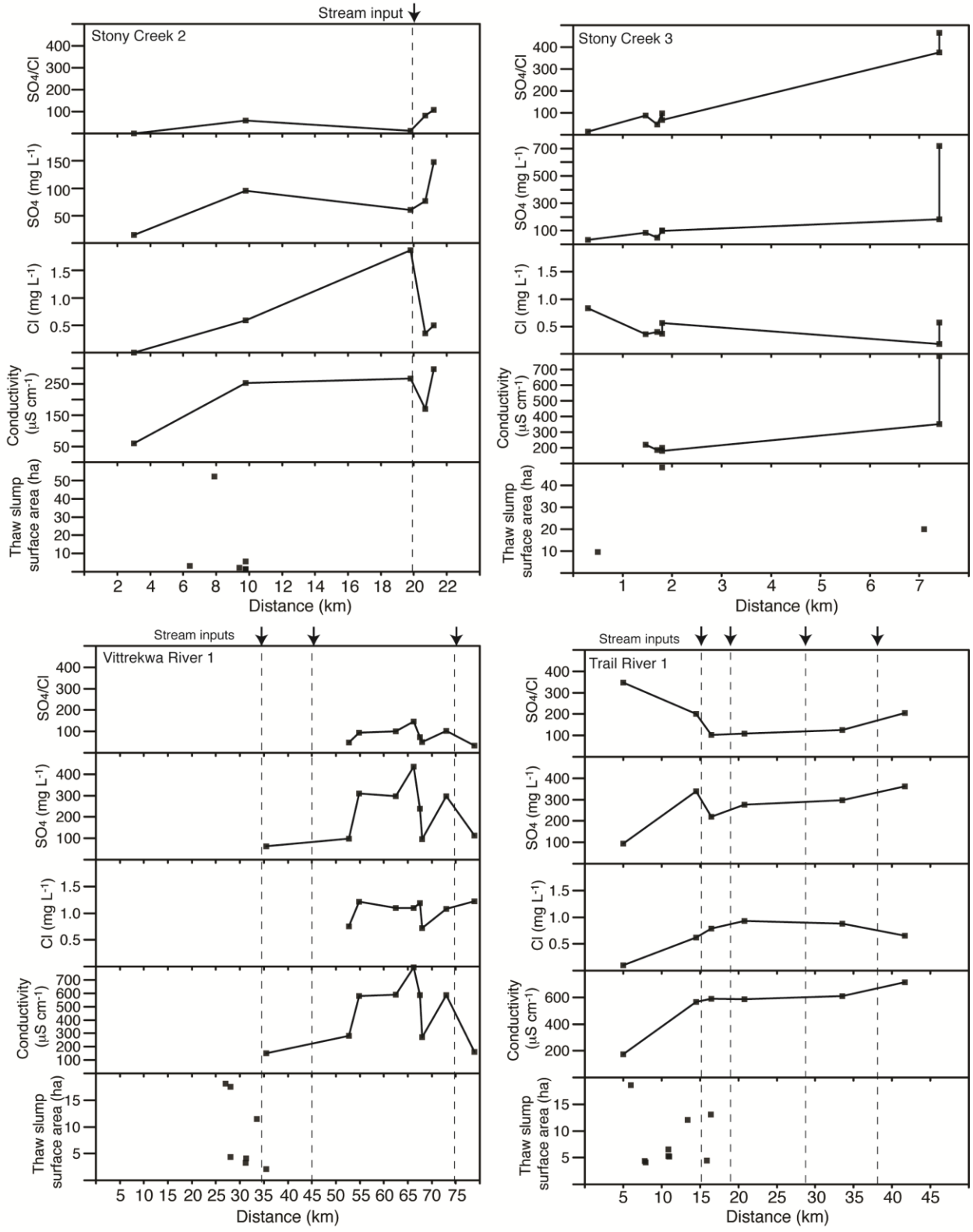

Figure 45 Relationship between the geochemical composition of streams (conductivity, SO_4, Cl, and SO_4/Cl) with respect to the distribution and surface area of thaw slumps along stream transects in the southern portion of the study area.

4.5 Relations between distribution and size of thaw slumps with geochemical composition of streams

This section examines the relations between the geochemical composition of streams (conductivity, SO_4, Cl, and SO_4/Cl) and four different slump parameters (number of slumps, slump density (1000km^2), total slump area (ha), and average slump size) at various spatial scales (4th level sub-basins, 5thlevel watersheds, and 6th level sub-watersheds).

For each hydrological scale, the figures show the linear correlation between the parameters (Fig. 46-48). As has been previously shown, the data is not normally distributed. For this reason, the more common R regression analysis could not be performed. The Fisher *zr* transformation transforms a skewed sampling distribution into normalized format. Table 9 shows the correlation (Zr value), between the parameters at the various scales.

Table 9 R-values indicating the relationship between four different slump parameters and four different hydro-geochemical parameters.

Fisher transformed	Zr			
	Number of slumps	Slump density (1000km^2)	Average slump area (ha)	Total surface area (ha)
Sub-basins				
Conductivity	0.27	0.38	**0.89**	0.56
Cl	0.74	0.44	**1.16**	**1.57**
SO_4	0.21	0.33	**0.88**	0.5
SO_4/Cl	-0.01	0.48	-0.23	-0.28
Watersheds				
Conductivity	-0.23	-0.27	**0.78**	-0.07
Cl	-0.41	-0.37	-0.09	-0.44
SO_4	-0.2	-0.21	**0.77**	-0.05
SO_4/Cl	0.23	0.17	0.41	0.19
Sub-watersheds				
Conductivity	0.01	0.3	0.23	0.18
Cl	-0.1	0.46	0.47	-0.09
SO_4	-0.05	0.14	0.19	0.11
SO_4/Cl	0.02	-0.19	0.17	0.5

4th level sub-basin

With only 7 sub-basins containing both slumps and stream water samples, trends are difficult to observe, and limited in their significance (Table 9, Fig. 46). The Zr-values in Table 9 show that the density of slumps as an important factor in explaining the variation of ionic concentration of SO_4 (Zr=0.88) and Cl (1.16) as well as conductivity (0.89). At this scale, total slump surface area shows important correlation to conductivity (Zr=1.57).

5th level watershed

The highest Zr-values at this scale are between geochemical concentrations and average slump surface area (Table 9, Fig. 47). Average slump surface area is responsible for three of the four hydro-geochemical parameters' highest Zr-values (conductivity, SO_4 and SO_4/Cl). The Zr-value between average slump surface area and conductivity is 0.78. The Zr-value between average slump surface area and SO_4 is 0.77. The Zr-value between average slump surface area and SO_4/Cl is 0.41. At the watershed scale, the correlation between stream geochemistry and number of slumps, slump density and total surface area is low.

6th level sub-watershed

Once again, the average slump surface area is the most correlated slump parameter with stream geochemistry, followed by slump density (Table 9, Fig. 48). The Zr-value between average slumps surface area and conductivity is 0.73. The Zr-value between average slumps surface area and SO_4 is 0.19. The Zr-value between average slumps surface area and SO_4/Cl is 0.17. This indicates that one of the most important factors influencing hydro-geochemistry is slump size and not the number of density of slumps.

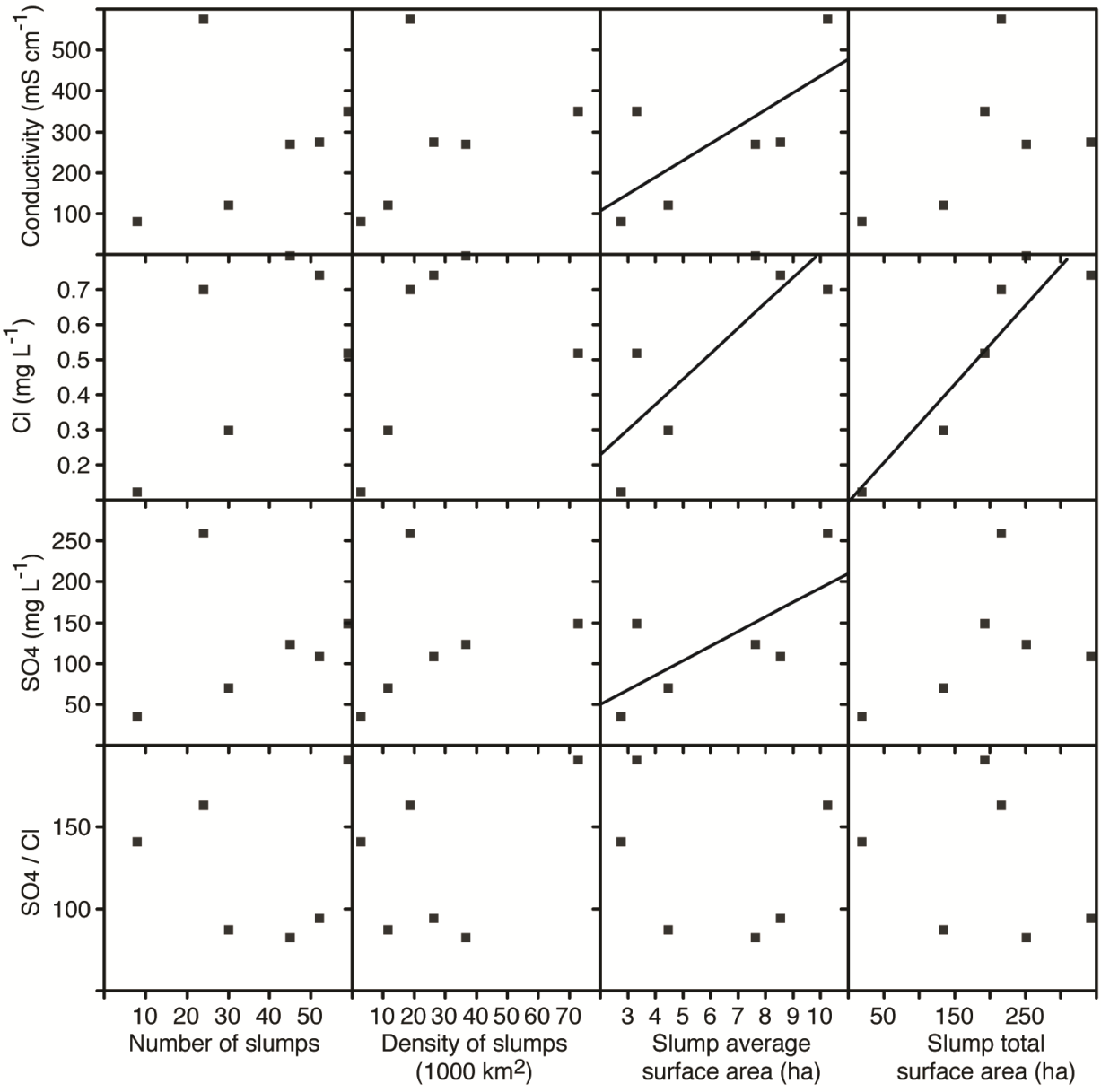

Figure 46. Relationships between hydro-geochemistry and slump parameters at the 4th level sub-basin, in the Richardson Mountain-Peel Plateau region.

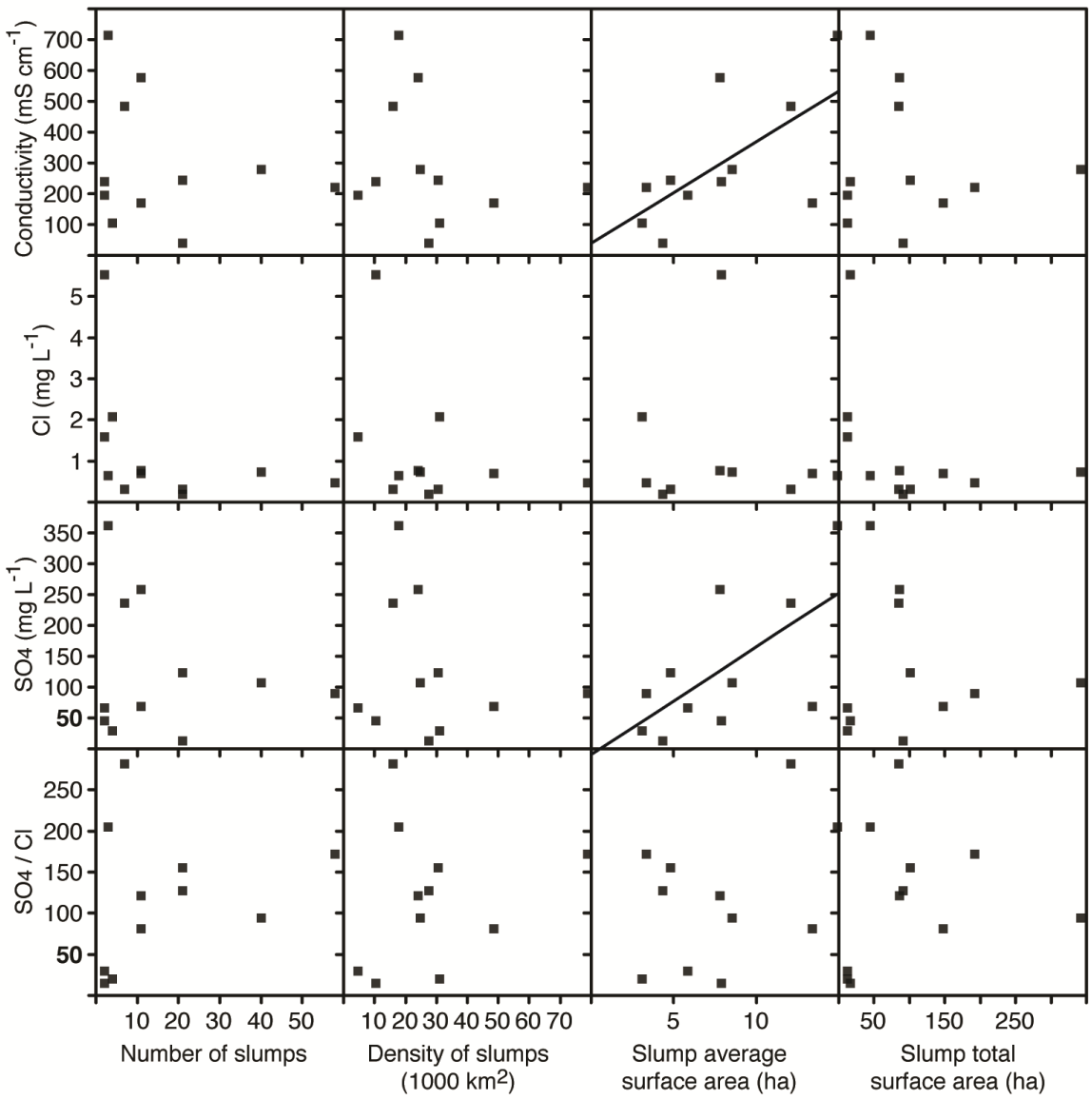

Figure 47. Relationships between hydro-geochemistry and slump parameters at the 5th level watershed, in the Richardson Mountain-Peel Plateau region.

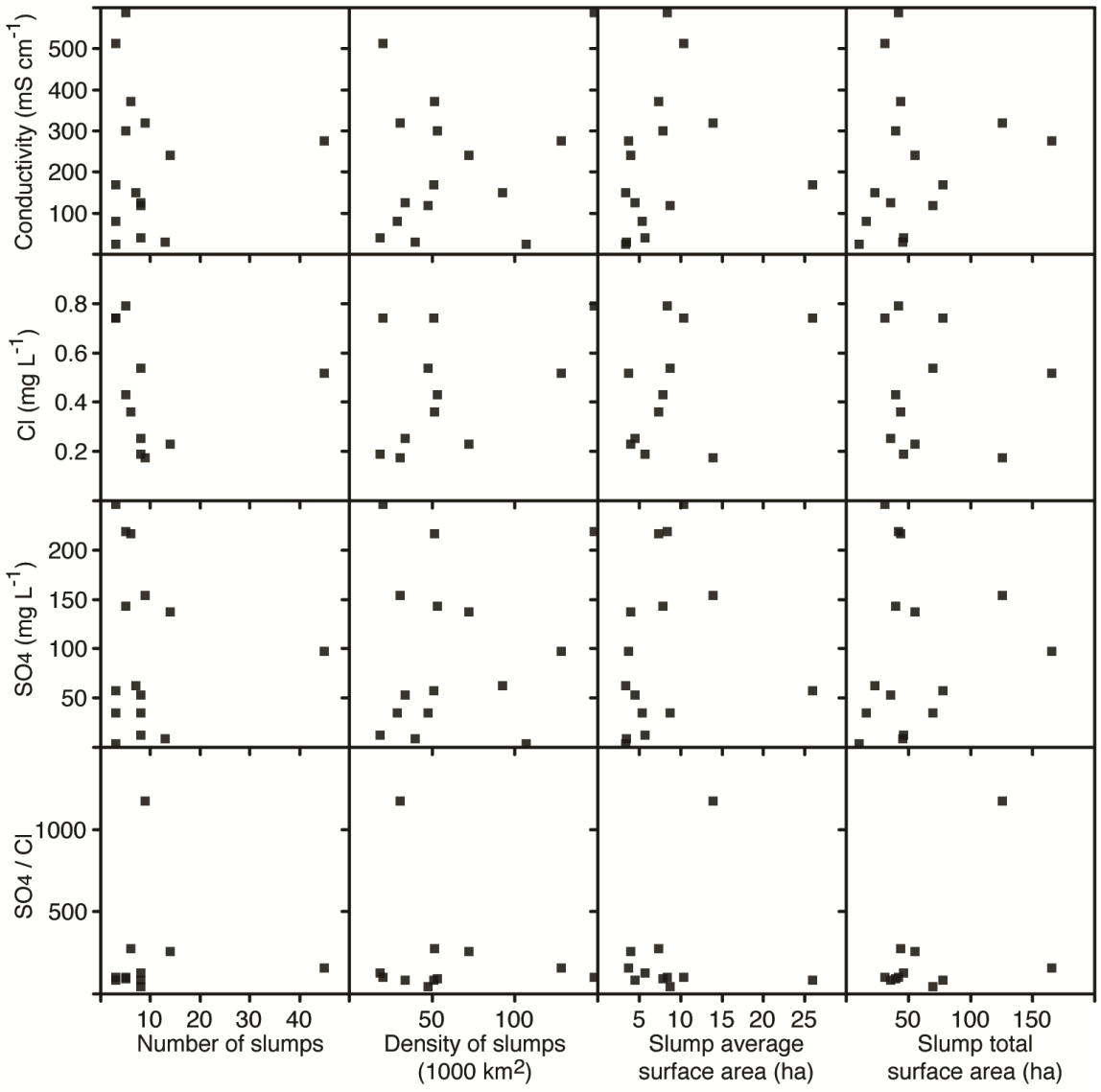

Figure 48. Relationships between hydro-geochemistry and slump parameters at the 6th level sub-watershed, in the Richardson Mountain-Peel Plateau region.

Chapter 5 – Discussion

This thesis aims to explore the spatial dimension of the impacts of slumps on the geochemical composition of streams. The goal of this thesis is to quantify the effects of thaw slumps on the geochemical composition of stream in the Richardson Mountains-Peel Plateau region within various hydrological units (sub-basin, watershed, sub-watershed). This chapter will discuss the results presented in the previous chapter.

5.1 Distribution of thaw slumps in the Richardson Mountains – Peel Plateau, NWT

All identified slumps in this study have occurred within the westward limit to the Laurentide Ice Sheet. This indicated that the area is home to a specific physical feature linked to the location of the ice sheet. Previous studies, as well as site visits, have shown the area in question is underlain by ice-rich permafrost, a necessary feature for the development and growth of retrogressive thaw slumps. As no slumps have developed west of the Laurentide Ice Sheet limit, and the area's surficial sediment properties are somewhat similar to the area to the east, it can be deduced that the area to the west is not underlain by important ice content. Furthermore, over half of identified slumps develop where morainal sediment covers the surface. This indicates once again the importance past glacial activity has had on today's landscapes.

Latitude plays an important role in the distribution of thaw slumps, which is evident at all scales of the study (Fig. 27, 30 and 33). Firstly, the higher number of slumps and the higher density of slumps occur at the mid-latitudes of the study area (between 67° and 68.5°). These characteristics indicate the area has an ideal combination of necessary properties for the initiation and the development of retrogressive thaw slumps, such as massive ground ice, good surficial sediment properties and abundant incoming solar radiation to consistently melt the exposed ice. Secondly, as the three different scales have shown, the larger slumps (average surface area of slumps) seem to be found further south in the study area, where conditions allow the slumps to grow for longer periods in the summer than in the northern portion of the study area. However, the study area's mid-latitude watersheds still have the highest cumulative slumping surface area because of the higher slump counts. The slumps are on average smaller than the ones found further south, but there are larger numbers of them combining for larger total slumping areas.

The distribution of slumps within the study area also highlights the importance of considering the role surficial sediments play in the initiation and development of retrogressive thaw slumps. As indicated in section 4.2, more than half of slumps are found in morainal sediment. As shown in section 2.3, the central and southern portions of the study area have large deposits of morainal sediment, which could impact the number and density of slumps as well as their size.

5.2 Relations between distribution and size of thaw slumps with geochemical composition of streams

The first analysis (4.1.1) looked at geochemical variations along single stream reaches. It can be observed that conductivity, SO_4 and SO_4/Cl values rise immediately following the presence of a slump (usually exceeding a certain size), and the values decrease in the following downstream kilometers. The different stream analyses do not show a link between slumping input and variations in Cl concentrations.

The spatial extent of the impact of thaw slumps within various scales of drainage units (section 4.2.2), performed at the sub-basin, watershed and sub-watershed levels, revealed the importance of slump size; the larger the individual slumps, the higher the geochemical values will be immediately downstream. For example, in Stony Creek 1, it can be observed that hydro-geochemical values are higher after certain slumps, though they are not as high as in other stretches because the slumps are smaller (all <10ha). According to Malone et al. (2013), SO_4/Cl > 300 in streams are indicative of slump impacted streams. Based on this threshold value, it appears that thaw slumps >5ha in surface area will impact stream geochemistry across sub-basins, watersheds and sub-watersheds scales. This is determined from the intersection of SO_4/Cl = 300 with average slump surface area in Figures 46, 47 and 48 meaning slumps smaller than 5ha do not seem to significantly impact downstream geochemistry, even combined with other small slumps.

The average surface area of slumps is the parameter having the largest impact on three of four hydro-geochemical parameters at the 5^{th} and 6^{th} levels (all but Cl, which has been concluded to not be significantly affected by slumping activity). The reason for the high correlation between conductivity, SO_4 and SO_4/Cl values and average slump size within a 5^{th} or 6^{th} level unit

and not, for instance, cumulative surface area of thaw slumps within a drainage unit, is that the size of individual slumps is the important factor. This means a drainage unit can contain a high number of slumps, but if the individual slumps are too small (<5ha), they will not have a significant impact on the geochemistry. However, a sub-basin, watershed or watershed with fewer but large individual slumps (>5ha) will show more significant geochemical disturbances.

One of the main conclusions this study makes is that slumps do not have the cumulative effects previously thought. For example, 10 slumps covering 5ha each (for a total of 50ha of slumping) do not have the same environmental impacts that a single 50ha slump has. As seen in section 4.4.1, there seems to be a size threshold when it comes to the impact of slumps on hydro-geochemistry. Slumps smaller than ~5ha have little geochemical impact, even when there are several in close proximity to one another. Slumps larger than this do impact the environment with higher conductivity values, as well as higher concentrations of SO_4 and higher ratios of SO_4/Cl.

5.3 Impact of scale

Appendix B shows the number of data points as well as the median, mean and standard deviation values of the five main geochemical properties (pH, conductivity, SO_4, Cl and SO4/Cl) as well as the number of slumps. This is shown for every unit at every scale (sub-basin, watershed and sub-watershed). At the sub-basin scale, there are many more sample sites than there are at the sub-watershed level. At the sub-basin scale, all units have more than 1 sample site with many having more than 20. At the sub-watershed scale, many units have only 1 or two samples while others have none, making their mean or median values not as accurate. For this reason, the relationship between slumps and geochemistry at the sub-basin scale (figures should be taken with more consideration than the relationships at the other scales.

5.4 Environmental impacts

Many of the measured geochemical values are outside the limits of CCME standards. For example, 248 of the 408 conductivity measurements (60%) are either below the minimum ideal threshold (<150µS/cm, mostly in the centre of the Rat sub-basin) or above the maximum ideal threshold (>500µS/cm, mostly in the Willow and Stony sub-basins). As shown in Table 2, this could significantly impact certain species of fish and macroinvertebrates, including diatoms. Of

the 414 SO_4 sample points, 101 were measured at being over the long-term maximum of 50ppm but below the short-term maximum of 100pm, while 157 more were measure being over the short-term maximum. These high levels of sulfate, especially those above 100ppm could have negative impacts of aquatic life. These high SO_4 values were found throughout the Richardson Mountains-Peel Plateau region. Very high concentrations were measured along the Willow sub-basin's main reach, in the northwestern and central portions of the Rat sub-basin, in the eastern portion of the Stony Creek sub-basin (near where it meets the Peel River), in the northwestern portion of the Vittrekwa sub-basin as well as along the main stretch of the Trail sub-basin. 39 measurements have shown soft or very soft water, both of which could negatively impact fish populations (Weiner, 2008). Additionally 109 sites had pH values low enough to be considered potentially harmful to fish, including the northwestern portions of the Vittrekwa sub-basin.

All this taken into account, the Richardson Mountain-Peel Plateau region has pockets of water not suitable or potential harmful for fish and other aquatic life. As has been shown, retrogressive thaw slumps impact the quality of the water supply, and so, could potentially, be creating adverse hydro-geochemical conditions for the promotion of a healthy ecosystem. Below we explore the distribution of these pockets of potentially harmful water with respect to the distribution of aufeis and drinking water source for the community of Aklavik.

5.3.1 Possible impact on drinking water

Figure 49 shows where the community of Aklavik sources their water. An important portion of it comes from the Willow and Rat River sub-basins, within the Peel River basin. In red are slumps covering more than 5ha, the identified minimum slump surface area that can impact downstream geochemistry. As can be seen, southern portions of the Rat River sub-basin and the central part of the Willow River sub-basin have large slumps indicating the possibility of reduced water quality. Drinking water standards are more strict than the standards for freshwater aquatic life therefore the presence of these large slumps may impact Aklavik's drinking supply and lead to necessary changes in the way the community manages their drinking water.

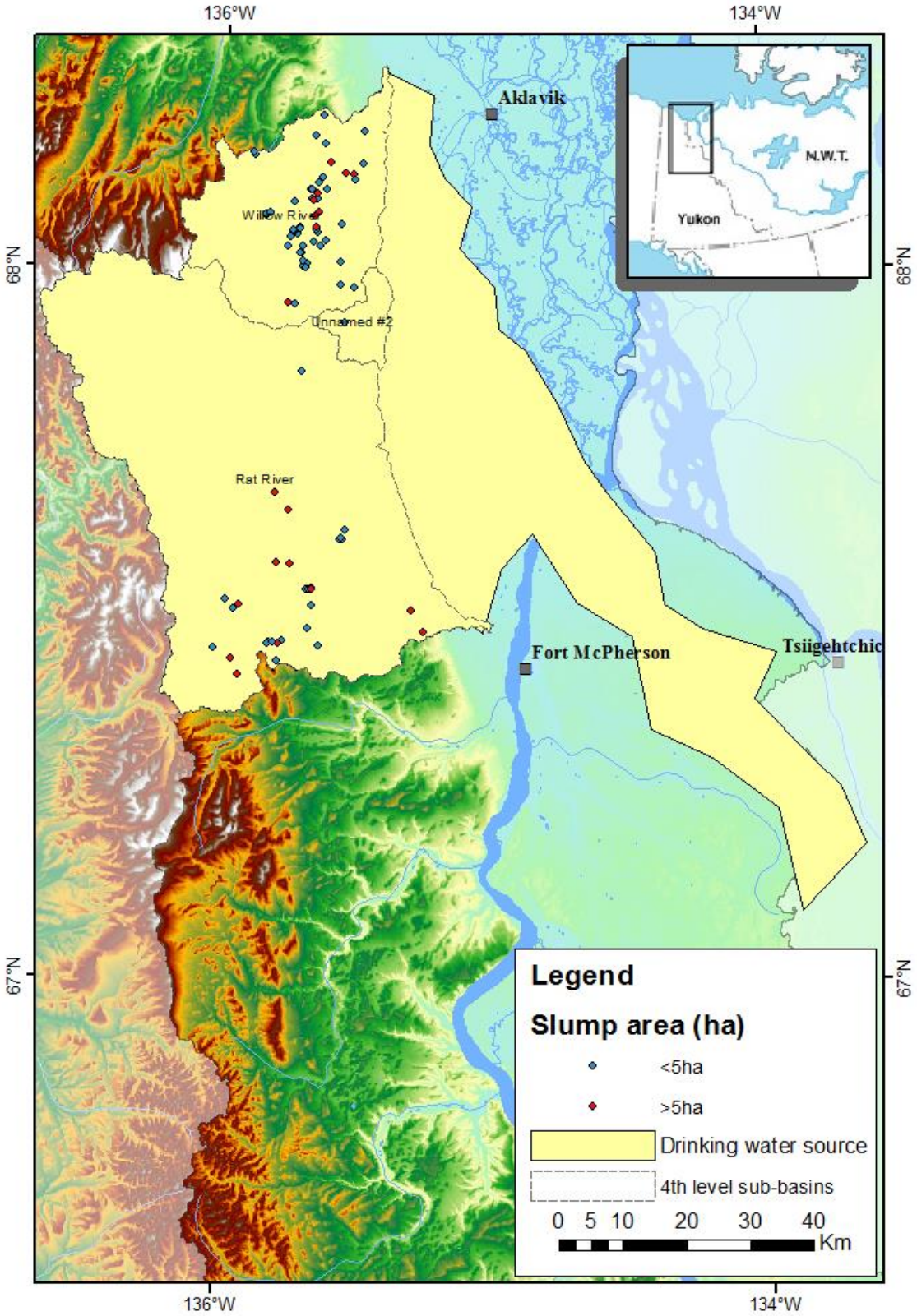

Figure 49 Area used as a source for drinking water in Aklavik (adapted from NWT Centre for Geomatics, GNWT, 2011).

Chapter 6- Summary and conclusions

This study on the impacts of thaw slumps on streams, sub-watersheds, watersheds and sub-basins has allowed a better understanding of slump distribution, stream geochemistry and the relationship between both. This study concluded that latitude plays an extremely important role in the distribution of thaw slumps. The study area's mid-latitudes (67°-68.5°N, Willow River, Rat River, Stony Creek and northern Vittrekwa sub-basins) had the highest number of slumps, the highest density of slumps as well as the largest cumulative slump area (sum of all slump area). However, in the areas further south are located the highest average surface areas, meaning the larger slumps (southern Vittrekwa River, Road River, Trail River sub-basins).

Analysis of single streams reaches demonstrated that conductivity, SO_4 and SO_4/Cl values rise immediately following a slump covering approximately 5ha or more. The larger the slump(s) along the stream, the larger the geochemical response will be. This analysis also showed that there is little to no relation between Cl and slumping. The analysis of slump's relationships with sub-watersheds, watersheds and sub-basins has shown once again that the size of individual slumps is the main factor in influencing downstream geochemistry. The R-values between average surface area and the geochemical parameters were the highest, showing the most correlation. There are not enough values at the sub-basin scale to identify trends. At the watershed level, average slump size explains up to 60% of the variation of geochemical parameters while up to 26% of the variation at the sub-watershed level is explained by slumping-acceptable levels in natural environments. This also shows that slumps have limited cumulative impact; a high number of small slumps do not have a similar impact to a small number of large slumps.

Slumping in the Richardson Mountains-Peel Plateau region has important environmental impacts. Many of the measured geochemical parameters, which increase in proximity to slumps, are outside the Canadian Council of Ministers of the Environment (CCME) standards. This means the Lower Peel basin has pockets of inadequate quality in respect to healthy freshwater aquatic life. More specifically, this unsuitable water could pose danger to fish spending months over-wintering in unfrozen water under aufeis and could lead to necessary changes in local communities' management of drinking water.

References

Arctic Climate Impact Assessment (ACIA). (2004). *Impacts of a warming arctic.* Cambridge University Press.

Bedient, P. B., Huber, W. C., & Vieux, B. E. (2008). In Stark H. (Ed.), *Hydrology and floodplain analysis* (4th ed.). New Jersey: Prentice Hall.

Bowden, W. B., Gooseff, M. N., Balser, A., Green, A., Peterson, B. J., & Bradford, J. (2008). Sediment and nutrient delivery from thermokarst features in the foothills of the North Slope, Alaska: Potential impacts on headwater stream ecosystems. *Journal of Geophysical Research, 113*(G02026), 12.

Bradford, M. J., Grout, J. A., & Moodie, S. (2001). Ecology of juvenile Chinook salmon in a small non-natal stream of the Yukon River drainage and the role of ice conditions on their distribution and survival. *Canadian Journal of Zoology, 79*, 2043-2054.

Brasseur, P., Kokelj, S., Fraser, R.,& Lacelle, D.(2014). Distribution of aufeis in eastern Yukon and adjacent Northwest Territories (Richardson and Mackenzie Mountains). Open File, Northwest Territories Geoscience Office.

Brooker, Alexander. (2014). *Investigating Changes in Retrogressive Thaw Slumps in the Richardson Mountains (Northwest Territories, Canada) based on Tasseled Cap Trend Analysis of Landsat Image Stacks.* (Master of Science in Earth Sciences, University of Ottawa).

Brooks, K. N., Folliott, P. F., Gregersen, H. M., & DeBano, L. F. (2003). *Hydrology and the management of watersheds* (3rd ed.). Iowa: Iowa State Press, A Blackwell Publishing Company.

Brown, J. (1998). In Ferrians O.J., Hegginbottom J.A. and Melnikov E. S.(Eds.), *Circum-arctic map of permafrost and ground ice conditions.* Boulder, CO: National Snow and Ice Data Center.

Brown, J., Hinkel, K.M. & Nelson, F.E. (2000). The circumpolar active layer monitoring (CALM) program: Research designs and initial results. *Polar Geography*, 24(3), 165-258.

Burn, C. R. (1997). Cryostratigraphy, paleogeography, and climate change during the early Holocene warm interval, western arctic coast, Canada. *Canadian Journal of Earth Sciences, 34*(7), 912-925.

Burn, C. R. (1998). The active layer: Two contrasting definitions. *Permafrost and Periglacial Processes, 9*(4), 411-416.

Burn, C. R. (2000). The thermal regime of a retrogressive thaw slump near Mayo, Yukon Territory. *Canadian Journal of Earth Sciences, 37*(7), 967-981.

Burn, C. R., & Kokelj, S. V. (2009). The environment and permafrost of the Mackenzie Delta area. *Permafrost and Periglacial Processes, 20*(2), 83-105.

Burn, C.R. & Friele, P.A. (1989). Geomorphology, vegetation succession, soil characteristics and permafrost in retrogressive thaw slumps near Mayo, Yukon Territory. *Arctic*, *42*, 31-40.

Burn, C.R. & Lewkowicz, A.G. (1990). Canadian Landforms Examples-17 Retrogressive Thaw Slumps, The Canadian Geographer, *34*(3), 273-276.

Canadian Council of Ministers of the Environment. (1987-2012). Canadian environmental qualitied guidelines summary table. Retrieved April 3, 2014, from http://st-ts.ccme.ca/

Canadian Council of Ministers of the Environment. (1999). *Canadian environmental quality guidelines glossary.*

Carrière, M. (2008). *Origins of Martian valley networks based on a comparative statistical analysis of Martian and terrestrial basin shape functions.* (Master of Science, University of Ottawa, Ottawa).

Catto, N.R. (1996). Richardson Mountains, Yukon-Northwest Territories: The northern portal of the postulated 'ice-free corridor'. *Quaternary International*, *32*, 3-19.

Circumpolar Active Layer Monitoring. (2012). CALM summary data table - northern hemisphere. Retrieved 01/15, 2013, from http://www.gwu.edu/~calm/data/north.html

Clark, I. D., & Lauriol, B. (1997). Aufeis of the Firth River basin, northern Yukon, Canada: Insights into permafrost hydrogeology and karst. *Arctic and Alpine Research, 29*(2), pp. 240-252.

Clark, I.D., Lauriol, B., Marschner, M., Sabourin, N., Chauret, Y., & Desrochers, A. (2004). Endostromatolites from permafrost karst, Yukon Canada : Paleoclimatic proxies for the Holocene hysithermal. *Canadian Journal of Earth Sciences, 41*, 397-399.

Day, S. J. S., Larivière, J. M., Friske, P. W. B., McNeil, R. J., Cairns, S. R., McCurdy, M. W., & Gal, L. P. (2005). *National geochemical reconnaissance, regional stream sediment and water geochemical data, Richardson Mountains, Northwest Territories (parts of NTS 106M, 107B, 116P and 117A) including analytical, mineralogical and kimberlite indicator mineral data from silts, heavy mineral concentrates and waters; geological survey of Canada* Open File 4670/Northwest Territories Geoscience Office, Contribution 0006.

Dyke, A., Andrews, J., Clark, P., England, J., Miller, G., Shaw, J., & Veillette, J. (2002). The Laurentide and Innuitian ice sheets during the last glacial maximum. *Quaternary Science Reviews, 21*(1-3), 9-31.

Ecosystem Classification Group. (2010). *Ecological regions of the Northwest Territories – Cordillera.* Yellowknife, NT, Canada: Department of Environment and Natural Resources, Government of the Northwest Territories.

Environment Canada. (2013). Climate normal and averages. Retrieved 06/05, 2013, from http://climate.weatheroffice.gc.ca/climate_normals/index_e.html

Environmental Systems Research Institute (ESRI). (2001). ArcGIS geostatistical analyst: Statistical tools for data exploration, modelling and advanced surface generation. Retrieved 05/21, 2013, from http://www.esri.com/~/media/Files/Pdfs/library/whitepapers/pdfs/geostat.pdf

ESRI. (2012). *ArcGIS 10.1.*

French, H. (2007). *The periglacial environment* (3rd ed.). New York: John Wiley & Sons, Ltd.

Frey, K., E., & McClelland, J., W. (2009). Impacts of permafrost degradation on Arctic River biogeochemistry. *Hydrological Processes, 23*(1), 169-182.

Gold, L. W., & Lachenbruch, A. H. (1973). Thermal conditions in permafrost-A review of North American literature. *Permafrost: The North American Contribution to the Second International Conference.* National Academy of Sciences, 3-23.

Heginbottom, J. A., Dubreuil, M. A., & Harker, P. A. (1995). *Canada-permafrost. in National Atlas of Canada, 5th ed. National Atlas information service* (Plate 2.1 MCR 4177 ed.). Natural Resources Canada, Ottawa.

Hill, .R., Mudie, P.J., Moran, K., & Blasco, S.M. (1985). A sea-level curve for the Canadian Beaufort shelf. *Canadian Journal of Earth Sciences, 22,* 1383-1393.

Jorgenson, M. T., Shur, Y. L., & Pullman, E. R. (2006). Abrupt increase in permafrost degradation in arctic Alaska. *Geophysical Research Letters, 33*(2).

Kane, D. L. (1981). Physical mechanics of aufeis growth. *Canadian Journal of Civil Engineering, 8*, 186-195.

Kauffmann, D.S., Ager, T.A., Anderson, N.J., Anderson, P.M., Andrews, J.T., Bartlein, P.J., Brubaker, L.B., Coats, L.L., Cwynar, L.C., Duvall, M.L., Dyke, A.S., Edwards, M.E., Eisner, W.R., Gajewski, K., Geirsdottir, A., Hu, F.S., Jennings, A.E., Kaplan, M.R., Kerwin, M.W., Lozhkin, A.V., MacDonald, G.M., Miller, G.H., Mock, C.J., Oswald, W.W., Otto-Bliesner, B.L., Porinchu, D.F., Ruhland, K., Smol, J.P., Steig, E.J., & Wolfe, B.B. (2004). Holocene thermal maximum in the western Arctic (0-180°W). *Quaternary Science Reviews, 23(5-6)*, 529-560

Keller, K., Blum, J. D., & Kling, G. W. (2007). Geochemistry of soils and streams on surfaces of varying ages in arctic Alaska. *Arctic, Antarctic and Alpine Research, 39*(1), 84-98.

Keller, K., Blum, J. D., & Kling, G. W. (2010). Stream geochemistry as an indicator of increasing permafrost thaw depth in an arctic watershed. *Chemical Geology, 273*(1-2), 76-81.

Kokelj, S. V., Lacelle, D., Lantz, T. C., Tunnicliffe, J., Malone, L., Clark, I. D., & Chin, K. S. (2013). Thawing of massive ground ice in mega slumps drives increases in stream sediment and solute flux across a range of watershed scales. *Journal of Geophysical Research: Earth Surface, 118*, 1-

Kokelj, S. V., & Lewkowicz, A. G. (1999). Salinization of permafrost terrain due to natural geomorphic disturbance, Fosheim peninsula, Ellesmere Island. *Arctic, 52*(4), 372-385.

Kokelj, S. V., & Burn, C. R. (2005). Geochemistry of the active layer and near-surface permafrost, Mackenzie Delta region, Northwest Territories, Canada. *Canadian Journal of Earth Sciences, 42*, 37-48.

Kokelj, S. V., & Burn, C. R. (2005). Near-surface ground ice in sediments of the Mackenzie Delta, Northwest Territories, Canada. *Permafrost and Periglacial Processes, 16*(3), 291-303.

Kokelj, S. V., Jenkins, R. E., Milburn, D., Burn, C. R., & Snow, N. (2005). The influence of thermokarst disturbance on the water quality of small upland lakes, Mackenzie Delta region, Northwest Territories, Canada. *Permafrost and Periglacial Processes, 16*(4), 343-353.

Kokelj, S. V., Lantz, T. C., Kanigan, J., Smith, S. L., & Coutts, R. (2009). Origin and polycyclic behaviour of tundra thaw slumps, Mackenzie Delta region, Northwest Territories, Canada. *Permafrost and Periglacial Processes, 20*(2), 173-184.

Kokelj, S.V. & Jorgenson, M.T. (2013) Advances in Thermokarst Research. *Permafrost and Periglacial Processes*, 24(2), 108-119.

Kokelj, S. V., Zajdlik, B., & Thompson, M. S. (2009). The impacts of thawing permafrost on the chemistry of lakes across the subarctic boreal-tundra transition, Mackenzie Delta region, Canada. *Permafrost and Periglacial Processes, 20*(2), 185-199.

Kokelj, S.V., Tunnicliffe, J., Lacelle, D., Lantz, T.C., Chin, K., & Fraser, R. (in review). Increased precipitation drives mega-slumps development and destabilization of ice-rich permafrost terrain, northwestern Canada.

Lacelle, D., Bjornson, J., Lauriol, B., Clark, I. D., & Troutet, Y. (2004). Segregated-intrusive ice of subglacial meltwater origin in retrogressive thaw flow headwalls, Richardson Mountains, NWT, Canada. *Quaternary Science Reviews, 23*(5-6), 681-696.

Lacelle, D., Lauriol, B., Zazula, G. D., Bassam, G., Utting, N., & Clark, I. D. (2013). Timing of advance and basal condition of the Laurentide ice sheet during the last glacial maximum, Richardson mountains, NWT. *Quaternary Research, 80(2),* 274-283.

Lacelle, D., Bjornson, J., & Lauriol, B. (2010). Climatic and geomorphic factors affecting contemporary (1950-2004) activity of retrogressive thaw slumps on the Aklavik plateau, Richardson Mountains, NWT, Canada. *Permafrost and Periglacial Processes, 21*(1), 1-15.

Lacelle, D., Brooker, A., Fraser, R.H., Kokelj, S.V. (in review). Effect of terrain factors and solar radiation on the distribution and growth of thaw slumps (1985-2011) in the Richardson Mountains-Peel Plateau region, northwestern Canada.

Lamirande, I., Lauriol, B., Lalonde, A. E., & Clark, I. D. (1999). La production de limon sur les terrasses de cryoplanation dans les monts Richardson, Canada. *Canadian Journal of Earth Sciences, 36*(10), 1645-1654.

Lamoureux, S. F., & Lafrenière, M. J. (2009). Fluvial impact of extensive active layer detachments, Cape Bounty, Melville Island, Canada. *Arctic, Antarctic, and Alpine Research, 41*(1), 59-68.

Lantuit, H., & Pollard, W. H. (2008). Fifty years of coastal erosion and retrogressive thaw slump activity on Herschel Island, southern Beaufort sea, Yukon Territory, Canada. *Geomorphology, 95*(1-2), 84-102.

Lantuit, H., Pollard, W. H., Couture, N., Fritz, M., Schirmeister, L., Meyer, H., & Hubberten, H. W. (2012). Modern and late Holocene retrogressive thaw slump activity on the Yukon coastal plain and Herschel Island, Yukon Territory, Canada. *Permafrost and Periglacial Processes, 23*(1), 39-51.

Lantz, T. C., & Kokelj, S. V. (2008). Increasing rates of retrogressive thaw slump activity in the Mackenzie Delta region, N.W.T., Canada. *Geophysical Research Letters, 35*(6).

Lauriol, B., Duguay, C. R., & Riel, A. (2002). Response of the Porcupine and Old Crow rivers in northern Yukon, Canada, to Holocene climatic change. *The Holocene, 12*(1), 27-34.

Lauriol, B., Cabana, Y., Cinq-Mars, J., Geurts, M., & Grimm, F. W. (2002). Cliff-top eolian deposits and associated molluscan assemblages as indicators of late Pleistocene and Holocene environments in Beringia. *Quaternary International, 87*, 59-79.

Lewis, T., Lafrenière, M. J., & Lamoureux, S. F. (2012). Hydrochemical and sedimentary responses of paired high Arctic watersheds to unusual climate and permafrost disturbance, Melville Island, Canada. *Hydrological Processes, 26*(13), 2003-2018.

Lewkowicz, A. G. (1985). Use of ablatometer to measure short-term ablation of exposed ground ice. *Canadian Journal of Earth Sciences, 22*, 1767-1773.

Lewkowicz, A. G. (1987). Headwall retreat of ground-ice slumps, Banks Island, Northwest Territories. *Canadian Journal of Earth Sciences, 24*(6), 1077-1085.

Lewkowicz, A. G. (2007). Dynamics of active-layer detachment failures, Fosheim Peninsula, Ellesmere Island, Nunavut, Canada. *Permafrost and Periglacial Processes, 18*, 89-103.

Lewkowicz, A. G., Bonnaventure, P. P., Smith, S. L., & Kuntz, Z. (2012). Spatial and thermal characteristics of mountain permafrost, northwest Canada. *Geografiska Annaler, Series A: Physical Geography, 94*(2), 195-213.

Lumb, A., Halliwell, D., & Sharma, T. (2006). Application of CCME water quality index to monitor water quality: A case of the Mackenzie River basin, Canada. *Environmental Monitoring and Assessment, 113*, 411-429.

Malone, L. (2013). *Impacts of retrogressive thaw slumps on the geochemistry of periglacial streams: Identifying a geochemical tracer of slump runoff at the watershed-scale.* (Master of Science in Earth Sciences, University of Ottawa).

Malone, L., Lacelle, D., Kokelj, S., & Clark, I. D. (2013). Impacts of hillslope thaw slumps on the geochemistry of permafrost catchments (Stony Creek watershed, NWT, Canada). *Chemical Geology, 356*, 38-49.

Mackay, J. R. & Dallimore, S.R.. (1992). Massive ice of the Tuktoyaktuk area, western Arctic coast, Canada. *Canadian Journal of Earth Sciences*, 29, 1235-1249.

McCammon, B. P., & USDA-Forest Service, Pacific Northwest Region. (2012). Recommended watershed terminology. Retrieved 08/28, 2014, from http://www.watershed.org/?q=node/187

Mesquita, P. S., Wrona, F. J., & Prowse, T.,D. (2010). Effects of retrogressive permafrost thaw slumping on sediment chemistry and submerged macrophytes in arctic tundra lakes. *Freshwater Biology, 55*(11), 2347-2358.

Muller, S. W. (1943). *Permafrost of permanently frozen ground and related engineering problems.* U.S. Geological Survey Report.

Murton, J. B. (1996). Thermokarst-lake-basin sediments, Tuktoyaktuk coastlands, western Arctic Canada. *Sedimentology, 43*(4), 737-760.

Murton, J. B. (2001). Thermokarst sediments and sedimentary structures, Tuktoyaktuk coastlands, western Arctic Canada. *Global and Planetary Change, 28*(1-2), 175-192.

Natural Resource Conservation Service - Iowa. (2008). *Watershed boundary dataset, twelve-digit hydrologic units (sub-watersheds) with hydrologic relevance in Iowa* (WBD edition 1; NRGIS edition 20110131 ed.). Fort Worth, Texas: U. S. Department of Agriculture, Natural Resources Conservation Service.

Natural Resource Conservation Service - United States Department of Agriculture. (2007). *Watersheds, hydrologic units, hydrologic unit codes, watershed approach, and rapid watershed assessments* (http://www.nrcs.usda.gov/Internet/FSE_DOCUMENTS/stelprdb1042207.pdf ed.)

Natural Resources Canada. (2005). National air photo library. Retrieved, 2013, from http://napl.cits.nrcan.gc.ca/wes/ClientDisplay/startEnglishClient.jsp?wes_portal_language_id=en_US&showLogin=null&width=1024&height=768

Norris, D. (1984). *Geology of the northern Yukon and northwest district of Mackenzie, 1:500,000*. Ottawa: Geological Survey of Canada. map1581A.

Northwest Territories Centre for Geomatics. (2011). Aklavik – Drinking Water Source Watershed map. Retrieved 07/09/2014, from http://www.geomatics.gov.nt.ca/maps/Aklavik_2011_LegendLimited_low.jpp

Osterkamp, T. E., & Romanovsky, V. E. (1999). Evidence for warming and thawing of discontinuous permafrost in Alaska. *Permafrost and Periglacial Processes, 10*(1), 17-37.

Rampton, V. N. (1982). *Quaternary geology of the Yukon coastal plain.* (No. Bulletin 317). Canada: Geological Survey of Canada.

Ritchie, J. C., Cwynar, L. C., & Spear, R. W. (1983). Evidence from north-west Canada for an early Holocene Milankovitch thermal maximum. *Nature, 305*(5930), 126-128.

Romanovsky, V. E., S. L. Smith, & H. H. Christiansen. (2010). Permafrost Thermal State in the Polar Northern Hemisphere during the International Polar Year 2007-2009: a synthesis. *Permafrost and Periglacial Processes*, 21, 106-116.

Rowland, J. C., Jones, C. E., Altmann, G., Bryan, R., Crosby, B. T., Hinzman, L.D., Kane, D.L., Lawrence, D.M., Mancino, A., Marsh, P., McNamara, J.P, Romanovsky, V.E., Toniolo, H., Travis, B.J., Trochim, E., Wilson, C. J. & Geernaert, G. L., (2010). Arctic landscapes in transition: Responses to thawing permafrost. *Eos, 91*(26), 229-230.

Simard, C. (2008). In Bianca Lam (Ed.), *Méthodes quantitatives: Approche progressive pour les sciences humaines* (4th edition ed.). Quebec: Modulo.

Smith, S. L., Romanovsky, V. E., Lewkowicz, A. G., Burn, C. R., Allard, M., Clow, G. D., Yoshikawa, K. & Throop, J. (2010). Thermal state of permafrost in North America: A contribution to the international polar year. *Permafrost and Periglacial Processes, 21*(2), 17-135.

United States Environmental Protection Agency (EPA). (2012). Water: Monitoring and assessment, 5.9 Conductivity. Retrieved 11/07, 2014, from http://water.epa.gov/type/rsl/monitoring/vms59.cfm

van Everdingen, R. O. (1976). Geocryological terminology. *Canadian Journal of Earth Sciences, 13*(6), 862-867.

Weiner, E. R. (2008). *Applications of environmental aquatic chemistry: A practical guide* (Second ed.). Florida: CRC Press Taylor and Francis Group.

Zazula, G. D., MacKay, G., Andrews, T. D., Shapiro, B., Letts, B., & Brock, F. (2009). A late Pleistocene steppe bison (*bison priscus*) partial carcass from Tsiigehtchic, Northwest Territories, Canada. *Quaternary Science Reviews, 28*(25-26), 2734-2742.

Appendix A: Hydro-geochemistry results

Year	Sample #	Latitude	Longitude	pH	Conductivity (µS/cm)	Al (ppm)	As (ppm)	Ca (ppm)	Cl (ppm)	Fe (ppm)	K (ppm)	Mg (ppm)	Na (ppm)	NO3 (ppm)	S (ppm)	SO4 (ppm)	Zn (ppm)
2010	**10-LM-01**	67.25505	-135.242	7.64	184.4	0.130	-	20.050	0.400	0.340	1.830	6.930	4.610	<0.025	-	50.380	-
2010	**10-LM-04**	67.2554	135.2484	8.1	108.9	0.050	-	14.180	0.195	0.430	0.550	3.130	1.570	<0.025	-	20.380	-
2010	**10-LM-05**	67.25419	-135.247	7.79	219.6	0.080	-	26.960	0.360	0.250	2.560	10.280	7.370	0.140	-	84.990	-
2010	**10-LM-06**	67.2635	135.219	7.06	664	-	-	107.370	0.740	<0.006	3.460	24.620	21.180	1.010	-	318.000	-
2010	**10-LM-10**	67.2586	135.2376	6.4	77.3	0.020	-	61.820	0.183	0.020	0.590	16.170	5.980	<0.025	-	24.530	-
2010	**10-LM-11**	67.2568	135.2367	6.92	2025	-	-	517.630	1.830	0.016	11.140	118.380	57.150	3.540	-	1782.000	-
2010	**10-LM-12**	67.2546	135.2307	6.82	1326	-	-	246.570	1.510	0.009	9.140	63.340	45.030	0.160	-	865.000	-
2010	**10-LM-14**	67.2519	135.2632	7.815	302	-	-	46.190	0.620	0.073	2.980	16.010	8.960	1.240	-	123.000	-
2010	**10-LM-16**	67.2521	135.2738	7.07	73.4	0.110	-	6.790	0.271	0.930	0.460	3.010	1.290	<0.025	-	21.510	-
2010	**10-LM-17**	67.2536	135.2732	7.1	95	-	-	14.280	1.260	0.557	1.160	6.230	3.390	0.570	-	34.000	-
2010	**10-LM-19**	67.253	135.2718	6.675	1352.5	-	-	167.750	3.110	0.013	12.660	54.320	70.710	0.060	-	648.000	-
2010	**10-LM-20**	67.2536	135.2732	7.21	2017	-	-	250.540	4.850	0.077	11.180	86.480	84.910	0.070	-	1100.000	-
2010	**10-LM-21**	67.2511	135.2726	7.35	226	0.070	-	14.510	7.511	0.340	1.610	11.710	13.450	0.040	-	52.360	-
2010	**10-LM-24**	67.23465	-135.237	7.72	230	0.030	-	25.850	0.380	0.060	1.030	7.770	6.810	0.020	-	56.580	-
2010	**10-LM-25**	67.2436	135.2768	7.36	143.6	0.120	-	14.590	0.818	1.110	1.530	6.640	4.640	<0.025	-	28.590	-
2010	**10-LM-26**	67.2322	134.5535	7.67	339	0.020	-	40.470	1.602	<0.006	0.550	15.750	3.360	0.160	-	63.040	-
2010	**10-LM-27**	67.25333	-134.549	7.94	331	0.030	-	40.970	1.830	<0.0006	0.890	15.920	3.340	0.140	-	62.990	-
2010	**10-LM-29**	67.2635	135.219	6.78	1464	-	-	232.020	2.500	<0.006	6.160	55.550	57.180	0.070	-	807.000	-
2010	**10-LM-30**	67.2568	135.2367	6.86	2700	-	-	537.010	3.800	<0.006	11.330	130.180	61.200	0.110	-	1866.000	-
2010	**10-LM-31**	67.2546	135.2307	7.03	1700	-	-	326.460	1.510	<0.006	10.280	80.500	45.960	0.070	-	1167.000	-
2010	**10-LM-32**	67.2285	134.5494	7.38	166	0.030	-	18.390	0.167	0.360	0.760	5.830	3.850	0.930	-	33.990	-
2010	**10-LM-33**	67.27123	-135.293	7.97	770	0.020	-	101.670	0.580	na	2.260	30.780	22.170	0.930	-	282.380	-
2010	**10-LM-36**	67.2713	135.3727	7.78	122.5	0.030	-	11.030	0.156	0.460	0.700	4.730	3.430	0.130	-	34.340	-
2010	**10-LM-37**	67.1368	-135.168	7.5	682	0.260	-	89.820	0.740	0.660	2.970	23.910	27.710	<0.025	-	295.940	-
2010	**10-LM-38**	67.3242	-135.142	7.83	267	0.080	-	31.960	1.870	0.220	1.090	8.640	7.040	<0.025	-	60.430	-
2010	**10-LM-39**	67.2519	135.2671	7.64	868	-	-	99.500	1.760	0.163	5.060	37.770	28.420	2.140	-	417.000	-
2010	**10-LM-40**	67.2625	135.5268	6.86	114.2	0.050	-	11.740	0.484	0.550	0.750	5.310	2.690	0.070	-	36.040	-
2010	**10-LM-41**	67.2536	135.2732	7	2893	-	-	342.530	7.410	0.015	15.420	118.750	118.330	0.550	-	1594.000	-

2010	**10-LM-42**	67.2529	135.271	7.1	2352	-	-	280.460	5.380	0.010	13.830	106.760	75.580	0.030	-	1355.000	-
2010	**10-LM-43**	67.5203	135.3034	6.79	362	0.060	-	23.760	10.538	10.690	2.450	16.540	17.880	0.110	-	50.910	-
2010	**10-LM-61**	67.2519	135.2671	7.13	159.8	-	-	18.540	4.360	0.259	1.230	6.930	4.330	0.390	-	62.590	-
2010	**10-LM-62**	67.252	135.2717	8.52	2515	-	-	338.020	3.600	0.138	13.270	124.580	93.060	<0.025	-	1390.360	-
2010	**10-LM-63**	67.253	135.2718	7.02	1495	-	-	145.580	5.620	0.046	13.270	53.680	100.430	0.120	-	797.060	-
2010	**10-LM-64**	67.5203	135.3034	6.88	118.8	0.090	-	10.670	0.534	0.270	0.400	4.400	14.650	<0.025	-	40.720	-
2011	**11-LM-10**	67.2519	135.2774	4.89	15.72	0.150	-	1.430	0.403	0.430	0.770	0.490	0.520	<0.025	-	1.960	0.014
2011	**11-LM-12**	67.2521	135.2738	5.48	16.77	0.140	-	1.580	0.486	0.340	0.920	0.550	0.510	<0.025	-	1.400	0.015
2011	**11-LM-13**	67.2518	135.2728	6.76	39.4	0.110	-	3.510	0.747	0.780	0.790	1.410	1.120	<0.025	-	9.340	0.009
2011	**11-LM-14**	67.2518	135.2619	6.96	135.4	-	-	23.740	1.080	0.283	2.530	7.510	6.230	1.020	-	61.000	-
2011	**11-LM-15**	67.252	135.2656	7.15	140	-	-	21.110	1.070	0.237	2.190	7.280	5.850	1.230	-	56.000	-
2011	**11-LM-16**	67.2522	135.2721	6.89	813	-	-	90.210	1.900	0.008	8.590	25.030	42.500	0.380	-	373.000	-
2011	**11-LM-17**	67.2545	135.2738	6.88	1062	-	-	118.050	2.640	<0.006	10.660	36.480	69.660	0.340	-	554.000	-
2011	**11-LM-18**	67.252	135.2738	8.07	248.5	0.020	-	19.850	0.246	0.020	0.720	9.860	5.300	<0.025	-	80.270	<0.003
2011	**11-LM-20**	67.2644	135.2159	7.76	537	-	-	60.320	0.940	<0.006	2.440	17.300	12.210	0.430	-	206.000	-
2011	**11-LM-21**	67.2621	135.2308	8.12	179.7	-	-	28.000	0.470	0.211	1.290	6.140	3.450	0.360	-	72.000	-
2011	**11-LM-22**	67.2569	135.2369	7.3	1943	-	-	609.560	2.000	<0.006	11.860	117.460	65.980	0.270	-	1897.000	-
2011	**11-LM-23**	67.2542	135.2311	7.23	1841	-	-	606.580	2.320	0.007	11.590	138.970	69.340	0.270	-	1905.000	-
2011	**11-LM-41**	67.2644	135.2159	8.01	519	-	-	64.080	0.840	-	2.770	14.180	11.440	0.390	-	201.000	-
2011	**11-LM-43**	67.2644	135.2159	7.79	500	-	-	78.920	1.100	-	2.520	15.900	18.290	0.850	-	232.000	-
2011	**11-LM-44**	67.2644	135.2159	8.2	620	-	-	60.010	0.160	0.127	1.650	25.200	12.720	0.440	-	242.000	-
2011	**11-LM-45**	67.2589	135.2362	7.71	389	-	-	57.620	3.810	0.049	2.080	12.250	8.040	0.550	-	189.000	-
2011	**11-LM-46**	67.2569	135.2369	7.47	2075	-	-	610.040	1.760	-	11.090	112.700	59.620	0.310	-	1738.000	-
2011	**11-LM-49**	67.2518	135.2728	6.82	37.7	0.130	-	3.400	0.165	0.480	0.460	1.540	1.410	<0.025	-	9.510	0.006
2011	**11-LM-50**	67.2545	135.2738	8.01	2379	-	-	332.500	4.760	-	10.480	92.410	93.020	5.040	-	1287.000	-
2011	**11-LM-51**	67.252	135.2656	8.14	1219	-	-	152.280	1.950	0.007	4.980	42.720	34.030	0.250	-	585.000	-
2011	**11-LM-52**	67.2518	135.2619	8.56	112	-	-	14.230	0.430	0.465	1.300	5.060	3.240	0.290	-	46.000	-
2011	**11-LM-53**	67.25419	-135.247	5.86	122.7	0.170	-	13.480	0.760	0.500	1.490	4.570	3.760	0.350	-	41.540	0.006
2011	**11-LM-55**	67.25505	-135.242	6.8	168.5	0.120	-	14.380	1.260	0.520	1.700	4.100	2.410	0.450	-	44.430	0.007
2011	**11-LM-56**	67.25419	-135.247	6.76	157.1	0.190	-	16.760	1.160	0.640	1.590	5.580	4.050	0.650	-	59.530	0.004

2011	**11-LM-58**	67.2644	135.2159	6.94	460	-	-	67.030	0.440	0.086	2.690	13.000	8.640	0.220	-	195.000	-
2011	**11-LM-60**	67.2569	135.2369	7.14	1920	-	-	605.850	2.330	-	10.880	130.920	64.160	0.250	-	1883.000	-
2011	**11-LM-61**	67.2542	135.2311	6.77	1829	-	-	614.650	8.375	-	20.720	133.370	66.240	1.010	-	2078.000	-
2011	**11-LM-63**	67.25419	-135.247	6.41	133.6	0.090	-	18.270	0.870	0.400	1.170	7.020	6.030	0.460	-	64.010	0.019
2011	**11-LM-64**	67.2536	135.2393	6.77	139.5	0.110	-	27.150	0.158	0.430	0.490	5.060	0.490	0.650	-	46.630	0.003
2011	**11-LM-65**	67.25662	-135.24	5.84	180.3	0.150	-	28.360	0.560	0.300	0.990	8.190	4.900	0.390	-	101.380	0.036
2011	**11-LM-66**	67.2569	135.2369	7.4	1330	-	-	605.400	1.668	0.018	12.810	124.580	72.680	<0.025	-	1863.000	-
2011	**11-LM-67**	67.2578	135.2379	7.03	342	-	-	76.740	0.419	0.010	2.500	14.950	7.540	0.410	-	199.000	-
2011	**11-LM-68**	67.2588	135.2378	5.74	136.6	0.630	-	17.750	0.134	0.890	0.310	4.990	4.100	0.340	-	61.840	0.070
2011	**11-LM-69**	67.2606	135.2356	4.45	154.5	0.510	-	22.110	0.150	0.760	0.770	5.560	1.280	4.860	-	75.600	0.053
2011	**11-LM-70**	67.2578	135.2379	6.75	203.8	-	-	32.740	0.470	0.286	1.150	8.960	5.070	0.410	-	100.000	-
2011	**11-LM-71**	67.25596	-135.24	6.71	200.3	0.100	-	31.700	0.370	0.350	0.980	8.590	4.950	0.380	-	99.040	0.008
2011	**11-LM-72**	67.2578	135.2379	7.18	2214	-	-	583.280	1.878	0.015	12.630	118.420	67.750	-	-	1770.000	-
2011	**11-LM-73**	67.25596	-135.24	7.17	155.8	0.070	-	25.470	0.390	0.430	0.970	7.120	4.840	-	-	69.800	0.008
2011	**11-LM-74**	67.2528	135.2717	6.72	1121	-	-	199.380	2.500	0.007	9.790	61.500	62.560	2.760	-	757.000	-
2011	**11-LM-74B**	67.2524	135.274	6.08	50.8	0.180	-	6.350	0.594	1.140	0.300	2.870	1.850	-	-	42.610	0.011
2011	**11-LM-74C**	67.253	135.273	5.78	1317	-	-	233.340	3.990	0.010	12.360	70.090	81.930	2.220	-	942.000	-
2011	**11-LM-75**	67.2961	-135.175	7.64	352	0.010	-	81.800	0.180	0.020	3.290	15.770	13.640	0.110	-	182.760	0.001
2011	**11-LM-77**	67.2961	-135.175	7.66	300	0.020	-	69.590	0.280	0.060	2.880	13.350	11.360	0.340	-	143.170	0.000
2011	**11-LM-78**	67.3275	-135.122	7.57	169.5	0.050	-	39.610	0.350	0.200	1.500	8.020	7.000	0.340	-	76.560	0.001
2011	**11-LM-80**	67.3373	-135.083	7.62	180.3	0.040	-	37.480	0.230	0.140	1.420	10.210	5.740	0.330	-	87.360	0.003
2011	**11-LM-81**	67.3878	-134.924	7.49	208.6	0.020	-	44.660	0.430	0.070	1.540	11.220	7.060	0.450	-	100.350	0.003
2011	**11-LM-82**	67.33799	-134.874	7.82	261.7	0.030	-	59.000	0.980	0.020	0.780	15.740	5.540	0.190	-	81.840	-
2013	**13-cp-1**	67.18027	-135.727	-	-	0.080	0.001	8.200	0.430	0.173	0.029	2.732	1.488	-	5.839	13.690	0.022
2013	**13-cp-4**	67.17715	-135.725	-	-	0.010	-	33.590	0.110	-	1.460	15.400	2.000	-	27.800	91.340	-
2013	**13-cp-7**	67.25219	-135.274	-	-	0.111	-	16.660	0.830	0.799	0.928	5.937	4.710	-	13.155	33.130	0.019
2013	**13-cp-10**	67.74394	-135.46	7.3	339	0.030	-	68.380	3.490	0.026	1.782	20.387	15.356	3.090	58.203	156.590	0.020
2013	**13-cp-12**	67.70822	-135.463	7.1	339	0.050	-	127.880	0.790	-	13.170	35.860	59.540	-	168.130	608.730	0.010
2013	**13-cp-14**	67.66671	-135.443	7.4	346	0.007	-	68.190	2.360	0.010	1.071	19.921	13.461	0.500	60.392	159.540	0.009
2013	**13-cp-16**	67.66869	-135.556	7.1	353	0.020	-	55.230	2.440	-	1.150	18.480	10.270	0.350	56.850	192.020	-
2013	**13-cp-18**	67.66807	-135.666	7.3	372	0.030	-	63.090	3.300	-	1.490	19.880	12.330	0.370	63.980	216.300	-

2013	**13-cp-19**	67.63116	-135.683	6.7	254	0.010	-	32.950	0.400	-	1.020	14.790	9.820	-	41.640	138.160	-
2013	**13-cp-20**	67.66451	-135.732	6.4	192	0.020	-	31.570	0.210	-	0.940	13.040	5.000	-	36.850	120.680	-
2013	**13-cp-21**	67.67781	-135.73	7.1	375	0.019	-	75.200	3.260	0.005	1.350	23.235	14.486	0.150	69.105	179.640	0.025
2013	**13-cp-22**	67.71595	-135.87	7.1	432	0.040	-	66.810	2.770	-	0.980	21.560	10.950	-	67.550	222.970	-
2013	**13-cp-23**	67.73087	-135.298	7.1	405	0.030	-	68.190	1.880	-	0.780	19.720	11.690	-	65.630	218.590	-
2013	**13-cp-24**	67.34444	-135.058	7.63	285.9	0.020	-	37.800	0.700	-	1.240	12.930	10.880	-	39.360	124.120	-
2013	**13-cp-25**	67.35261	-135.379	7.6	281.4	0.005	0.003	41.210	0.790	0.004	1.922	15.247	12.714	-	42.619	108.570	0.029
2013	**13-cp-26**	67.35261	-135.349	7.56	280.9	-	-	35.210	0.800	-	1.810	13.620	11.210	-	40.440	131.840	0.040
2013	**13-cp-27**	67.28628	-135.338	7.6	252.5	0.010	-	33.370	0.590	0.010	1.000	10.390	10.600	-	31.770	95.310	-
2013	**13-cp-28**	67.36725	-135.389	7.67	269	0.010	-	37.690	0.250	-	1.210	14.360	9.320	-	42.930	132.800	-
2013	**13-cp-29**	67.34978	-135.482	7.6	226	0.010	-	31.930	0.320	-	1.360	13.210	8.570	-	38.300	119.050	-
2013	**13-cp-30**	67.30475	-135.55	7.5	240	0.010	-	39.790	0.150	-	2.000	14.200	9.140	0.030	43.680	137.630	-
2013	**13-cp-31**	67.24506	-135.764	7.6	295	0.007	-	65.600	0.310	0.002	1.206	16.165	5.455	-	55.757	145.820	0.001
2013	**13-cp-32**	67.29628	-135.175	7.5	785	0.070	-	215.380	0.570	-	5.100	37.910	37.770	-	215.960	718.110	0.010
2013	**13-cp-33**	67.32814	-135.11	7.9	297	0.010	0.010	45.820	0.500	-	1.770	15.100	11.880	-	47.250	147.740	0.020
2013	**13-cp-34**	66.63178	-134.652	7.52	714	0.040	0.010	94.970	0.650	-	1.750	29.950	30.630	-	109.380	361.090	-
2013	**13-cp-35**	66.57686	-134.771	8.13	608	0.040	-	89.640	0.880	-	1.720	26.050	24.880	-	92.590	297.130	-
2013	**13-cp-36**	66.55547	-135.009	7.49	585	0.040	-	85.140	0.930	-	1.500	24.780	22.760	-	85.720	276.570	0.020
2013	**13-cp-37**	66.55122	-135.083	7.93	588	0.023	0.006	97.210	0.790	-	1.952	28.695	26.819	0.020	83.394	218.680	0.006
2013	**13-cp-38**	66.53475	-135.134	7.12	567	0.010	-	39.860	0.620	-	1.820	26.090	51.020	-	101.560	338.720	0.080
2013	**13-cp-39**	66.53231	-135.31	5.99	174.3	0.060	-	16.030	0.100	0.090	1.020	8.000	9.860	0.010	29.710	94.200	0.060
2013	**13-cp-40**	66.45525	-135.265	8.05	484.4	0.030	0.010	82.120	0.310	-	0.800	24.410	6.670	-	72.840	236.370	-
2013	**13-cp-41**	66.50897	-135.126	7.98	553	0.030	-	74.100	0.750	-	1.270	22.390	13.590	-	69.840	240.610	-
2013	**13-cp-42**	67.15697	-135.146	7.8	585	0.030	-	66.940	1.080	-	2.010	26.180	20.290	-	83.660	297.280	-
2013	**13-cp-43**	67.18333	-135.24	7.85	587	0.008	-	82.440	1.190	-	2.624	32.215	27.117	0.020	89.669	238.070	0.006
2013	**13-cp-44**	67.18475	-135.275	7.76	794	0.030	-	76.350	1.100	-	2.090	29.440	56.800	-	122.780	435.480	-
2013	**13-cp-45**	67.15014	-135.282	7.86	588	0.020	-	69.640	1.100	-	2.030	28.460	20.360	-	90.660	297.860	-
2013	**13-cp-46**	67.11833	-135.374	7.83	578	0.020	-	71.810	1.210	-	2.270	28.360	20.190	-	92.550	308.620	-
2013	**13-cp-47**	67.12814	-135.461	7.27	790	-	-	89.600	1.700	0.001	4.013	39.594	76.881	0.040	151.275	413.840	0.020

Appendix B. Results per drainage unit.

Sub-basin

BFR

parameter	# samples	median	mean	standard deviation
conductivity	8	80.0	93.8	54.5
SO4	8	35.0	41.5	26.3
Cl	2	0.1	0.1	0.0
SO4/Cl	2	140.9	140.9	96.5
pH	8	5.5	5.3	0.7
# of slumps	8			

Rat

parameter	# samples	median	mean	standard deviation
conductivity	198	120.0	182.8	485.0
SO4	199	43.3	95.9	396.5
Cl	52	0.3	1.3	1.6
SO4/Cl	52	70.0	195.5	188.5
pH	8	6.9	6.7	1.1
# of slumps	30			

Stony Creek

parameter	# samples	median	mean	standard deviation
conductivity	192	283.7	555.3	635.1
SO4	88	123.6	430.4	601.6
Cl	82	0.8	1.5	1.8
SO4/Cl	185	72.4	112.1	164.5
pH	190	7.0	6.8	1.2
# of slumps	45			

Trail

parameter	# samples	median	mean	standard deviation
conductivity	8	576.0	534.2	148.6
SO4	8	258.6	257.9	77.6
Cl	8	0.7	0.6	0.3
SO4/Cl	8	163.1	186.3	84.4
pH	8	7.7	7.5	0.7
# of slumps	24			

Unnamed #2

parameter	# samples	median	mean	standard deviation
conductivity	6	865.0	1033.3	562.9
SO4	6	437.8	534.3	331.8
Cl	2	0.3	0.3	0.0
SO4/Cl	2	454.3	454.3	68.5
pH	6	7.8	7.8	0.1
# of slumps	1			

Vittrekwa

parameter	# samples	median	mean	standard deviation
conductivity	52	275.0	293.0	198.6
SO4	84	123.5	262.9	373.6
Cl	48	0.4	3.0	13.8
SO4/Cl	46	95.9	172.9	244.7
pH	81	6.6	6.6	0.8
# of slumps	52			

Willow River

parameter	# samples	median	mean	standard deviation
conductivity	35	350.0	651.4	653.6
SO4	36	149.0	480.6	691.9
Cl	22	0.5	6.0	20.0
SO4/Cl	22	191.4	202.2	118.2
pH	36	7.0	6.8	0.8
# of slumps	59			

Watershed

BFR8

parameter	# samples	median	mean	standard deviation
conductivity	8	80.0	93.8	54.5
SO4	8	35.0	41.5	26.3
Cl	2	0.1	0.1	0.0
SO4/Cl	2	140.9	140.9	96.5
pH	8	5.5	5.3	0.7
# of slumps	8			

Rat 2

parameter	# samples	median	mean	standard deviation
conductivity	13	230.0	381.5	492.4
SO4	13	92.7	231.7	410.8
Cl	5	0.1	1.6	2.6
SO4/Cl	5	90.3	253.0	251.2
pH	13	6.3	6.0	0.9
# of slumps	1			

Rat 4

parameter	# samples	median	mean	standard deviation
conductivity	41	200.0	212.7	142.0
SO4	42	66.5	146.6	446.2
Cl	15	1.6	1.5	1.2
SO4/Cl	15	29.7	138.0	188.2
pH	42	7.1	6.9	0.8
# of slumps	2			

Rat 5

parameter	# samples	median	mean	standard deviation
conductivity	16	105.0	156.8	142.8
SO4	16	29.5	95.4	151.7
Cl	8	2.1	2.2	0.8
SO4/Cl	8	20.4	51.8	88.1
pH	16	6.9	6.8	0.4
# of slumps	4			

SC3

parameter	# samples	median	mean	standard deviation
conductivity	10	245.0	207.2	87.7
SO4	10	123.0	98.9	47.0
Cl	6	0.3	0.4	0.3
SO4/Cl	6	155.4	159.5	96.3
pH	10	7.5	10.0	0.6
# of slumps	21			

Rat 7

parameter	# samples	median	mean	standard deviation
conductivity	2	240.4	240.4	121.6
SO4	2	45.8	45.8	5.1
Cl	2	5.5	5.5	5.0
SO4/Cl	2	15.0	15.0	13.2
pH	2	6.8	6.8	0.0
# of slumps	2			

Rat 8

parameter	# samples	median	mean	standard deviation
conductivity	60	40.0	65.7	65.8
SO4	60	12.7	24.3	32.3
Cl	3	0.2	0.2	0.1
SO4/Cl	3	127.5	161.4	108.7
pH	60	6.7	6.5	0.6
# of slumps	21			

SC1

parameter	# samples	median	mean	standard deviation
conductivity	3	285.9	254.4	52.6
SO4	3	124.1	119.7	24.8
Cl	3	0.5	0.5	0.2
SO4/Cl	3	109.0	104.9	30.7
pH	3	7.6	7.7	0.1
# of slumps	1			

SC2

parameter	# samples	median	mean	standard deviation
conductivity	74	301.0	746.9	74.0
SO4	76	112.2	481.1	76.0
Cl	73	0.9	1.7	73.0
SO4/Cl	73	80.9	120.3	73.0
pH	74	7.1	7.1	74.0
# of slumps	11			

TR2

parameter	# samples	median	mean	standard deviation
conductivity	1	714.0	714.0	0.0
SO4	1	361.1	361.1	0.0
Cl	1	0.7	0.7	0.0
SO4/Cl	1	205.0	205.0	0.0
pH	1	7.5	7.5	0.0
# of slumps	3			

Tr6

parameter	# samples	median	mean	standard deviation
conductivity	1	484.4	484.4	0.0
SO4	1	236.4	236.4	0.0
Cl	1	0.3	0.3	0.0
SO4/Cl	1	281.4	281.4	0.0
pH	1	8.1	8.1	0.0
# of slumps	7			

Un21

parameter	# samples	median	mean	standard deviation
conductivity	4	865.0	1015.0	323.3
SO4	4	437.8	521.2	190.5
Cl	2	0.3	0.3	0.0
SO4/Cl	2	454.3	454.3	68.5
pH	4	7.8	7.8	0.1
# of slumps	1			

VR3

parameter	# samples	median	mean	standard deviation
conductivity	50	280.0	299.3	199.8
SO4	53	108.9	157.7	140.3
Cl	15	0.7	0.7	0.5
SO4/Cl	15	94.1	243.4	370.7
pH	50	6.4	6.4	0.8
# of slumps	40			

WR2

parameter	# samples	median	mean	standard deviation
conductivity	27	220.0	395.6	390.2
SO4	27	96.4	340.8	662.1
Cl	14	0.5	8.0	24.8
SO4/Cl	14	171.4	177.2	104.5
pH	28	7.0	68.0	0.1
# of slumps	58			

TR4

parameter	# samples	median	mean	standard deviation
conductivity	6	576.0	512.6	152.2
SO4	6	258.6	244.3	77.4
Cl	6	0.8	0.7	0.3
SO4/Cl	6	121.5	167.4	87.1
pH	6	7.7	7.4	0.7
# of slumps	11			

Sub-watersheds

BFR8

parameter	# samples	median	mean	standard deviation
conductivity	8.0	80.0	93.8	54.5
SO4	8.0	35.0	41.5	26.3
Cl	2.0	0.1	0.1	0.0
SO4/Cl	2.0	140.9	140.9	96.5
pH	8.0	5.5	5.3	0.7
# of slumps	8			

Rat 2a

parameter	# samples	median	mean	standard deviation
conductivity	13.0	230.0	381.5	492.4
SO4	13.0	92.7	231.7	410.8
Cl	5.0	0.1	1.6	2.6
SO4/Cl	5.0	90.3	253.0	251.2
pH	13.0	6.3	6.0	0.9
# of slumps	1			

Rat 4d

parameter	# samples	median	mean	standard deviation
conductivity	17.0	150.0	185.2	115.4
SO4	17.0	69.4	77.7	59.9
Cl	6.0	2.4	1.9	1.2
SO4/Cl	6.0	25.0	94.9	110.6
pH	17.0	7.0	6.9	0.3
# of slumps	2			

Rat 8b

parameter	# samples	median	mean	standard deviation
conductivity	24.0	30.0	43.8	50.9
SO4	24.0	8.8	15.5	23.0
Cl	0.0			
SO4/Cl	0.0			
pH	24.0	6.1	6.0	0.5
# of slumps	13			

Rat 8c

parameter	# samples	median	mean	standard deviation
conductivity	36.0	50.0	80.4	70.4
SO4	36.0	15.1	30.1	36.1
Cl	3.0	0.2	0.2	0.1
SO4/Cl	125.0	101.6	161.9	178.1
pH	36.0	6.9	6.9	0.3
# of slumps	8			

Rat 5b

parameter	# samples	median	mean	standard deviation
conductivity	6.0	190.0	190.8	139.9
SO4	6.0	58.3	88.4	85.2
Cl	4.0	2.1	2.3	0.6
SO4/Cl	4.0	18.3	19.4	7.4
pH	6.0	7.1	6.9	0.3
# of slumps	1			

Rat 5c

parameter	# samples	median	mean	standard deviation
conductivity	2.0	25.0	25.0	5.0
SO4	2.0	3.7	3.7	1.0
Cl	0.0			
SO4/Cl	0.0			
pH	2.0	6.3	6.3	0.1
# of slumps	3			

Rat 7d

parameter	# samples	median	mean	standard deviation
conductivity	2.0	240.4	240.4	121.6
SO4	2.0	45.8	45.8	5.1
Cl	2.0	5.5	5.5	5.0
SO4/Cl	2.0	15.0	15.0	13.2
pH	2.0	6.8	6.8	0.0
# of slumps	1			

SC3a

parameter	# samples	median	mean	standard deviation
conductivity	1.0	80.0	80.0	0.0
SO4	1.0	34.6	34.6	0.0
Cl	0.0			
SO4/Cl	0.0			
pH	1.0	6.6	6.6	0.0
# of slumps	3			

Sc3c

parameter	# samples	median	mean	standard deviation
conductivity	3.0	280.9	277.1	5.7
SO4	3.0	131.8	124.4	11.2
Cl	3.0	0.8	0.6	0.3
SO4/Cl	3.0	60.8	102.5	66.3
pH	3.0	7.6	7.6	0.0
# of slumps	2			

SC3d

parameter	# samples	median	mean	standard deviation
conductivity	3.0	240.0	205.0	91.2
SO4	3.0	137.6	103.1	54.7
Cl	2.0	0.2	0.2	0.1
SO4/Cl	2.0	256.1	256.1	82.5
pH	3.0	7.5	7.3	0.4
# of slumps	14			

SC3e

parameter	# samples	median	mean	standard deviation
conductivity	3.0	226.0	182.0	79.8
SO4	3.0	119.1	90.4	46.2
Cl	1.0	0.3	90.4	46.2
SO4/Cl	1.0	137.3	137.3	0.0
pH	3.0	6.5	6.7	0.6
# of slumps	2			

TR2a

parameter	# samples	median	mean	standard deviation
conductivity	1.0	714.0	714.0	0.0
SO4	1.0	361.1	361.1	0.0
Cl	1.0	0.7	0.7	0.0
SO4/Cl	1.0	205.0	205.0	0.0
pH	1.0	7.5	7.5	0.0
# of slumps	1			

TR4d

parameter	# samples	median	mean	standard deviation
conductivity	1.0	588.0	588.0	0.0
SO4	1.0	218.7	218.7	0.0
Cl	1.0	0.8	0.8	0.0
SO4/Cl	1.0	102.2	102.2	0.0
pH	1.0	7.9	7.9	0.0
# of slumps	5			

TR4h

parameter	# samples	median	mean	standard deviation
conductivity	2.0	370.7	370.7	196.4
SO4	2.0	216.5	216.5	122.3
Cl	2.0	0.4	0.4	0.3
SO4/Cl	2.0	274.6	274.6	73.0
pH	2.0	6.6	6.6	0.6
# of slumps		6		

SC2a

parameter	# samples	median	mean	standard deviation
conductivity	68.0	370.5	799.8	68.0
SO4	69.0	189.0	525.6	69.0
Cl	68.0	0.9	1.7	68.0
SO4/Cl	69.0	83.7	124.7	69.0
pH	68.0	7.1	7.1	68.0
# of slumps	3			

SC2b

parameter	# samples	median	mean	standard deviation
conductivity	6.0	118.4	147.7	6.0
SO4	6.0	35.2	43.5	6.0
Cl	4.0	0.5	0.8	4.0
SO4/Cl	4.0	43.5	45.1	4.0
pH	6.0	7.2	7.2	6.0
# of slumps	8			

VR3a

parameter	# samples	median	mean	standard deviation
conductivity	50.0	280.0	299.3	199.8
SO4	53.0	108.9	157.7	140.3
Cl	15.0	0.7	0.7	0.5
SO4/Cl	15.0	94.1	243.4	370.7
pH	50.0	6.4	6.4	0.8
# of slumps	3			

VR3g

parameter	# samples	median	mean	standard deviation
conductivity	3.0	150.0	126.7	33.0
SO4	3.0	62.5	57.0	8.5
Cl	0.0			
SO4/Cl	0.0			
pH	3.0	6.4	6.4	0.1
# of slumps	7			

WR2a

parameter	# samples	median	mean	standard deviation
conductivity	1.0	660.0	660.0	0.0
SO4	1.0	348.8	348.8	0.0
Cl	1.0	0.5	0.5	0.0
SO4/Cl	1.0	267.6	267.6	0.0
pH	1.0	4.5	4.5	0.0
# of slumps	1			

WR2d

parameter	# samples	median	mean	standard deviation
conductivity	4.0	100.0	95.0	55.5
SO4	4.0	44.2	42.3	26.7
Cl	3.0	0.1	0.1	0.0
SO4/Cl	3.0	174.1	149.6	83.1
pH	4.0	6.2	6.3	0.3
# of slumps	2			

WR2e

parameter	# samples	median	mean	standard deviation
conductivity	22.0	275.0	438.2	406.1
SO4	23.0	97.5	379.4	708.1
Cl	10.0	0.5	11.1	28.7
SO4/Cl	10.0	156.9	176.5	110.3
pH	23.0	7.2	7.1	0.6
# of slumps	45			

VR3c

parameter	# samples	median	mean	standard deviation
conductivity	3.0	300.0	456.7	235.8
SO4	5.0	142.9	164.8	134.7
Cl	3.0	0.4	0.7	0.7
SO4/Cl	3.0	89.8	136.0	124.7
pH	3.0	6.5	6.7	0.4
# of slumps	5			

VR3h

parameter	# samples	median	mean	standard deviation
conductivity	1.0	100.0	100.0	0.0
SO4	1.0	41.1	41.1	0.0
Cl				
SO4/Cl				
pH	1.0	6.3	6.3	0.0
# of slumps	1			

TR6d

parameter	# samples	median	mean	standard deviation
conductivity	1.0	484.4	484.4	0.0
SO4	1.0	236.4	236.4	0.0
Cl	1.0	0.3	0.3	0.0
SO4/Cl	1.0	281.4	281.4	0.0
pH	1.0	8.1	8.1	0.0
# of slumps	2			

Un21b

parameter	# samples	median	mean	standard deviation
conductivity	3.0	860.0	830.0	49.7
SO4	3.0	423.6	412.7	37.2
Cl	2.0	0.3	0.3	0.0
SO4/Cl	2.0	454.3	454.3	68.5
pH	3.0	7.7	7.7	0.1
# of slumps	1			

VR3f

parameter	# samples	median	mean	standard deviation
conductivity	22.0	320.0	309.5	155.8
SO4	23.0	154.4	192.3	158.2
Cl	2.0	0.2	0.2	0.0
SO4/Cl	2.0	1173.0	1173.0	45.7
pH	22.0	6.4	6.3	0.6
# of slumps	9			

VR3i

parameter	# samples	median	mean	standard deviation
conductivity	12.0	125.0	142.5	76.0
SO4	12.0	52.8	64.8	39.1
Cl	1.0	0.3	0.3	0.0
SO4/Cl	1.0	81.7	81.7	0.0
pH	12.0	6.0	5.8	0.6
# of slumps	8			